UNIVERSITY OF COPENHAGEN

Tropical Cyclones in the Southwest Indian Ocean

And Their Impacts on Vanilla Cultivation in Madagascar

Matea Elise Marinkovic

Master's Thesis
MSc Climate Change

Supervised by:
Jens Hesselbjerg Christensen
with special thanks to Martin Drews

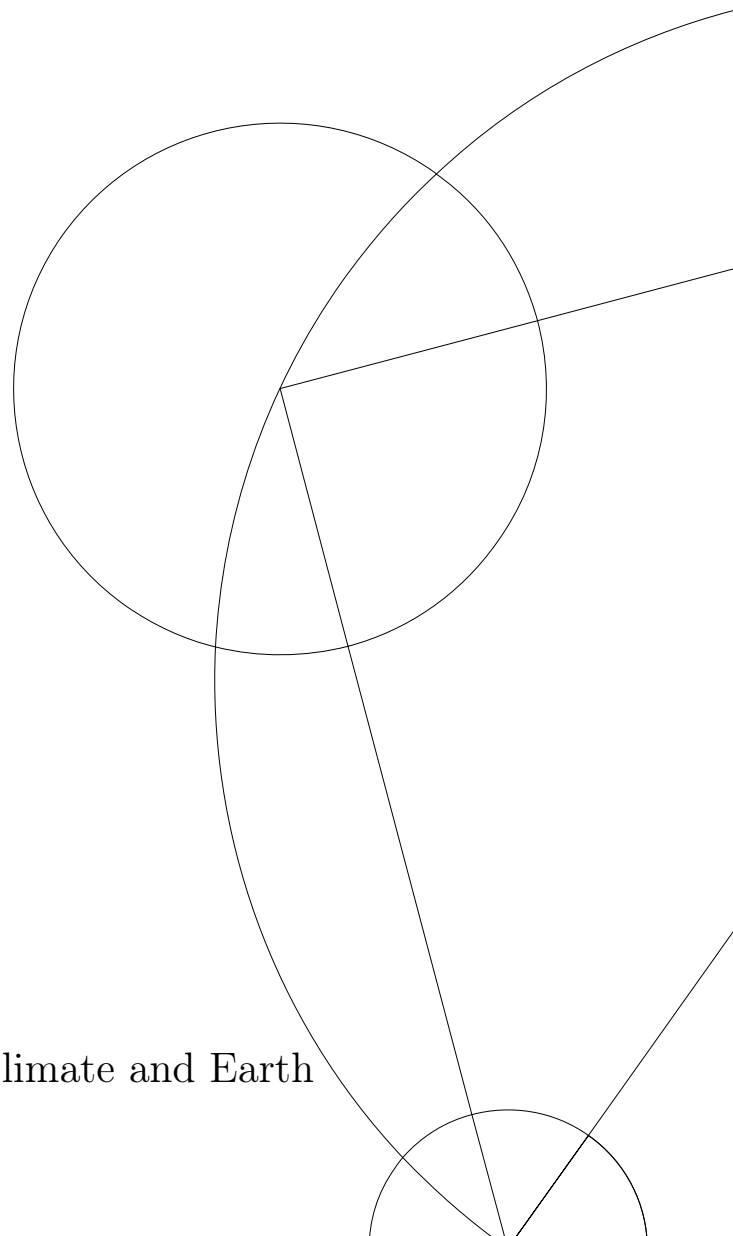

May 31st, 2023
Niels Bohr Institute - Physics of Ice, Climate and Earth

Abstract

Tropical cyclones (TCs) are some of the most destructive weather-related atmospheric features, responsible for significant impacts by way of strong winds, heavy precipitation, storm surges and flooding to the areas that they impact. This study examines the future trends of TCs in the Southwest Indian Ocean (SWIO) region under a changing climate and assesses their impacts on vanilla agriculture in Madagascar in particular. TC tracks calculated with a tracking algorithm from model simulations and observational data is used to for comparison. Calculated TC tracks are verified against model output to confirm TC track identification. Statistical analysis is conducted to evaluate trends in the frequency, intensity, and duration of TCs under a future climate, as well as mean sea level pressure as an indicator of normalized damage. The study finds agreement with global trends of increasing TC intensity and duration but with uncertainties due to methodological limitations and model resolution challenges. The results suggest that higher-intensity TCs and prolonged exposure to extreme weather pose risks to coastal communities and agriculture in the SWIO, particularly vanilla production in Madagascar. To improve the analysis, incorporating more models at higher resolutions, and considering natural variability factors is recommended.

Acknowledgements

To my supervisor Jens, thank you for the many hours of patient instruction, explanation, and your excitement for my thesis topic. To Susanne, thank you for introducing me to climate models and supporting me in my application to KU, as well as in the late stages of the thesis with your thoughtful feedback. I would additionally like to thank my colleagues at IFF for the inspiration in contextualizing climate model work, as well as Martin Drews, for the help in the initial development of the thesis topic and scope.

To my close friends Andrea, Ida, and Rebekka; Thank you for your love, support, encouragement, thoughtful conversations, help in times of code-crisis, and for long coffee breaks and lunches in the sun at PICE, as well as throughout this masters program. Thank you Nick, for the unquestioning support throughout the thesis process and for giving me a computer to write this thesis with. Finally, I would like to thank my family for their encouragement from afar, and their support as I left home to pursue my passion for climate in Denmark.

List of Figures

1 **Southwest Indian Ocean Region** . . . 2
2 **Theoretical Model of the Main Tropical Cyclone Structures** . . . 6
3 **Model Simulations Undertaken by the PRIMAVERA Project** . . . 12
4 **Spatial Distribution of TC Frequency** . . . 19
5 **Tropical Storms in the 1953 Calendar Year from Control Simulation Output** . . . 20
6 **Example Tropical Storm Track** . . . 21
7 **Example Tropical Storm Track Wind Speeds** . . . 21
8 **Mean Wind Field of Example Storm** . . . 22
9 **Wind Field of Example Storm - Max Daily Values** . . . 23
10 **Mean Vorticity Field of Example Storm** . . . 23
11 **Distribution of TC Frequency in the SWIO Basin** . . . 25
12 **Distribution of TCs Intensity** . . . 26
13 **Distribution of the Duration of TCs** . . . 26
14 **Distribution of the Duration of TCs with Sustained Wind Speeds $>$ 35 m/s** . . . 27
15 **Regression of the Frequency of TCs per TC Season** . . . 28
16 **Regression of the Duration of TCs** . . . 28
17 **Percentile 5-Year Running Mean of TC Duration** . . . 29
18 **Regression of the Intensity of TCs** . . . 30
19 **Percentile 5-Year Running Mean of TC Intensity** . . . 30
20 **Distribution of the Frequency of TCs per TC Season Passing Near Land** . . . 31
21 **Distribution of Intensity (max sustained wind) for TCs Passing Near Land** . . . 32
22 **Distribution of the Duration of TCs Passing Near Land** . . . 33
23 **Distribution of the Duration of TCs with Sustained Wind Speeds $>$ 35 m/s** . . . 33
24 **Regression of the Frequency of TCs per TC Season Passing Near Land** . . . 34
25 **Regression of the Duration of TCs Passing Near Land** . . . 35
26 **Percentile 5-Year Running Mean of TC Duration - Near Land** . . . 35
27 **Regression of the Intensity of TCs Passing Near Land** . . . 36
28 **Percentile 5-Year Running Mean of TC Intensity Near Land** . . . 37
29 **Distribution of the Frequency of Landfall TCs per TC Season in the SWIO** . . . 38
30 **Distribution of Intensity for TCs Making Landfall** . . . 38
31 **Distribution of the Duration of TCs Making Landfall** . . . 39
32 **Distribution of the Duration of TCs Making Landfall with Sustained Wind Speeds $>$ 35 m/s** . . . 40
33 **Regression of the Frequency of TCs per TC Season Making Landfall** . . . 40
34 **Regression of the Duration of TCs Making Landfall** . . . 41
35 **Percentile 5-Year Running Mean of Landfall TC Duration** . . . 42
36 **Regression of the Intensity of TCs Making Landfall** . . . 42
37 **Percentile 5-Year Running Mean of Landfall TC Intensity** . . . 43
38 **Distribution of MSLP** . . . 44
39 **Linear Regression of MSLP of all TCs in the SWIO** . . . 45
40 **Percentiles of MSLP versus Season** . . . 45
41 **Distribution of the Frequency of TCs per TC Season in Two EC-Earth3P-HR Ensemble Members** . . . 63
42 **Distribution of Intensity of TCs in Two EC-Earth3P-HR Ensemble Members** . . . 64
43 **Distribution of Duration of TCs in Two EC-Earth3P-HR Ensemble Members** . . . 64
44 **Linear Regression of the Frequency of TCs per TC Season in Two EC-Earth3P-HR Ensemble Members** . . . 65

45 **Linear Regression of the Intensity of TCs in Two EC-Earth3P-HR Ensemble Members** . . . 65
46 **Percentile 5-Year Running Mean of SWIO TC Intensity for Two EC-Earth3P-HR Ensemble Members** . . . 66
47 **Linear Regression of the Duration of TCs in Two EC-Earth3P-HR Ensemble Members** . . . 66
48 **Percentile 5-Year Running Mean of SWIO TC Duration for Two EC-Earth3P-HR Ensemble Members** . . . 67
49 **Distribution of MSLP for TCs in Two EC-Earth3P-HR Ensemble Members** . . . 67
50 **Linear Regression of the MSLP of TCs in Two EC-Earth3P-HR Ensemble Members** . . . 68
51 **Percentile 5-Year Running Mean of SWIO TC MSLP for Two EC-Earth3P-HR Ensemble Members** . . . 68

List of Acronyms

AR6 Assessment Report 6

CMIP6 Coupled Model Intercomparison Project Phase 6

GCMs Global Climate Models

HighResMIP High Resolution Model Intercomparison Project

ITCZ Inter-Tropical Convergence Zone

IPCC The Intergovernmental Panel on Climate Change

KDE Kernel Density Estimate

MSLP Mean Sea Level Pressure

NH Northern Hemisphere

RF Radiative Forcing

SH Southern Hemisphere

SSTs Sea Surface Temperatures

SWIO Southwest Indian Ocean

TC(s) Tropical Cyclone(s)

WGI Working Group 1

W.R.T With Respect To

Contents

Abstract ii

Acknowledgements iii

List of Acronyms vi

1 Introduction 1

2 Background 4

3 Data and Methods 10
3.1 Data . . . 10
3.2 Methods . . . 14
3.2.1 Identification of Storm Tracks . . . 14
3.2.2 Confirmation of TC Conditions in Model Output . . . 14
3.2.3 All-Basin Analysis . . . 15
3.2.4 Landfall and Near-Land TC Analysis . . . 17
3.2.5 Damage Estimation . . . 18

4 Results 19
4.1 Identification and Confirmation of Tropical Cyclone Tracks . . . 19
4.1.1 Identification . . . 19
4.1.2 Confirmation . . . 22
4.2 Tropical Cyclone Track Analysis . . . 24
4.2.1 All Basin . . . 25
4.2.2 Near-Land . . . 31
4.2.3 Landfall . . . 37
4.3 Damage Estimation . . . 44
4.4 Results Summary . . . 46

5 Discussion 48
5.1 Discussion of Methods: How well does the tracking algorithm method represent observed tropical cyclones? . . . 48
5.2 Discussion of Results: What do future tropical cyclone seasons look like in the SWIO? . . . 50
5.3 Discussion of Impacts: How will future tropical cyclones impact vanilla agriculture in the SWIO, particularly in Madagascar? . . . 51

6 Conclusion and Outlook 53

Bibliography 62

A Appendix 63

1 Introduction

Tropical cyclones (TCs) are some of the most destructive weather-related atmospheric features, responsible for significant impacts by way of strong winds, heavy precipitation, storm surges and flooding to the areas that they impact. TCs are weather systems that occur on a synoptic scale, spanning hundreds of kilometers, and develop over warm tropical oceans near to the equator (Redmond et al., 2015). In the Southwest Indian Ocean (SWIO), TCs are particularly significant due to the vulnerability of the coastal populations and the frequency and intensity of storms in the region, with greater than 5 named storms forming on average each year (Mavume et al., 2009; Seneviratne et al., 2021). TCs in the SWIO can have a devastating impact on the lives and livelihoods of the people living in the region, as well as the local economies and infrastructure. It is therefore important to utilize available data and analysis to better understand how TCs in SWIO basin are impacting the region, with the purpose of better understanding future trends to inform environmental, social, and economic adaptation efforts. This study aims to examine TC features in the SWIO and, in particular, how they might impact the region's vanilla agriculture under a changing climate through the use of observations and global climate model simulations.

Between February and March of 2023, Tropical Cyclone Freddy crossed the Southern Indian Ocean, persisting for an unprecedented 5 weeks and 2 days and producing the highest accumulated cyclone energy (ACE) of any TC on record (Cappucci, 2023). Initially forming in the Australian basin in early February, Freddy rapidly intensified into a Category 4 storm before entering the Southwest Indian Ocean basin, where it continued to strengthen (WMO, 2023). At its peak, Freddy reached 1 minute maximum sustained winds of 270 km/hr. The TC first made landfall in Madagascar, causing some weakening, before re-intensifying in the Mozambique Channel. Freddy then made landfall again in the southeast, causing significant damage. The final death toll attributed to Freddy exceeded 1400 people, making it the third deadliest TC on record (Reuters, 2023). The impact of recent events such as TC Freddy, highlights the need for a better understanding of TC trends in the SWIO to inform social, economic, and agricultural adaptation efforts.

TCs have a significant impact on the SWIO region. In particular, the island of Madagascar experiences more TCs than any other African country, which brings heavy rain, high winds, and flooding to the island (E. C. Jones & Murphy, 2009). A unique feature of Madagascar is that northeastern Madagascar is the global center of vanilla agriculture production, responsible for 80-85% of the world's natural vanilla (C.D, 2018; Martin et al., 2021). Weather conditions from TC activity can be particularly damaging to vanilla crops, which are sensitive to excess water and wind (Correll, 1953). Correll (1953) further notes that excessive rainfall can cause vanilla vines to become waterlogged, which can damage the plant and make it more susceptible to diseases, as well as high winds can also damage the vines, which can reduce yield and quality of the vanilla beans. Additionally, flooding can wash away soil and nutrients, which can have a negative impact on the growth of the plants. In some cases, TCs can cause widespread damage to vanilla farms, leading to significant economic losses for farmers and the industry as a whole (Correll, 1953). In 2017, for example, TC Enawo caused extensive damage to vanilla crops in Madagascar, leading to a sharp increase in vanilla prices on the global market (Probst et al., 2017).

TC genesis and intensification are complex processes that require a combination of favorable atmospheric and oceanic conditions. One of the primary factors that contributes to TC formation and intensification is warm sea surface temperatures (SSTs) of a minimum of 26°C (Singh & Koll, 2022). This warm water provides the energy necessary for the storm to intensify, as it evaporates and rises, creating a low-pressure system that draws in more warm and moist

air from the surrounding area (Laing & Evans, 2011). A high mid-level tropospheric humidity allows for the formation of deep convection and cloud development, and when there is such abundant moisture in the mid-troposphere, it can also fuel the storm's growth and intensification as moist air rises and cools, releasing latent heat and further fueling the storm (Laing & Evans, 2011). A low vertical wind shear is also critical for TC genesis and to maintain intensification without disrupting the storm's structure (Gray, 1998).
The SWIO is a unique body of water due in part to its wide range of interactions between the ocean and atmosphere, which can be responsible for both encouraging and/or inhibiting TC genesis in this basin (Fitchett, 2018). During the austral summer, SSTs tend to range from 28°C to 30°C, which meets the threshold for temperatures warm enough to provide the energy needed for TCs to form and intensify (Skirving et al., 2020). High atmospheric moisture near the equator in this region can additionally contribute to the formation of deep convection and cloud development, further fueling a storm's growth.
The SWIO region extends from the southern tip of the African continent, near the Cape of Good Hope, to the equator, and includes the island nations of Madagascar, Mauritius, Seychelles, and Comoros, as well as smaller islands including the French overseas territories of Réunion and Mayotte, as shown in Figure 1.

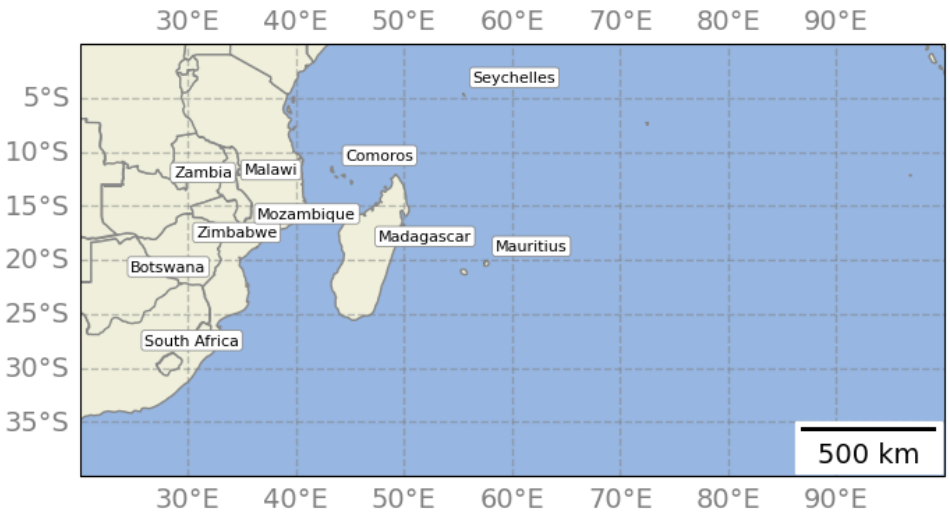

Figure 1: **Southwest Indian Ocean Region** Country boarders and labels included for reference.

TCs and other extreme weather events are naturally highly variable, making the detection and attribution more uncertain than the detection and attribution of the elements by which such events occur, such as large-scale precipitation and temperature trends (Seneviratne et al., 2021). Local physical processes and mechanisms are often the driving force of TC events, which makes projections challenging due to global climate models (GCMs) ability to accurately capture these contributing factors. Despite these challenges, GCMs generally tend to estimate TCs to be intensifying as the Earth warms due to climate change impacts (Grinsted et al., 2019).
When investigating the impacts that TCs have on the region as well as the projected changes in the TCs themselves due to the impacts of climate change, low resolution GCMs (with horizontal resolution >100 km) do not adequately capture the observed TCs, and it is widely recognized that TC intensity and structure improve with increased GCM resolution(Redmond et al., 2015) (Strachan et al., 2013).
As previously mentioned, this study aims to evaluate the future trends of TCs under a changing climate in the SWIO, and assess how these future trends will impact the region and in particular its vanilla agriculture. To this end, storm tracks derived from EC-Earth3P-HR model simulations *control-1950* and *highres-future* conducted using the Coupled Model Intercompar-

ison Project Phase 6 (CMIP6) High Resolution Model Intercomparison Project (HighResMIP) protocol, by the PRIMAVERA project group, have been used. This study uses only data from the SWIO basin and only storms from the period beginning on the 1st of October 1980 through the 30th of May 2015 were considered (more details in Section 3.1). A TC tracking algorithm (*TRACK*) is used to calculate storm tracks from the model simulation output. Further cross checks between the model output and the calculated storm tracks are made to verify the algorithm output. To this end, distribution and regression analysis is conducted to derive future trends from modeled simulations incorporating a high emissions climate change scenario, and then compared to a control model as well as observational trends for the SWIO basin. Future damages are estimated using MSLP as predictor.

This study is carried out for the purpose of addressing several questions. First, how well does the tracking algorithm method applied to model data represent observed tropical cyclones from best track data? Second, what do future tropical cyclone seasons look like in the SWIO basin under a high emissions changing climate scenario? Third, how will future tropical cyclones impact vanilla agriculture in the SWIO, specifically on the island of Madagascar?

2 Background

Increases in both frequency and intensity of extreme weather events such as TCs are often cited as some of the most dangerous projected impacts under anthropogenic climate change conditions (Fitchett, 2018).The extreme weather events referred to in this study as tropical cylones (TCs) have varying naming conventions depending on the region in which they occur. The Atlantic Ocean and Northeastern Pacific Ocean (including the Gulf of Mexico and the Caribbean Sea) refer to storms with sustained winds of at least 119 km/h (74 mph) as hurricanes, while in the Northwestern Pacific Ocean (including the South China Sea and the Philippine Sea) these same types of storms are referred to as typhoons (WMO, 2016). In the Indian Ocean and the Southwestern Pacific Ocean (including the seas around Australia and Indonesia) they are referred to as tropical cyclones. In the South Pacific Ocean, east of the International Date Line, they are referred to as cyclones. This study focuses on the SWIO region, and therefore the nomenclature of storms in this region is tropical cyclones (TCs).
Despite varying names, TCs all share similar characteristics, as they have a well defined life cycle, which can be delimited into classifications. The first stage of a TC is known as a disturbance, where a low pressure area forms over the ocean with a high SST, potentially with converging wind patterns (Laing & Evans, 2011). If conditions are favorable, the disturbance will intensify into a tropical depression, which is characterized by maximum sustained winds speeds of 60 km/h (about 38 mph), with a closed circulation of winds and a defined center of low pressure. As the storm further intensifies, the next classification is a tropical storm, characterized by maximum sustained wind speeds between 62 and 117 km/h (39 and 73 mph). When storms reach this intensity, the storm will be named to avoid confusion amongst, as there can be more than one TC occurring at the same point in time (WMO, 2016). As a classified tropical storm, the storm will cause significant impacts such as heavy rainfall, strong winds, and storm surge in coastal areas. If the storm continues to intensify, it can reach Category 1 TC status on the Saffir-Simpson Hurricane Wind Scale. The Saffir-Simpson Hurricane Wind Scale is a 1-5 rating based on the storm's maximum sustained wind speed, not accounting for other potential impacts including storm surge, heavy precipitation and flooding (NOAA, n.d.). See the remaining classifications from the Saffir-Simpson Hurricane Wind Scale in Table 2.1, with the category number increasing as the intensity increases.

Category	Sustained Wind Speeds	Type of Damage Due to Winds
1	119-153 km/h 74-95 mph 64-82 kt	Very dangerous winds will produce some damage.
2	154-177 km/h 96-110 mph 83-94 kt	Extremely dangerous winds will cause extensive damage.
3 (major)	178-208 km/h 111-129 mph 96-112 kt	Devastating damage will occur.
4 (major)	209-251 km/h 130-156 mph 113-136 kt	Catastrophic damage will occur.

Table 2.1 continued from previous page

5 (major)	252 km/h or higher 157 mph or higher 237 kt or higher	Catastrophic damage will occur.

Table 2.1: The Staffir-Simpson Hurricane Wind Scale with associated types of damage due to sustained wind speeds. Further description of the type of damage with examples can be found at (NOAA, n.d.).

As the storm encounters less favorable environmental conditions (such as cooler ocean temperatures, increased vertical wind shear, land masses, or traveling too close or too far from the equator), the storm will begin to weaken, transitioning to an extratropical or subtropical storm before dissipation (S. C. Jones et al., 2003). The transition process involves the formation of a new frontal boundary, or a transition zone, between the tropical and extratropical air masses (Merrill, 1993). As the TC moves regions of higher latitudes, it may interact with this new boundary and begin to lose its warm core structure. This can lead to changes in the storm's wind and pressure patterns, and a weakening of the storm's core.
One of the key differences between tropical and extratropical storms is the distribution of winds around the storm. TCs have a compact and symmetrical wind field around the eye of the storm, while extratropical storms have a more asymmetrical and diffused wind field around the eye (Bowyer, 2000). As a TC transitions to an extratropical storm, the storm's wind field may become more spread out and less concentrated around the center of the storm. During this transition, the storm may also start to produce more frontal precipitation, which is different from the convective precipitation associated with TCs (Foley & Hanstrum, 1994). This can lead to increased rainfall over a broader area, as well as a potential for strong winds.
However, TCs are complex weather systems driven by a combination of atmospheric, oceanic and geographic features. Six main features (see Table 2.2) are necessary for tropical cyclogenesis to occur. Note, however, that if all six conditions are met, it is still possible that cyclogenesis will not occur (Gray, 1998).

Tropic Feature Number	Tropic Feature
1	Sufficient ocean thermal energy: SST >26°C for the first 60 meters of depth
2	Enhanced mid-tropospheric relative humidity: at 700 hPa
3	Enhanced lower troposphere relative vorticity
4	Low vertical shear of horizontal winds
5	Conditional instability
6	Adequate Coriolis Force Effect: Genesis site location at least 5 degrees latitude away from the equator

Table 2.2: Tropic features that are necessary for cyclogenesis to occur. Features 1, 2, and 5 are thermodynamic parameters supporting deep convection, whereas dynamic features 3, 4, and 6 support the likelihood of genesis (McBride & Zehr, 1981).

Throughout all mature TCs, several key structural elements are present. The (i) boundary layer inflow, (ii) eyewall, (iii) cirrus cloud shield, (iv) rainbands, and (v) upper tropospheric outflow (as seen in figure 2a) are found in all tropical depressions and tropical storms. As storms become more intense, a (vi) clear central eye becomes visible from satellite (as seen in Figure 2a).

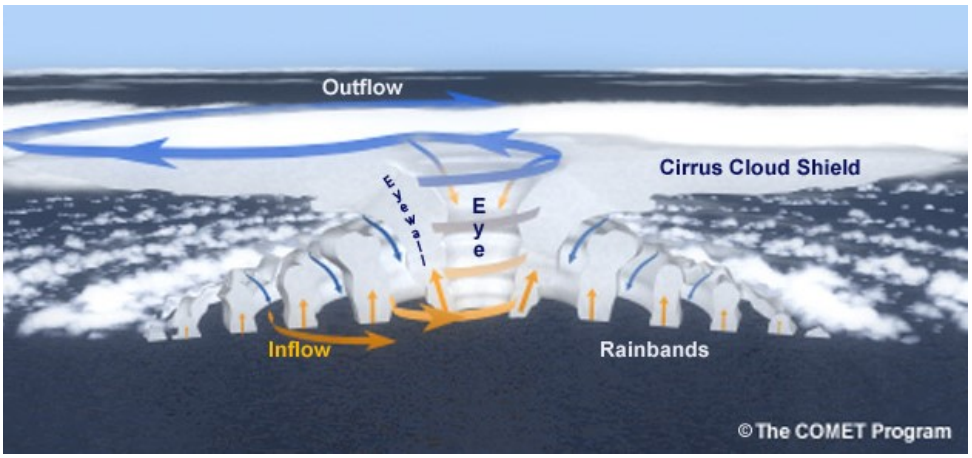

(a)

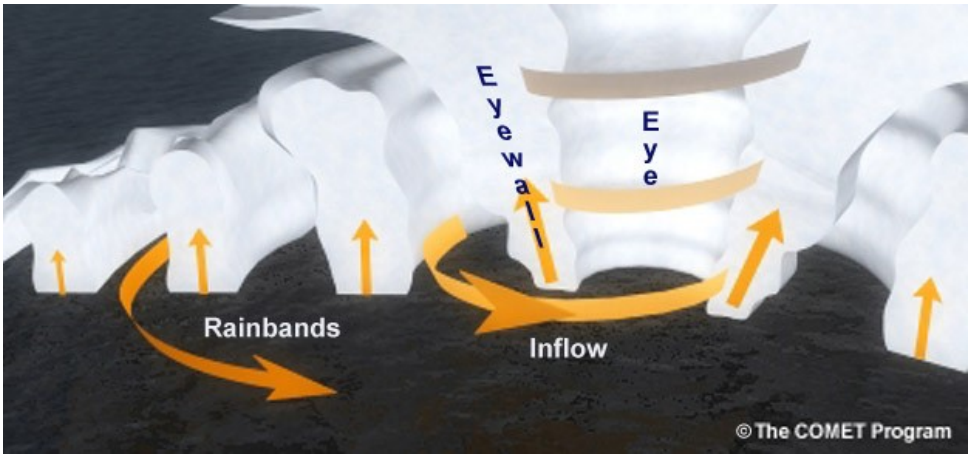

(b)

Figure 2: **Theoretical Model of the Main Tropical Cyclone Structures**(a) Specifically highlighting the inflow, eye, eyewall, cirrus shield, rainbands, and upper tropospheric outflow. (b) Additional view of the boundary layer flow of a TC. Both (a) and (b) can be found in (Laing & Evans, 2011)

As previously mentioned, TCs are synoptic-scale systems and therefore must spin cyclonically (Laing & Evans, 2011). In the Northern Hemisphere (NH), TCs spin counter-clockwise (anti-clockwise) while in the Southern Hemisphere (SH), they spin clockwise. The wind pattern within a TC is characterized by inward cyclonic flow at lower levels, which spirals upward within the zones of deep convection, such as the central eyewall or spiral rainbands. At higher altitudes, just below the tropopause, the wind spirals outward. These dynamics are depicted in (Figure 2b), which provides an illustration of the fundamental aspects of TC systems and is an example of a NH cyclone. The clear central eye region is characterized as being relatively calm with low wind speeds and the lowest surface pressure, with an band of thunderstorms surrounding the eye known as the eyewall where the highest wind speeds are located.
As a TC passes over water, a 'cold-wake' is formed, referring to the area of ocean water that is left cooler than the surrounding water (Chen et al., 2017). This cooling effect is caused by the mixing of colder water from deeper layers of the ocean with warmer surface water, which

occurs as strong winds and waves churn up the ocean during the passage of the TC. The size and intensity of the cold wake depend on various factors, such as the size and intensity of the storm, the speed of its movement, and the oceanographic conditions in the area (Karnauskas et al., 2021). In general, larger and more intense storms tend to create larger and more pronounced cold wakes.

The IPCC AR6 WG1 Chapter 11 report on Weather and Climate Extreme Events in Changing Climate provides valuable insights into the mechanisms and drivers of TCs, observed trends in TC activity, model evaluation and projections for the late 21st century (Seneviratne et al., 2021), noting that there is low confidence in most reported long-term trends in TC frequency and intensity-based metrics. TCs are complex weather phenomena influenced by various mechanisms and drivers. These include large-scale atmospheric circulations, such as the Hadley and Walker circulations (which will be further discussed later in this chapter), which play a crucial role in the formation and intensification of TCs (Seneviratne et al., 2021). Additionally, internal variability on different time scales contributes to the behavior and characteristics of these storms. When assessing trends in TC frequency and intensity metrics, there is limited confidence due to data limitations in so called 'best-track' data (as used in this study and outlined in section 3.1) (Schreck et al., 2014). However, studies including Kang and Elsner (2012), Kishtawal et al. (2012), Kossin et al. (2013), and Mei and Xie (2016), and Balaguru et al. (2018) among others conducted during the satellite era have provided some evidence of positive trends in TC intensity and rapid intensification events. This suggests that TCs are becoming stronger and more capable of undergoing rapid strengthening over shorter periods of time. Furthermore, there have been observations of changes in TC characteristics, including a poleward migration of peak intensity (Kossin et al., 2014) and a global slowdown in translation speed (Kossin, 2018). These observed shifts in behavior have significant implications for regions like the SWIO vulnerable to TC impacts. To gain a better understanding of TC behavior and improve projections, different models have previously been evaluated for performance. Higher-resolution models (as used in HighResMIP, further described in Section 3.1) have shown better performance in capturing TC properties more realistically, including their size, structure, and track patterns (C. D. Roberts et al., 2018). This suggests that finer-scale details and interactions between the storm and its environment play a crucial role in accurately simulating TCs.

Looking ahead to the late 21st century, projections suggest a decrease in the total number of TCs globally (Knutson et al., 2020). This decrease is expected to be more significant at the weaker end of the intensity spectrum, indicating a potential shift towards fewer but stronger storms. Furthermore, the proportion of intense TCs, particularly those classified as Category 4 or 5, is projected to increase (Knutson et al., 2020; Murakami et al., 2012). This implies that regions already susceptible to powerful storms may be facing a higher frequency of extremely destructive TCs in the future. In addition to changes in intensity, other aspects of TC behavior are also projected to undergo transformations. Precipitation rates associated with TCs are expected to increase globally, due to increased low-level moisture convergence caused by regional increases in wind intensities (Seneviratne et al., 2021). This means that when these future TCs do occur, they will likely exhibit more powerful winds and heavier rainfall, posing greater risks in terms of infrastructure damage, flooding, and other hazards.

When examining the formation and behavior of TCs in the SWIO basin in particular, there are several key atmospheric, oceanic, and geographic elements that influence the formation of TCs, as noted in (Seneviratne et al., 2021). In particular, the presence of Hadley and Walker cells, the Inter-tropical Convergence Zone (ITCZ), the Madden-Julian Oscillation (MJO), the Indian Ocean Dipole (IOD), and the El Niño Southern Oscillation (ENSO), as well as the land masses of this region and ocean currents have been shown to influence this basin.

Hadley cells are large-scale atmospheric circulation patterns that are driven by solar heating

and play a significant role in the formation of tropical cyclones (Lu et al., 2007). The SWIO is located in the region of a Hadley cell, where warm, moist air rises at the equator and flows towards the poles at higher altitudes. This creates a region of low pressure, which can lead to the formation of disturbances that can develop into TCs. It is relevant to note, however, that despite the rise in atmospheric and sea surface temperatures (SSTs) over the past century, studies have shown that there has been no significant increase in the number of tropical cyclones in various regions of the world (Fitchett & Grab, 2014; Malherbe et al., 2013). In fact, climate models predict a decrease rather than an increase in the occurrence and landfall of tropical cyclones in the coming century (Seneviratne et al., 2021). This trend is attributed to the strengthening of atmospheric factors that hinder TC formation, in part due to an increase in vertical shear resulting from the expansion of the Hadley cell in this region (Lu et al., 2007). Ash and Matyas (2012) notes the IOD plays a large role TC track influences, particularly due to the role of the IOD surface temperature anomaly.

Walker cells are another atmospheric circulation pattern that can influence TC formation in the SWIO. These cells are driven by temperature differences between the western and eastern portions of the ocean basin and can create regions of low and high pressure that can impact TC development (Saji & Yamagata, 2003). For example, during El Niño events, the Walker cell weakens, leading to warmer SSTs and more favorable conditions for TC formation (M. R. Jury, 1993). Additionally, land masses of the region impact the intensification of TCs as when TCs make landfall, they can weaken or dissipate due to the friction and disruption caused by the terrain. In addition, the shape and location of land masses can impact the path and intensity of TCs as they move across the ocean.

This region also boasts the Inter-Tropical Convergence Zone (ITCZ); a tropical belt of deep convective clouds that migrates between averate latitudes of 20°N and 8 °S in the boreal summer and boreal winter respectively, influencing seasonal rainfall variation (Schneider et al., 2014). During the southward shift in the boreal winter (austral summer), the ITCZ brings with it the increased moisture and instability, which can contribute to the formation of cyclones. The SWIO is also impacted by the Madden-Julian Oscillation (MJO); a dominant mode of variability in the tropical atmosphere (Maloney & Hartmann, 2000). In certain phases of the MJO where low easterly anomalies of the MJO over the Indian Ocean shift to westerly anomalies, the number of TCs can increase twofold (Zhang, 2013).

One of the most major land masses in the SWIO is the island country of Madagascar. TCs cross the island almost every austral summer, causing flooding, landslides, coastal storm surges, as well as loss of life and property (M. Jury, 2022). As previously mentioned, Madagascar is the global center for vanilla production, a crop and economy which is often put at risk by TC activity around the island (Brownell et al., 2009). Madagascar is an impoverished country, with lacking infrastructure throughout the country, which lends towards considerable vulnerability (Brown, 2009). Madagascar's position in the global vanilla economy is based on price and quality, while TCs, considered by the Malagasy to be unpredictable-short term events which impact quality and supply, are now being used internationally as a driver on price and demand on Malagasy vanilla (Brown, 2009). The resulting situation is one where Madagascar focuses on yields and quality of vanilla, without support systems for vanilla farmers which has in part prevented the establishment of adequate resources to combat the impact of TCs on the region (Brown, 2009).

The cultivation of vanilla in Madagascar is mainly carried out by small-scale farmers (Laney, 2004). Growing vanilla is very labor intensive, as pollination is often done by hand, due to the limited amount of natural pollinators present in Madagascar (Brown, 2009). TC damage during the early months of the year are a large threat to vanilla production, and since the plants flower from October-December, the weather conditions play a large role in the size of the crop (Correll, 1953). With a proper balance of rain and sun, the yield is strong, while too

much rain (as when a TC occurs) causes the plant to develop more in the vine, rather than the vanilla bean producing flowers, limiting crop yield. There is a significant concern about the impact of TCs on the vanilla industry in Madagascar, as it could result in a decline in the country's economic growth and the livelihoods of the small-scale farmers who depend on vanilla cultivation, as well as disrupt the global vanilla supply chain. This concern prompted this study to examine TC features in the SWIO and how they might impact the region's vanilla agriculture under a changing climate.

3 Data and Methods

3.1 Data

Global climate models (GCMs) are tools that are instrumental for the understanding of climate. Such models are based on physical laws and allow for numerical simulations, where the climate system is characterized by a broad range of spatial scales and timescales (Rummukainen, 2010). As a result, GCMs can capture large-scale climate features including atmospheric and oceanic circulations, as well as broad patterns (for example) in temperature and precipitation. In the past, the limited computing resources available for climate models have placed restrictions on the horizontal resolution of GCMs, which has resulted in a lack of realistic simulation of TCs, especially in terms of their intensity and structure (Redmond et al., 2015). Likewise, while horizontal resolution is limited, the effective resolution is often lower due to numerical calculation within the model, although effective resolution is not considered in this study (Grotch & MacCracken, 1991). GCMs can have horizontal resolutions of up to hundreds of kilometers and employ parameterizations to represent the sub grid-scale processes. This level of horizontal resolution is generally considered insufficient to simulate TCs, and therefore a tracking algorithm is used to identify and track TC-like features in GCM output (Strachan et al., 2013).
In order to combat the concerns with the horizontal resolution of GCMs, this study focuses on model simulations conducted using the Coupled Model Intercomparison Project Phase 6 (CMIP6) High Resolution Model Intercomparison Project (HighResMIP) protocol, by the PRIMAVERA project, which aims to assess both standard and enhanced horizontal resolution simulations of the atmosphere and ocean (PRIMAVERA, n.d.). The experiments are tiered and include atmosphere only as well as coupled ocean-atmosphere runs for the period of 1950-2050, although only a portion of this available time is utilized in this study, and will be discussed later in this section. The HighResMIP protocol is described with further detail in R. J. Haarsma et al. (2016), and is summarized by the PRIMAVERA project in Figure 3 .
The collection of datasets created by the PRIMEVERA project with tropical storms tracks derived from the CMIP6 HighResMIP model simulations and calculated by the *TRACK* algorithm are listed in Table 3.1. The overview presented in Table 3.1 does include multiple atmosphere and ocean nominal resolutions for each model, due to the fact that each model has sub-distinctions based on resolution. For example, EC-Earth3P includes both EC-Earth3P and EC-Earth3P-HR, with EC-Earth3P-HR at a higher resolution. More information on the models and higher-resolution simulations can be found in (R. J. Haarsma et al., 2016). Note that due to time and computing restraints, only EC-Earth3P-HR was used for this study.

Model Name	Contact Institute	Atmosphere Nominal Resolution	Ocean Nominal Resolution	References
CMCC-CM2	CMCC	100 km 25 km	25 km 25 km	(Cherchi et al., 2019)
CNRM-CM6	CERFACS	250 km 50 km	100 km 25 km	(Voldoire et al., 2019)
EC-Earth3P	EC-Earth, KNMI, SHMI, BSC, CNR	100 km 50 km	100 km 25 km	(R. Haarsma et al., 2020)
ECMWF-IFS	ECMWF	50 km	100 km	(C. D. Roberts et al., 2018)

Table 3.1 continued from previous page

		25 km	25 km	
HadGEM3 GC3.1	MOHC, UREAD, NERC	250 km	100 km	(Williams et al., 2018)
		100 km	25 km	(Kuhlbrodt et al., 2018)
		50 km		(Menary et al., 2018)
				(M. J. Roberts et al., 2019)
MPIESM-1-2	MPI-M	100 km	40 km	(Gutjahr et al., 2019)
		50 km	40 km	

Table 3.1: Overview of models used by the PRIMAVERA project as part of the CMIP6 HighResMIP model simulations and additionally have calculated TC tracks by the *TRACK* algorithm. This overview includes information on the model name, contact institute(s) for the respective model, the nominal resolution for both atmosphere and ocean, as well as further references.

The PRIMEVERA project employs the *TRACK* algorithm to calculate tropical storm tracks, which are then made available as Climate Model Output Rewriter (CMOR) formatted NetCDF files. These files are organized into separate files for each hemisphere and cover all years of the HighResMIP experiments' simulated period (M. Roberts, 2019). An overview of the simulations with tropical cyclone tracks calculated can be seen in Table 3.2.

Simulation Name	Simulation Period	Run Type
highresSST-present	1950-2014	Atmosphere only
highresSST-future	2015-2050	Atmosphere only
control-1950	1950-2050	Coupled Atmosphere-Ocean
hist-1950	1950-2014	Coupled Atmosphere-Ocean
highres-future	2015-2050	Coupled Atmosphere-Ocean

Table 3.2: Overview of the simulations with TC tracks calculated using the *TRACK* algorithm by the PRIMAVERA project.

In this study, the EC-Earth3p-HR model is represented in the analysis by only one model run: ensemble member r1i1p2f1. Note that an additional ensemble member is examined in Appendix A The 'ripf' indicates individual members of an ensemble of simulations by their characteristics, where r indicates the realization (i.e. initial conditions), i the initialization method, p differences in model physics and f the forcing data used (Taylor et al., 2018). The various realizations, indicated by r, correspond to model runs with the same configurations but initiated from distinct initial conditions, thereby capturing the internal climate variability of the model. However, due to computational and time limitations, this study does not fully incorporate multiple realizations of each model, which would enable the consideration of this variability.
This study makes use of the *control-1950* coupled atmosphere-ocean simulation as well as the *highres-future* coupled atmosphere-ocean simulation forced using IPCC scenario SSP5-8.5. The *control-1950* and *highres-future* simulations are part of the second tier of simulations following

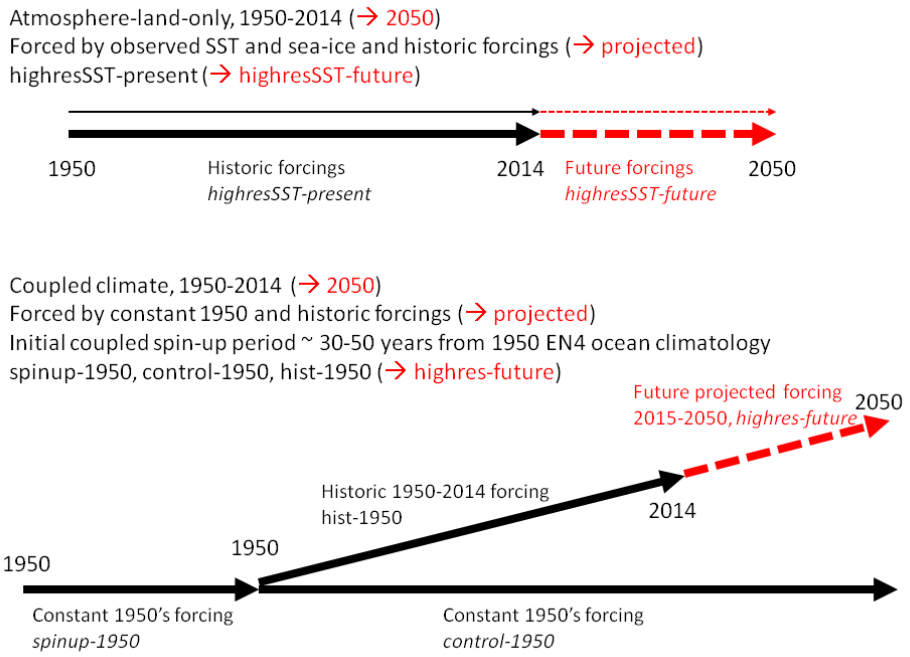

Figure 3: **Model Simulations Undertaken by the PRIMAVERA Project** PRIMAVERA tiered simulations following the CMIP6 HighResMIP protocol. This study utilizes the *control-1950 simulation* and the *highres-future* simulation. More information on simulations can be found in (R. J. Haarsma et al., 2016), diagram retrieved from (PRIMAVERA, n.d.).

the HighResMIP protocol. These coupled atmosphere-ocean simulations aim at addressing questions of model bias in mean state and variability (R. J. Haarsma et al., 2016). *Control-1950* is the HighResMIP answer to pre-industrial control, utilizing 1950s fixed forcing of GHG for a 1950s (10 year mean) climatology. The *highres-future* simulation forcing is based on CMIP6 SSP5.8.5, a very high emissions scenario where global $C0_2$ doubles by 2050 (IPCC, 2021). All models shown in table 3.1 have both *control-1950* and *highres-future* simulations of tropical storm tracks calculated by the *TRACK* algorithm, although only EC-Earth3p-HR ensemble member r1i1p2f1 is used in this study. The *TRACK* algorithm is an object-based tracking method which detects vorticies in the SH as minima in the 850 hPa relative vorticity field (at 6 hour time intervals), further details of which are outlined in (Hodges, 1995, 1999). In addition to the *TRACK* algorithm, tropical storm tracks are also available as calculated by the *TempestExtremes* algorithm, more details of which can be found in (Ullrich & Zarzycki, 2017) and (Zarzycki & Ullrich, 2017). Although both tracking algorithms employ the use of a feature tracking variable (vorticity for *TRACK* and MSLP for *TempestExtremes*) and have similar functionality, *TRACK* was selected for the inclusion of a greater variety of models with calculated tropical storm tracks, which allows for an expansion of the model and ensemble usage in future analysis past the scope of this study.

In order to evaluate the algorithm with respect to the model, model output from CMIP6 experiments using EC-Earth3p-HR was used, with the same ensemble member r1i1p2f1. From the *control-1950* experiment, daily mean near surface wind speed values (*sfcWind*), daily maximum near surface wind speed values (*sfcWindmax*) as well as mean atmospheric relative vorticity taken over 850, 700 and 600 hPa on a T63 spectrally truncated grid (*vortmean*) on a 6 hour time scale (Consortium (EC-Earth), 2018).

In order to evaluate the algorithm plus the model with respect to their variability under cur-

rent climate conditions, observational data is also taken into consideration. Observed tropical cyclone data from the International Best Track Archive for Climate Stewardship (IBTrACS) is used (Knapp et al., 2010). This study uses only data from the SWIO basin, and only storms from the period beginning on the 1st of October 1980 through the 30th of May 2015 were considered, to prevent issues of data heterogeneity from earlier storms occurring prior to the satellite era (Fitchett, 2018). Further details on the IBTrACS project methods and statistics related to the Indian Ocean data can be found in (Levinson et al., 2010).

3.2 Methods

The following steps of the analysis are conducted using Python, for which the code has been made available online[1].

3.2.1 Identification of Storm Tracks

The initial TC track identification and tracking methodology follows a similar method to that in Bengtsson et al. (2007) and Manganello et al. (2012), and is based on the *TRACK* algorithm (henceforth referred to as *TRACK*), a full explanation of which can be found in (Hodges, 1995, 1999). In this study, *TRACK* was utilized to detect vorticies in the SH as maximum in the 850-hPa relative vorticity field, available every 6 hours, with values greater than $5x10^{-6}s^{-1}$ at a spectral resolution of T63. Relative vorticity is used as a feature tracking variable, as it focuses on a smaller spatial scale than other fields and therefore thought to be a better indicator of tropical vorticies (Bengtsson et al., 2007). At this point, no differentiation is made between TCs and other synoptic systems, as every system that satisfies the tracking criteria are obtained. All calculated tracks at this point are filtered to ensure cyclogenesis occurs from October 1st - May 31st (the austral summer). Additionally, tracks not having a maximum sustained wind speed (peak intensity) occuring within the SWIO basin are filtered as out of scope to this study. It is important to note that in order to separate TCs from other synoptic systems captured by *TRACK*, a number of criteria (or filters) can be applied. The following criteria have been considered in this study, focusing on TC surface conditions:

1. Lifetime of $\geq$ 2 days.
2. Cyclogenesis occurring over ocean.
3. Difference in vorticity between 850 hPa and 250 hPa > 0, indicating a warm core condition.

Additional criteria such as vorticity max at each level between 850 and 250 hPa have not been included due to time and computing constraints, although this criteria would be useful in indicating a coherent vertical structure condition of the TCs.

3.2.2 Confirmation of TC Conditions in Model Output

To confirm that the aforementioned method of TC track identification is agreeing with the null hypothesis that *TRACK* is calculating TC-like systems (after filtering for TC criteria is applied), several checks were utilized to verify example TCs against model output from CMIP6 experiments using EC-Earth3p-HR. An example calculated storm from the *control-1950* simulation was selected at random to compare to model output. The TC track, along with wind speeds were visualized for the track (see Figures 6 and 7). From the model output of the *control-1950* experiment, daily mean near surface wind speed values (*sfcWind*), daily maximum near surface wind speed values (*sfcWindmax*) as well as mean atmospheric relative vorticity (*vortmean*) data was taken for the same time period as the duration of the calculated storm and animated on a daily time scale in order to visualize these conditions over the same area as the calculated storm track. An assumption is made that visual correlation between (in particular) high vorticity in the *vortmean* variable following a similar path to the calculated

[1]Code used in this study is available at https://github.com/MateaMarinkovic/Master-Thesis-Marinkovic.git

storm track (figure 6), represents confirmation of the method used in section 3.2.1. This was then repeated for an additional calculated storm in the *control-1950* experiment, as well as a calculated storm in the *highres-future* experiment.

3.2.3 All-Basin Analysis

Data frames are created for the observational, control and future simulations containing information on the TC season in which the TC occurs, the start and end date of each TC, as well as the duration (in days) of the storm and the maximum sustained wind speed for each storm in m/s. The TCs in these data frames include storms that occur throughout the entire basin, both that do and do not make landfall. As TCs in the SH occur over the austral summer (in this study, October - May) the 'season' of each storm is notated by a single year, based on the year of the first portion of the season (October-December). For example, a TC occurring in the 1980-1981 season would be notated with the season of 1980, regardless if the TC actually occurred in (for example) February of 1981. The data frames are then verified to ensure that TCs within the proper time frame are included. TCs are additionally grouped by season to calculate the number of TCs occurring in each season.

Linear Regression Analysis

Linear regression analysis is performed for observational, *control-1950*, and *highres-future* TC tracks. This regression analysis is performed in order to determine the correlations between the season in which the TC(s) occur and the number of TCs per season, as well as for the duration of the TCs and the sustained wind (Uyanık & Güler, 2013). This rests on the assumption that as the TC seasons progress (time progresses), this progression captures the impact of a changing climate and therefore, as time increases, the relationship between changing climate conditions and different aspects of TCs would be captured. In this study, the linear regression analysis is conducted with the Python library statsmodels, specifically through the implementation of Ordinary Least Squares (OLS) regression (Seabold & Perktold, 2010).
OLS regression assumes a linear relationship between the variables and aims to find the best fit line that minimizes the sum of the squared differences between the observed values of the dependent variable and the predicted values generated by the model (Weaver & Wuensch, 2013). This approach was selected due to its allowance for understanding of the relationships between the variables, as well as the ability to make predictions on the relationships between the variables. OLS regression additionally lends itself well to statistical measures that assess how well the fit of the model is. By assessing the fit, it is possible to determine the degree to which the model captures underlying patterns and variability.
In this study, the correlation between variables is calculated as the Pearson correlation coefficient (r). The Pearson correlation coefficient is calculated using the Python library scipy, specifically the pearson r function, which is represented by Equation 3.1, where m_z is the mean of vector x and m_y is the mean of vector y (Scipy, n.d.). The Pearson correlation coefficient (or Pearson's r) is used to assess the linear association between time and various dependent variables (Taylor, 2001). The dependent variables tested include the frequency of TCs per TC season, the duration of each TC, and the intensity of each TC measured by the maximum sustained wind speed.

$$r = \frac{\sum(x - m_x)(y - m_y)}{\sum(x - m_x)^2 \sum(y - m_y)^2} \tag{3.1}$$

Additionally, the study calculates p-values (the probability of the coefficient values being 0) for each OLS regression to assess the statistical significance of the coefficients with Equation 3.2 where xbar is the mean coefficients of the sample and the SE represents the coefficients standard error. The test statistic is translated to p-value with a t-value table. These p-values play a crucial role in determining whether the coefficients differ significantly from zero. In this study, specifically, the objective is to assess whether the season has a significant impact on any of the dependent variables under investigation. If the corresponding p-value is less than 0.05, the null hypothesis stating that the season does not have a significant impact on any of the dependent variables is rejected. This statistical significance assessment allows for more informed interpretations of the regression results.

$$teststatistic = \frac{(\overline{x} - 0)}{SE} \tag{3.2}$$

Percentile Analysis

The linear regression analysis was further broken down by percentiles; the 25th, 50th (median) and 75th percentile. Percentiles were calculated with the Python library Numpy percentile function (NumPy, n.d.). By analyzing the running means within these percentile ranges, it allows the examination of how the dependent variables behave in different ranges of their distribution. 5-year running means are utilized, and compared across datasets to observe how the dependent variable trends differ.

Distribution Analysis

Distributions analysis using histograms of the frequency of TCs per TC season, the duration of each TC and the intensity of each TC were also taken. The histogram is a graphical representation that organizes the data into bins, displaying the count of data falling into each bin. In this study, this allows for an understanding of the underling shape of the data to be considered. For distributions of frequency and duration, a bin width of 1 TC season and 1 day (respectively) was utilized, while for the distribution of sustained wind speeds, a bin width of 5 meters per second is used.

To accompany the distribution analyses, a Kruskal-Wallis p-value is calculated across the three distributions being compared for each variable; distribution of the observational data, distribution of the *control-1950* simulated TCs, and distribution of the *highres-future* simulated TCs. The Kruskal-Wallis test is a non-parametric statistical test used to compare the distributions of three or more independent groups, as present in the distribution analysis of this study, with three distributions of the same variable from different datasets (Theodorsson-Norheim, 1986), (Kruskal & Wallis, 2012). The Kruskal-Wallis test can aid in the determination of statistically significant differences in the distributions. The null hypothesis states that there are no significant differences between the distributions of the three datasets. Data from all datasets is then ranked in ascending order, irregardless of dataset origin. A test statistic is then calculated, measuring the overall difference between the ranked data of the three datasets, as shown in Equation 3.3:

$$H = (N-1)\frac{\sum_{i=1}^{g} n_i(\overline{r_i} - \overline{r})^2}{\sum_{i=1}^{g}\sum_{j=1}^{n_i}(r_{ij} - \overline{r})^2} \tag{3.3}$$

Where N is the total number of data points across all datasets, g is the number of datasets, n_i is the number of data points in each dataset, r_{ij} is the rank of each data point (j) amongst all data points in dataset (i), r_i is the average rank of all data points in dataset (i) and r is the average of all r_{ij}. Once the test statistic is computed, it is compared to the critical value from the distribution with degrees of freedom equal to the number of datasets less one. The Kruskal-Wallis p-value represents the probability of observing a test statistic as extreme as the one calculated, assuming the null hypothesis is true. If the p-value is below a predetermined significance level (0.05), we reject the null hypothesis and conclude that there are significant differences between the distributions. If the p-value is above the significance level, we fail to reject the null hypothesis. If the p-value is statistically significant (less than 0.05), it suggests that the distributions represented by the three histograms are significantly different. Alternatively, if the p-value is not significant, it indicates that there is insufficient evidence to conclude that the distributions differ significantly.

3.2.4 Landfall and Near-Land TC Analysis

The TCs present in the SWIO basin are further identified as TCs that do or do not make landfall within the region. For the purposes of this study, landfall storms are defined as storms that at some point in their path leave the ocean and cross land. It is important to note that no distinction was made between TCs that move at some angle to the coastline rather than perpendicular to the coast at landfall (Kaplan & DeMaria, 1995). Likewise, no distinction was made for TCs that make landfall more than once, returning to the ocean several times.
For this analysis, the TC tracks are identified with the same methodology as described in section 3.2.1. Both landfall and near-land TC identification methods are separated into two sections, observational data and modelled data. For the observational data, landfall values are given in the IBTrACS dataset, and defined as the nearest location to land within the upcoming 6 hours of a storm (Knapp et al., 2010). This can be interpreted as a landfall flag, with a value of 0 meaning landfall within the next 6 hours and >0 meaning no landfall within the next 6 hours. Landfall forcasts are based on the storm center, and values less than or equal to 100 km indicate that land was likely impacted by the system even though the center was not directly over land, as well as the opposite that the system was impacted by land formation at this distance (Barbary et al., 2019). For the purposes of this study, a distance (from land) of 1 km or less as a landfall value is considered to be equivalent to landfall for both the observational data and the modelled data, while a distance of 100 km or less is considered to be near-land. The number of landfall TCs per season is then calculated for TCs in the observational dataset. For modelled data in the *control-1950* calculated TCs and the *highres-future* calculated TCs, TCs that have been previously filtered to have a maximum intensity within the SWIO basin are considered. The longitude values for points along each TC track are normalized to be within -180 and 180 degrees, then a global land mask is applied to identify if each point in the TC tack is on land or over ocean. For TCs without points on land, the point that is closest to land then has a distance from land calculated utilizing the Haversine formula, which determines the great-circle distance between two points given their longitudes and latitudes (Prasetya et al., 2020). TCs are then filtered by the landfall value to signify if they are either landfall, near-land or other TCs. TCs that are considered landfall and near-land are then used for analysis.
Linear regression analysis as well as percentile analysis and distribution analysis with the corresponding statistical analysis as described in Section 3.2.3 are also applied to the landfall TC subset.

3.2.5 Damage Estimation

While there is no singular geophysical quantity that perfectly encapsulates the damage that TCs will cause, Bakkensen and Mendelsohn (2016) and Klotzbach et al. (2020) have identified mean sea level pressure (MSLP) as a skillful predictor of normalized damage. Normalization provides an estimate of how much damage a TC would hypothetical cause if it were to make landfall given identified levels of exposure and wealth where it made land. While normalized damage can be calculated (for example) by damage in terms of equivalent area of total destruction as in Grinsted et al. (2019), or as an adjustment of population, inflation, and wealth per-capita as in Weinkle et al. (2018), direct economic damage data and insured losses data amongst other social and economic data used in these methods is largely unavailable as a robust resource for the SWIO region. Therefore, this study utilized mean sea level pressure (MSLP) as a an indicator of damage, as a part of an proposed extended Saffir-Simpson Scale as shown in Table 3.3. With MSLP as a more skillful predictor of TC normalized damage, as well as with the assumption that the Saffir-Simpson scale was developed to characterize the risk of TCs to society, the proposed scale from Klotzbach et al. (2020) is used as a future damage estimate in this study (Klotzbach et al., 2020). For damage estimation analysis, the TC tracks are identified with the same methodology as described in section 3.2.1. Linear regression analysis, percentile analysis and distribution analysis as well as the the corresponding statistical analysis as described in section 3.2.3 are also applied to for damage estimation.

Category	Max-Sustained Wind (kt)	Min Sea Level Pressure (hPa)
1	64 - 82	976 - 990
2	83 - 95	961 - 975
3	96 - 112	946 - 960
4	113 - 136	926 - 945
5	>136	<926

Table 3.3: Extended Saffir-Simpson Scale with minimum sea level pressure included as proposed by Klotzbach et al. (2020).

4 Results

This chapter first presents the results from the identification of tropical storm tracks by the *TRACK* algorithm and subsequent confirmation of TC-like conditions in GCM output, followed by analysis of observational data, as well as the *control-1950* calculated TCs and the *highres-future* calculated TCs (henceforth referred to as the control and future simulations) at the basin, near-land and landfall TC perspective in Section 4.2. Section 4.3 then examines how normalized damage might be predicted via the Staffir - Simpson scale though the inclusion of MSLP.

4.1 Identification and Confirmation of Tropical Cyclone Tracks

4.1.1 Identification

Figure 5 shows three maps of the SWIO basin with spatial distributions of TC track frequency. Observations show the narrowest spatial distribution of all all three, with most TCs passing around 15°S, and few TC tracks traveling north of 10°S or south of 30°S. The control simulation with 1950s RF shows a greater density of TC tracks, as well as more tracks making landfall. There are higher numbers of tracks passing just northeast of Madagascar, as well as in the Mozambique Channel as compared to observed TC tracks. Notable from the control simulation is the high amount of tracks passing within 5°of the equator, as well as south of 30°S. The future simulation with SSP5-8.5 forcing shows the fewest highly dense areas, and is more closely representative of the observed TC tracks in that regard. However, similarly to the control simulation, the future simulation has a large number of tracks that pass within 5°of the equator as well as south of 30°S.

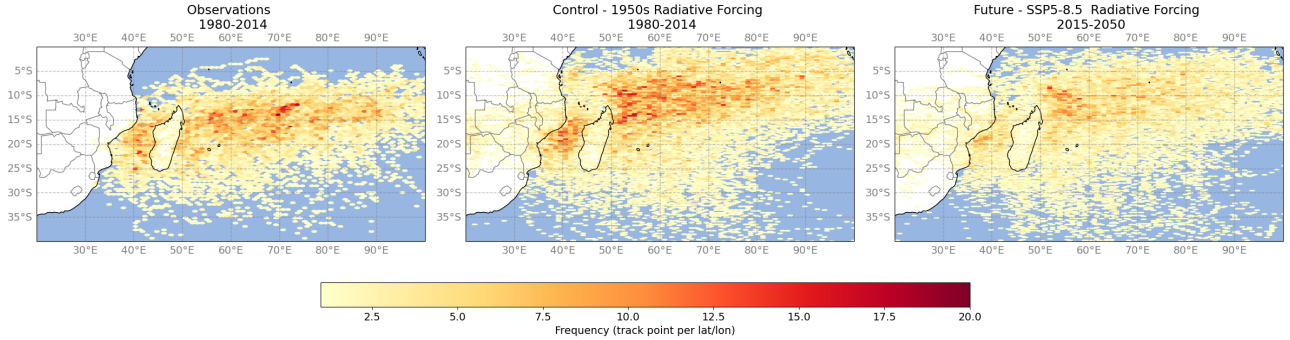

Figure 4: **Spatial Distribution of TC Frequency** Track density (frequency of track occurrence at each latitude and longitude) represented in (left) observational best-track data, (center) the control simulation and (right) the future simulation. Red areas indicate regions with a high frequency of TC tracks passing though. Note additional few occurrences of TC tracks passing onto land, both in Madagascar and on continental Africa.

Figure 5 shows an example of calculated tropical storms for the calendar year of 1953 from the control simulation. Note that this Figure represents storms from a calendar year, not a TC season, therefore storms from the end of the 1952 season and the beginning of the 1953 season are included. Also note that storms in this Figure can be described as TC-like but not as TCs, as they have not been confirmed as TCs with the methodology outlined in Sections 3.2.1 and 3.2.2, and will be referred to as tropical storms. A calendar year is plotted for the purpose of

more easily identifying an example tropical storm as storms from the same season often have overlapping tracks.

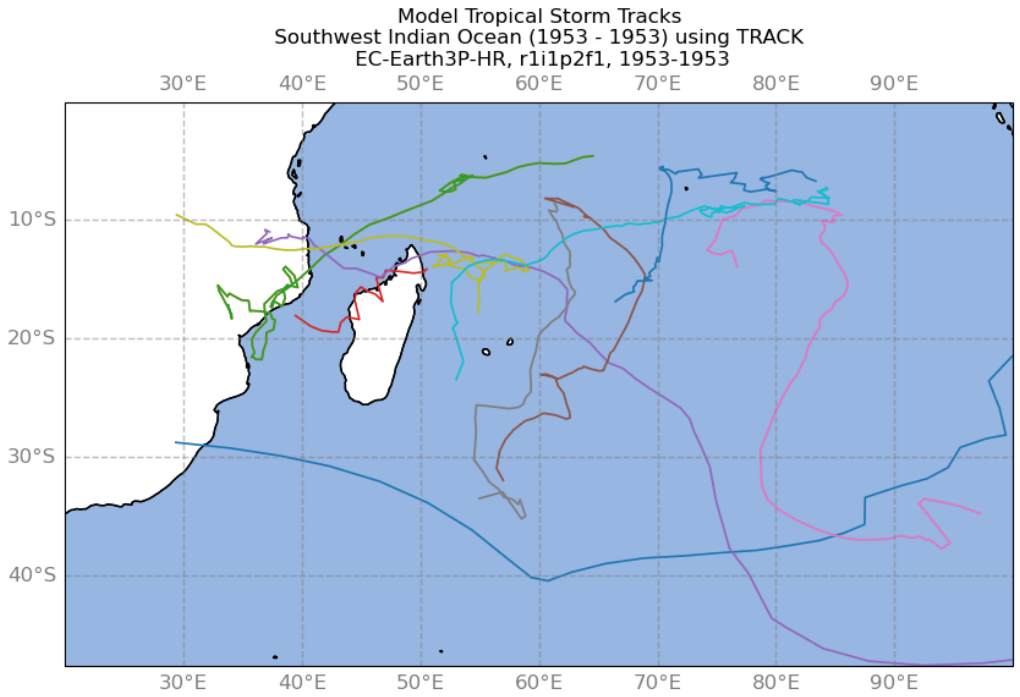

Figure 5: **Tropical Storms in the 1953 Calendar Year from Control Model Output** Tropical storm tracks as calculated from EC-Earth3P-HR ensemble member r1i1p2f1, showing storms from January 1953-December 1953 in the control simulation with 1950s radiative forcing. Each track is denoted with a different color and note that although some tracks extend beyond the mapped area, their peak sustained wind speeds occur within the shown area.

Figure 6 shows a singular TC track for the same 1953 year in the control simulation, along with wind speed labels for every fourth point of the track. This particular storm begins just northeast of Madagascar, travels southwest throughout its lifetime and makes landfall in Mozambique before traveling again over ocean in the Mozambique Channel before making landfall again several times and eventually dissipating over land. This modeled tropical storm begins on the 24th of November and ends on the 18th of December, in the 1953 radiative forcing year of the model simulation. Clustered track points in this storm track indicate a slow moving storm, as track points are identified on 6 hour intervals. Wind speeds for this storm can be seen in Figure 7.

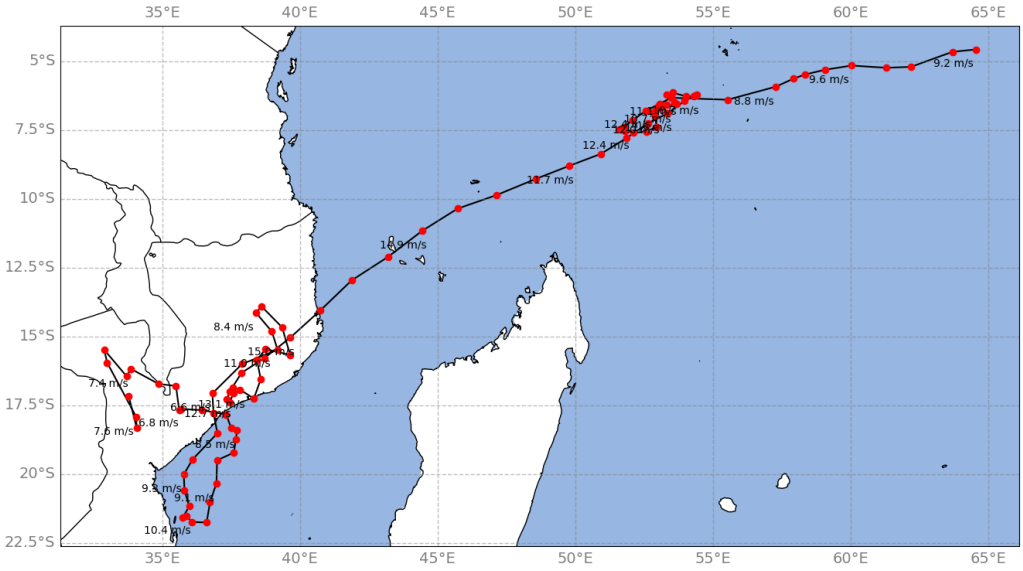

Figure 6: **Example Tropical Storm** Tropical storm track in the 1953 calendar radiative forcing year from control simulation output. Red points indicate observations at 6 hour intervals (one point for every 6 hours). Wind speeds in m/s are included at every 4th time step. Track can be seen from a broader perspective in green in Figure 5

.

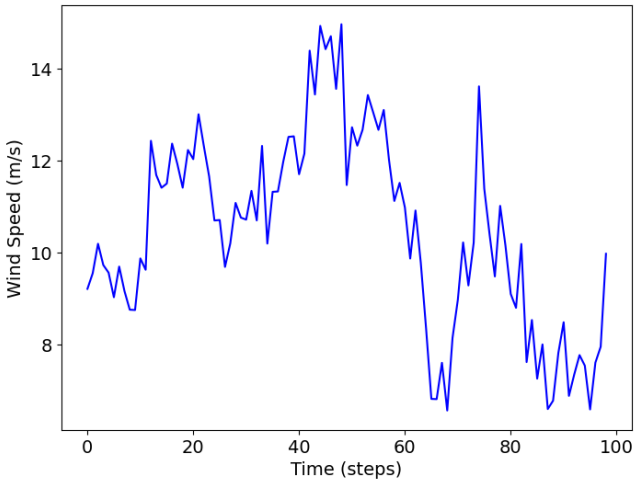

Figure 7: **Example Tropical Storm Track Wind Speeds** Tropical storm track in the 1953 calendar radiative forcing year from control simulation output. Wind speeds plotted in m/s.

4.1.2 Confirmation

Figure 8 is an animation that shows the daily mean wind field in which the example storm from Section 4.1.1 is occurring. Note that for all animations to be viewed, the document must be opened with Adobe Acrobat Reader. As this animation loops, a small area of high wind speeds relative to the displayed scale is visible following a similar path to the calculated tropical storm track. There is, however, many other areas of high wind speeds, making a distinct storm difficult to identify.

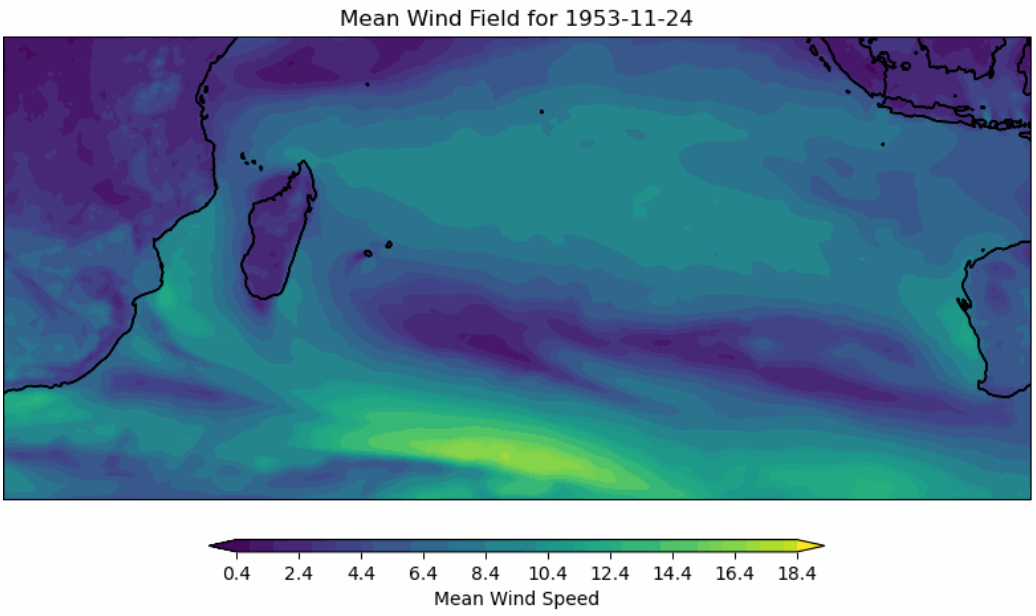

Figure 8: **Mean Wind Field of Example Storm** Mean wind speed values displayed as an animation for the SWIO wind field. Time steps are set as the same time as the calculated example storm in Figure 5 and wind speeds are shown in m/s. Note that in print form, animation will display only the first day.

Figure 9 shows the max wind field near surface winds, considering only the maximum daily value in each frame, as opposed to the mean wind field in Figure 8. With this animation, a high wind speed center is more easily identifiable following a similar track to the calculated storm track. However, high wind speeds at the southern end of the basin add a lot of noise to both this animation as well as the animation in Figure 8. Also note that when similar animations are created for storm tracks with faster moving storms (storms that cross a greater distance throughout their lifetime, as opposed to the example storm here), a center of high wind speeds is far less clear as the storm passes through the basin at daily resolution and blurs the high wind speed centers.

Relative vorticity is used as a feature tracking variable by TRACK, as it focuses on a smaller spatial scale than other fields and is therefore thought to be a better indicator of tropical vorticies. As an additional verification of the algorithm, Figure 10 shows the mean vorticity averaged over 850, 700, and 600 hPa. In the early frames of the animation, it is possible to see an area of low pressure forming at the beginning of the area where the tropical storm track was calculated, rotating, and following the same storm track path with much greater clarity than as shown by near surface wind speeds in Figure 8 and 9. This indicates visual confirmaton that TC-like conditions can be found in model output for the same (similar) areas where tropical storm tracks have been calculated.

As a result of the confirmation of TC-like conditions in near-surface winds and mean vorticity for the same time periods as the *TRACK* algorithm calculated tropical storms, this study then

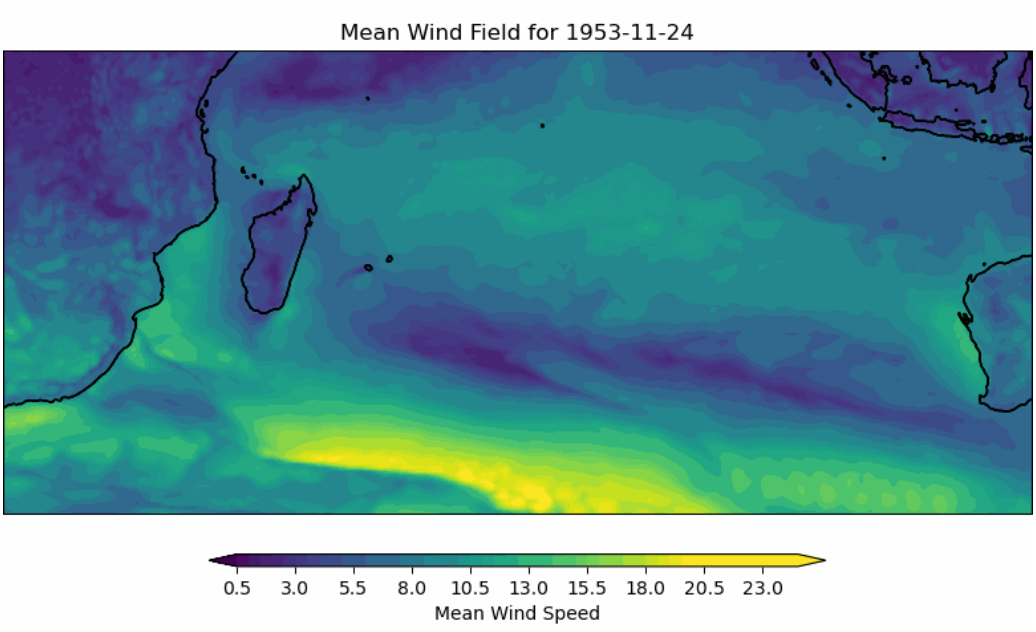

Figure 9: **Wind Field of Example Storm - Max Daily Values** Max daily wind speed values displayed as an animation for the SWIO wind field. Time steps are set as the same time as the calculated example storm in Figure 5 and wind speeds are shown in m/s. Note that in print form, animation will display only the first day. Additional note, Figure should read 'Max Wind Field and Max Wind Speed" instead of mean.

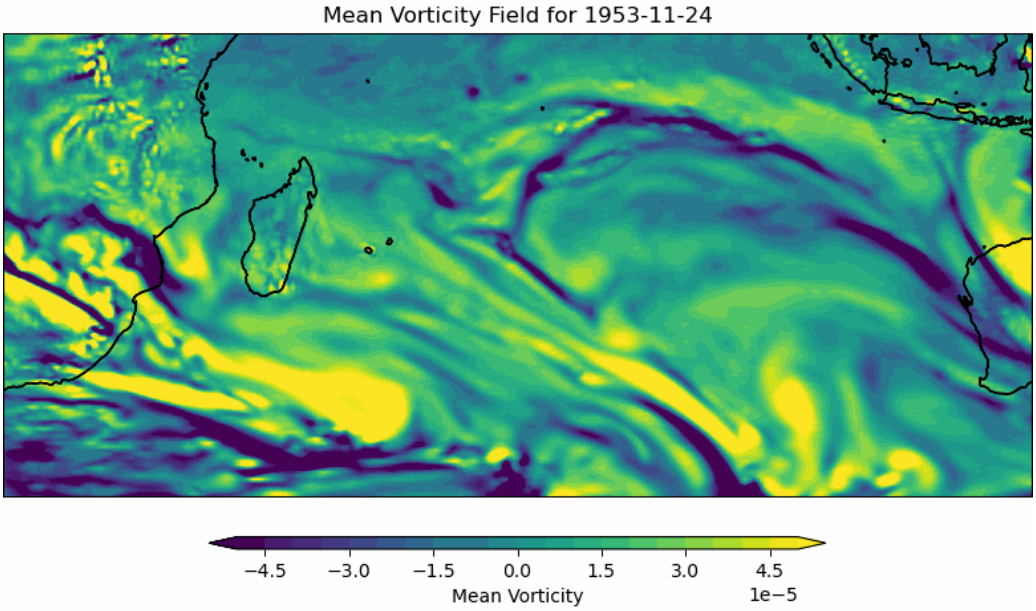

Figure 10: **Mean Vorticity Field of Example Storm** Mean vorticity over 850, 700, and 600 hPa displayed as an animation for the SWIO. Time steps are set as the same time as the calculated example storm in Figure 5 and vorticity is measured in rotations per second. Note that in print form, animation will display only the first day.

assumes that methods for identification of TCs in model output (as outlined in Section 3.2.1) are robust enough for analysis.

4.2 Tropical Cyclone Track Analysis

The following section presents the results of applying the linear regression, percentile and distribution analysis to the calculated TCs for the entire SWIO region for both the control and future simulations compared to the same analysis performed on the observed TCs. Note that for all subsequent sections, distribution analysis plots include observational TC data, as well as results from the control and future simulations, with kernel density estimate (KDE) smoothing. Note that for linear regression and percentile analysis, the control and future simulations are plotted on the same axes and delimited with a vertical dashed line to indicate the continuation of time between the two simulations, as the control simulation includes the 1980/1981 TC season through the 2014/2015 TC season, while the future simulation includes the 2015/2016 season through the 2049/2050 season. Shaded areas around the linear fits in the linear regression analysis represent the a 95% confidence interval of the regression fit calculated as the mean coefficients of the sample plus or minus the t-score multiplied by standard error multiplied by the mean coefficients of the sample. Table 4.1 outlines the number of TCs utilized in this study for the different analysis and across observations, as well as model simulations.

	Observations	*Control-1950* Simulation	*Highres-Future* Simulation
All TCs in the SWIO	359	397	292
Near Land TCs	140	115	68
Landfall TCs	94	169	122

Table 4.1: The resulting count of TCs in observation, as well as the two model simulations for all basin, TCs near land, and TCs that make landfall.

4.2.1 All Basin

The analysis in this subsection includes all TCs that have the maximum sustained wind speeds present within the previously defined boundaries of the SWIO basin, irregardless of where the TC track begins or ends.
Figure 11 shows the distribution of the frequency TCs occur over time (in each TC season). The observed TCs show a normal distribution, with a peak between 10 and 12 TCs per season. The control simulation shows a much flatter curve, with a slight peak around 13 TCs per TCs season. This peak at a slightly greater frequency can be indicative of either more TC-like conditions being produced in the model simulations compared to observations, or that what has been identified as a TC following the methods in Section 3.2.1 might not have been a TC if the same conditions were to have occurred in observation. Both interpretations are likely in this instance. The future simulation has a higher peak than both the observations and control simulation, between 8 and 10 TCs per TC season. This can be interpreted as an indication that in a warmer climate, there will be fewer TCs occurring in each season than are currently observed. The statistical significance of these three distributions as described in Section 3.2.3 confirms with a p-value of 2.6606e-05 that the distributions represented by the three histograms are significantly different across all TCs in the SWIO basin.

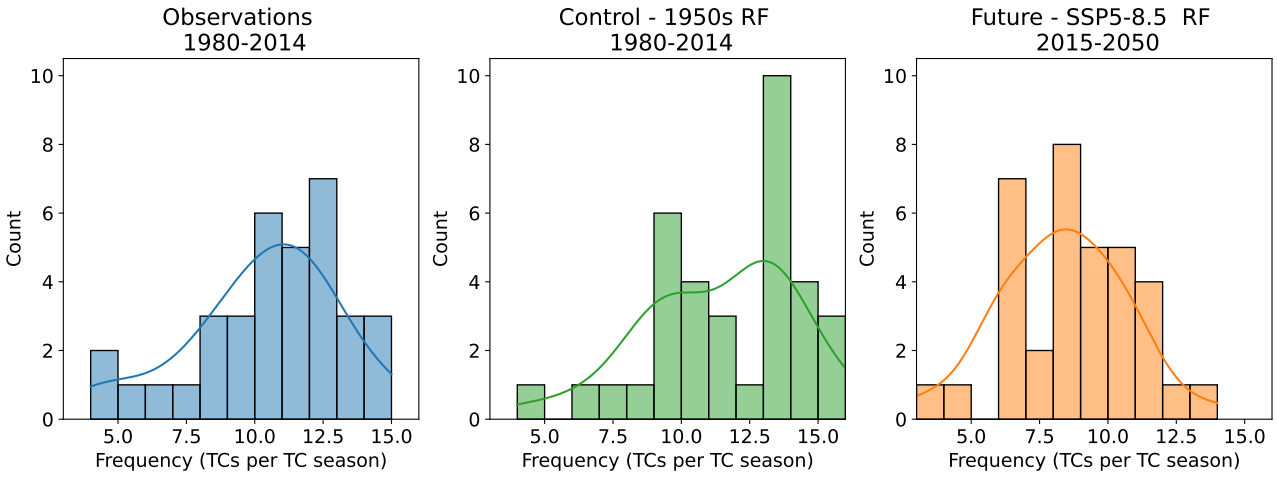

Figure 11: **Distribution of TC Frequency in the SWIO Basin** (Left) Frequency of TCs observed TCs. (Center) Frequency of TCs in the control simulation with 1950s radiative forcing. (Right) Frequency of TCs in the future simulation forced with SSP5-8.5. Kruskal-Wallis p-value of 2.6606e-05.

Figure 12 shows the distribution of intensity (measured in maximum sustained wind speeds; m/s) for each TC. Here it can be noted that the observed intensities have a somewhat flat distribution, with a slight plateau at lower intensities between 20 and 30 m/s. The observed intensities have tails extending well in both directions, representing the full range of very weak TCs to TCs with the highest intensities. In the control and future simulations, a high peak at between 20 and 30 m/s and a lack of intensity greater than around 50 m/s is shown. The lack of tails extending to intensities greater than 50 m/s in both the control and future simulations is attributed to the limit given by the model resolution. With a horizontal resolution of 50 km, the GCM used in this study does not have a high enough resolution to detect more intense storms than what is shown. The statistical significance of these intensity distributions confirms with a p-value of 2.6579e-22 that the intensities greatly vary between observations and the control and future scenarios.
Figure 13 shows the distribution of the duration (in days) of each TC. The observed duration of TCs show a high peak of TCs that last around 10 days, with very few TCs surviving for longer

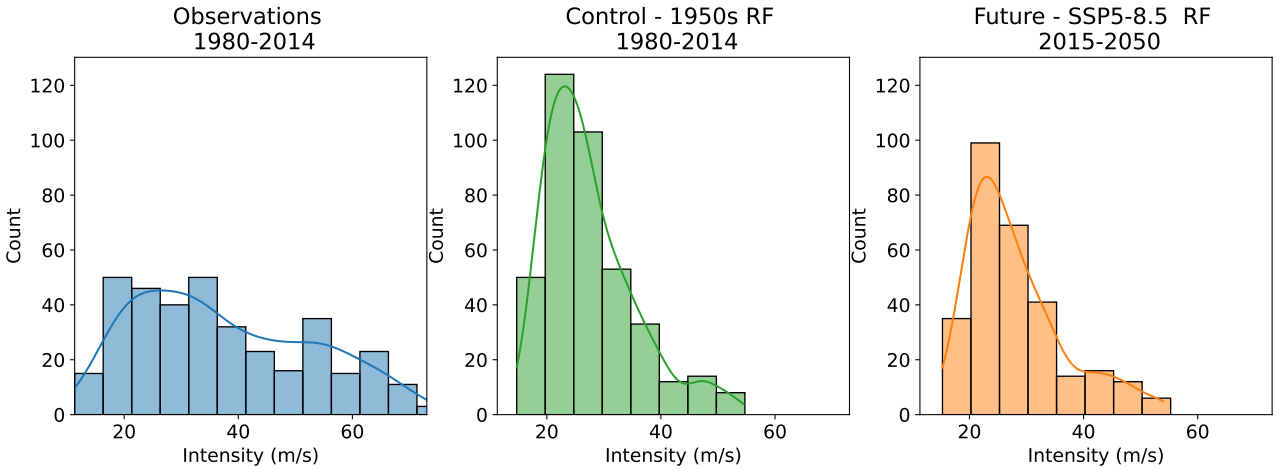

Figure 12: **Distribution of TCs Intensity** (Left) Intensity (max sustained wind in m/s) of observed TCs. (Center) Intensity of TCs in the control simulation with 1950s radiative forcing. (Right) Intensity of TCs in the future simulation forced with SSP5-8.5. Kruskal-Wallis p-value of 2.6579e-22.

than 20 days. The control and future simulations, however, show a much flatter distribution than observations. The control simulation has a slight peak from 15-25 days, with a much longer tail extending past 40 days. The peak in the future simulation is flatter still, with a similar extended tail. The control and future simulation distributions indicate that there is perhaps not a great enough weight on factors that would cause a TC in observation to dissipate, such as traveling too close or too far from the equator and transitioning into an extratropical or subtropical storm. This distinction between TC dissipation and extratropical and subtropical transition was not made by the identification method as outlined in Section 3.2.1, and therefore could account for the extended duration shown in the simulations. The statistical significance confirms with a p-value of 8.9581e-84 that these distributions are indeed significantly different.

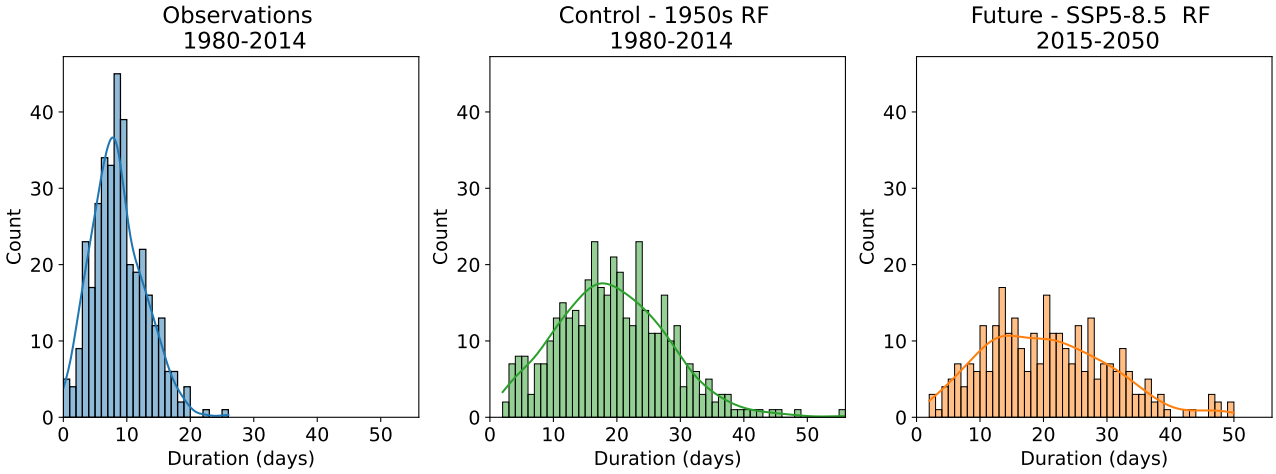

Figure 13: **Distribution of the Duration of TCs** (Left) Duration of observed TCs. (Center) Duration of TCs in the control simulation with 1950s radiative forcing. (Right) Duration of TCs in the future simulation forced with SSP5-8.5. Kruskal-Wallis p-value of 8.9581e-84.

The question of if the more intense TCs have a greater duration can also be asked, and Figure 14 shows the distribution of duration of TCs greater than 35 m/s. The observations show a high peak of TCs surviving less than 15 days and not exceeding 25 days, while both the control

and future simulations show a similar, flattened curve with a slight peak around the tail of the observations. The control and future simulations indicate that (similarly to Figure 13 in the model scenarios the accounting for transition to an extratropical or subtropical and subsequent definition of a TC and a beginning of either of these types of storms is necessary to more accurately reflect observations.

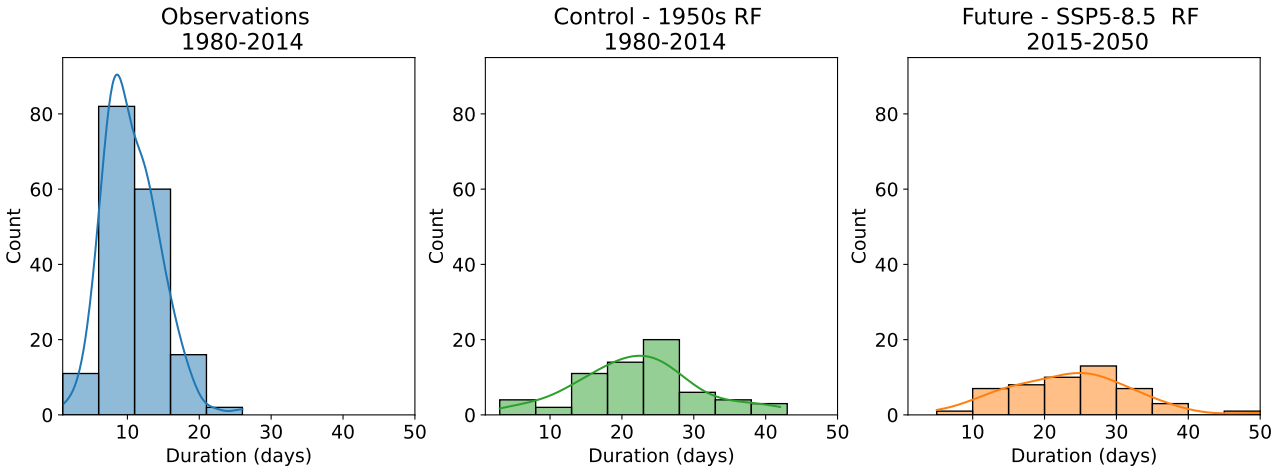

Figure 14: **Distribution of the Duration of TCs with Sustained Wind Speeds $>$ 35 m/s** (Left) Duration of observed TCs. (Center) Duration of TCs in the control simulation with 1950s radiative forcing. (Right) Duration of TCs in the future simulation forced with SSP5-8.5. Kruskal-Wallis p-value 7.5912e-31.

Figure 15 shows a linear regression fit of the observed frequency of TCs per TC season. The observational data shows a very weak positive if not negligible relationship between time and the number of storms, suggesting that the a warming climate over time does not have a significant impact on how frequently TCs occur. The control simulation regression fit is very similar to the observations, with a very weak negative (if not negligible) relationship, suggesting time does not have any significant impact on the number of storms in a TC season. Under a warmer climate in the future simulation, the regression fit shows a weak negative linear relationship between time and the number of TCs in a TC season. Figure 15 can be interpreted to represent very low if not negligible changes in the number of TCs occurring in the SWIO, rather even a slight decrease in the future number of storms in each season under a warmer climate.
Figure 16 shows a linear regression fit of duration of each TC per TC season. The observational data shows a weak positive linear relationship between time and the duration of individual TCs, indicating that as the climate warms the duration of TCs have been slightly increasing. The p-value of 0.0002 indicates that this is statistically significant, and supports the presence of some correlation between a warmer climate and an increased duration of TCs. The control and future simulations, however, show weaker positive (if not negligible) relationships with low statistical significance. This indicates that although there is some observational evidence to suggest an increase in duration with a warmer climate, this is not reflected in the model simulations.
It can therefore be asked if broader duration categories (short-lasting storms and long-lasting storms) show any differences than the regression in Figure 16. Figure 17 shows 5-year running mean of the 25th, 50th (median) and 75th percentiles of the duration values. The observational percentiles closely follow the shape of the regression in Figure 16, and do not show a great difference between the upper (75th) and lower (25th) percentiles to indicate there is a difference between the longer lasting and shorter lasting TCs as the climate warms. The control and future simulation percentiles show greater variation from one another, similarly to observations do not show enough of a spread to indicate that there is a difference between longer lasting and shorter lasting TCs as the climate warms.

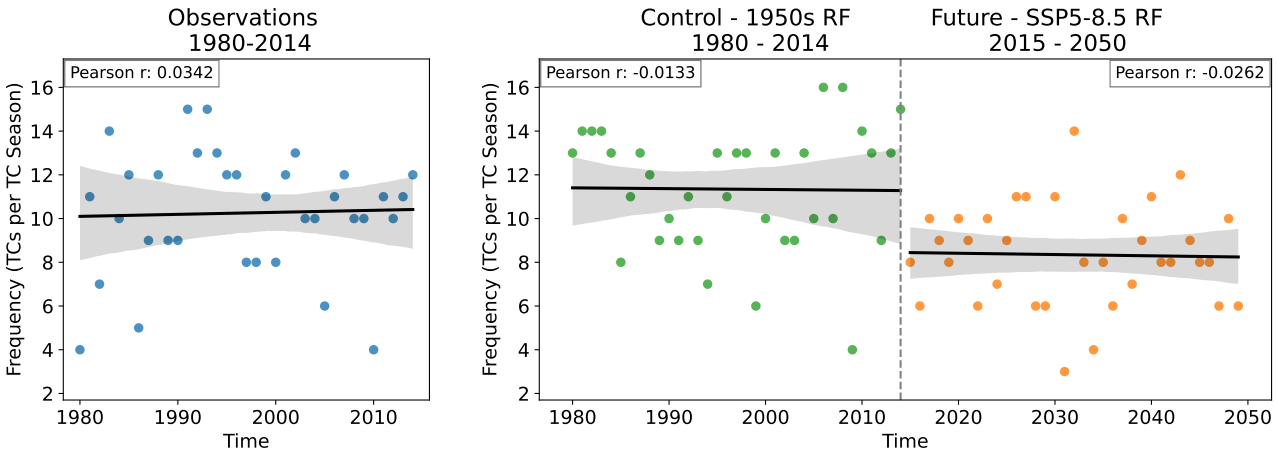

Figure 15: **Regression of the Frequency of TCs per TC Season** (Left) Linear regression of observed frequency of TCs in each TC season across the SWIO basin, each point representing an individual season. (Right) Linear regression of TCs in each TC season in the control simulation with 1950s radiative forcing and the future simulation forced with SSP5-8.5.

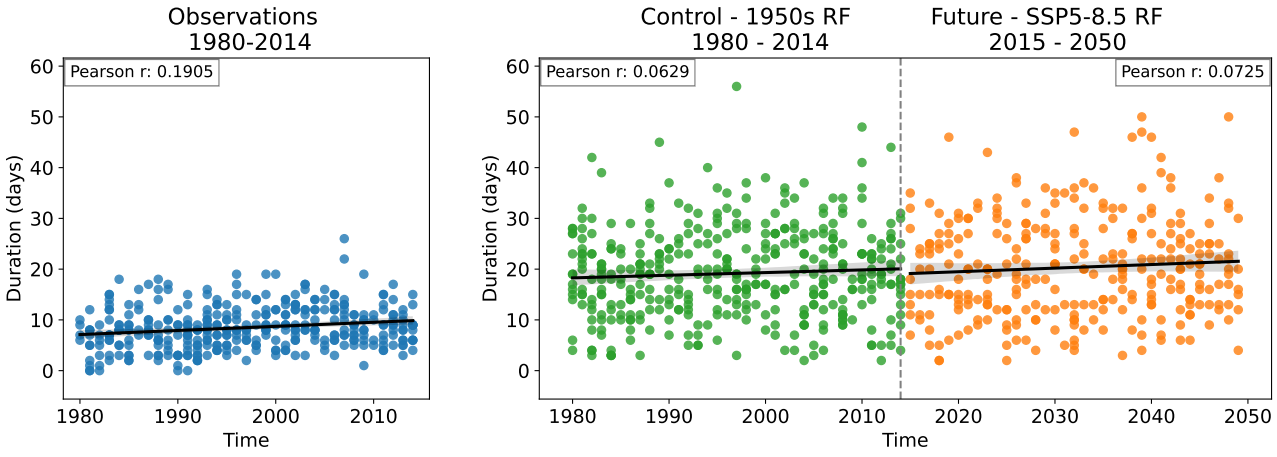

Figure 16: **Regression of the Duration of TCs** (Left) Linear regression of observed duration of TCs in each TC season across the SWIO basin, each point representing an individual TC. (Right) Linear regression of TC duration in each TC season in the control simulation with 1950s radiative forcing and the future simulation forced with SSP5-8.5.

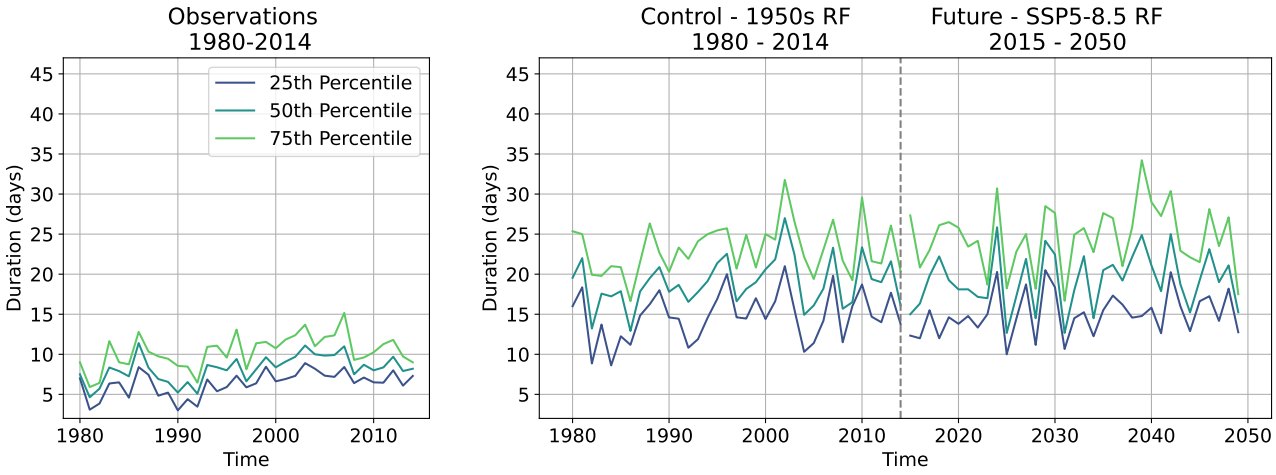

Figure 17: **Percentile 5-Year Running Mean of TC Duration** (Left) 5-year running mean of the 25th, 50th and 75th percentile of the duration of observed TCs in the SWIO. (Right) 5-year running mean of the 25th, 50th and 75th percentile of the control simulation with 1950s radiative forcing and the future simulation forced by SSP5-8.5. Control and future simulations are delimited with a vertical dashed line.

Figure 18 shows a linear regression fit of intensity of each TC per season measured in sustained wind speeds (m/s). The observed TCs show a weak positive linear relationship between the season and the intensity of individual TCs , indicating that as time passes and therefore the climate warms, the intensity of TCs have been slightly increasing. The p-value of 0.0002 indicates that this is statistically significant, and supports the presence of some correlation between a warming climate and an increased intensity of TCs. Both the control and future simulations show a negligible relationship between intensity and time, with low statistical significance, indicating almost no relationship between the season and the intensity of the TCs. The discrepancy between the observations and the control and future simulations could be in part due to the model's limited horizontal resolution, which prohibits the model from identifying the most intense TCs as the would be in observation. With the inclusion of higher intensity TCs in the control and future simulations, this might result in trends more similar to the observed TC intensities.

Similarly to the duration results, it can also therefore be asked if the broader intensity categories (low intensity and high intensity TCs) show any differences than the regression in Figure 18. Figure 19 shows 5-year running mean of the 25th, 50th (median) and 75th percentiles of the duration values. The observational percentile running means reflect the shift in maximum wind speeds seen in Figure 18, with gradual increases in all three percentiles. The control and future simulations do not display any noticeable shifts in the the percentiles as the climate warms, therefore indicating that there is no considerable difference in the relationship between a warmer climate and the intensity of storms as shown in the model.

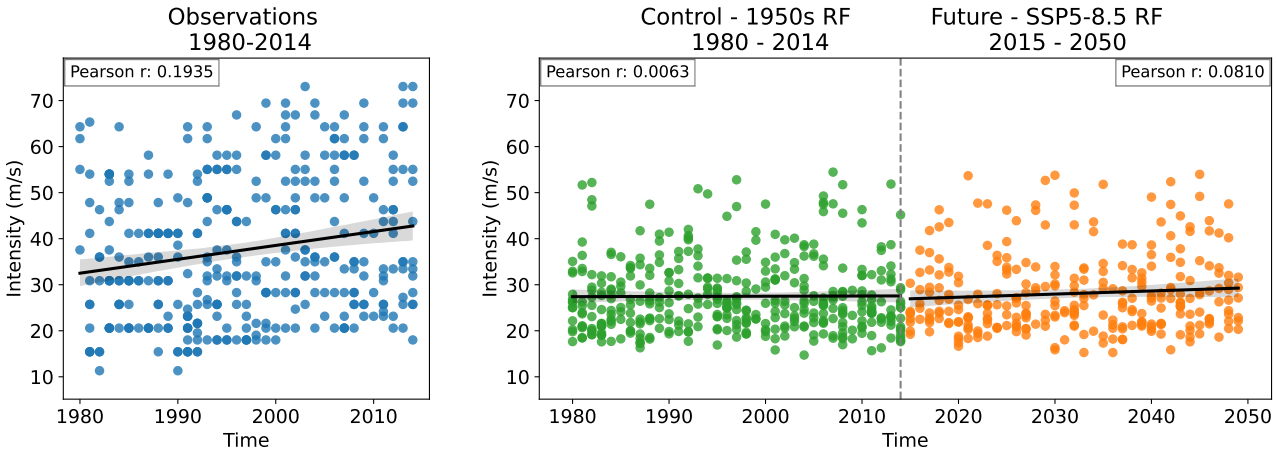

Figure 18: **Regression of the Intensity of TCs** (Left) Linear regression of observed maximum intensity (measured in max sustained wind speeds in m/s) of TCs in each TC season across the SWIO basin, each point representing an individual TC. (Right) Linear regression of TC intensity in each TC season in the control simulation with 1950s radiative forcing and the future simulation forced with SSP5-8.5.

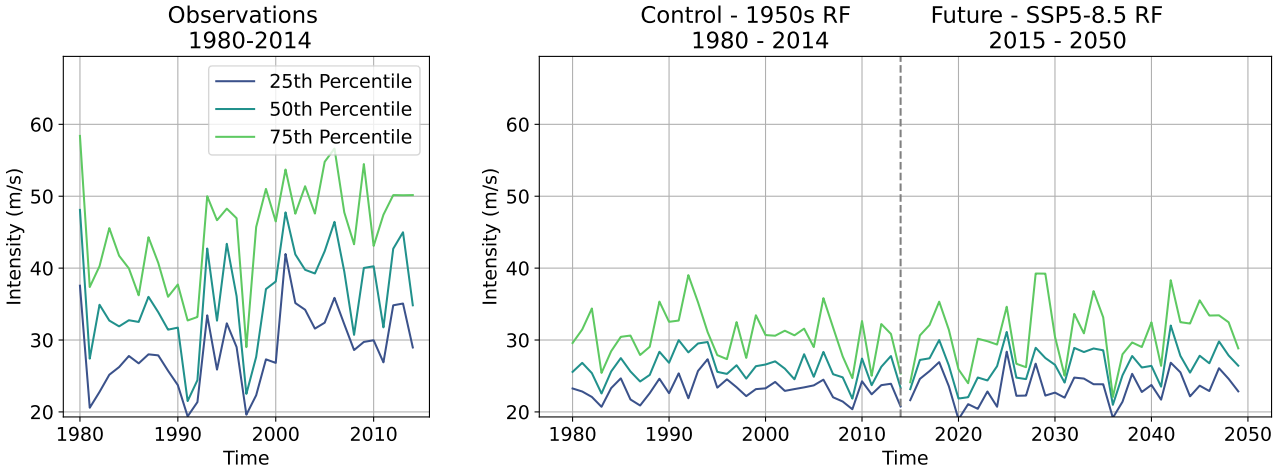

Figure 19: **Percentile 5-Year Running Mean of TC Intensity** (Left) 5-year running mean of the 25th, 50th and 75th percentile of the max intensity of observed TCs in the SWIO. (Right) 5-year running mean of the 25th, 50th and 75th percentile of the control simulation with 1950s radiative forcing and the future simulation forced by SSP5-8.5. Control and future simulations are delimited with a vertical dashed line.

4.2.2 Near-Land

The analysis in this subsection includes all TCs that have the maximum sustained wind speeds present within the previously defined boundaries of the SWIO basin, irregardless of where the TC track begins or ends, as well as an additional criteria that the TC track must pass near land, as defined in Section 3.2.4. From the values shown in Table 4.1 alone, it seems that the control simulation identifies more TCs passing near land than observations would indicate, with a greater proportion of them passing near land than both the observed TCs and the future simulation TCs. The future simulation has a comparable number of identified TCs to the observed TCs, but still with a higher proportion of those TCs passing near land than is observed.
Figure 20 shows the distribution of the frequency of TCs in each TC season that pass near land. The observational TCs show first a slight plateau around 2 TCs per season, with a peak between 4 and 6 TCs per season. It is also notable that there is no season with greater than 10 TCs passing near land. The control simulation shows a peak around 2 TCs per season, with a plateau around 5 TCs per season. The future simulation shows one distinct peak at 2 TCs per season, with no frequency extending past 4 TCs per TC season. These distributions can be indicative of more TCs being identified as passing near land in the model simulations (particularly in the control simulation) compared to observations. Additionally, similarly to Section 4.2.1 what has been identified as a TC following the methods in Section 3.2.1 might not have been a TC if the same conditions were to have occurred in observation, and therefore too many TCs might be considered. Both interpretations are likely in this instance. The statistical significance of these three distributions as described in 3.2.3 confirms with a p-value of 1.2799e-05 that the distributions represented by the three histograms are significantly different across the TCs that pass near land in the SWIO basin.

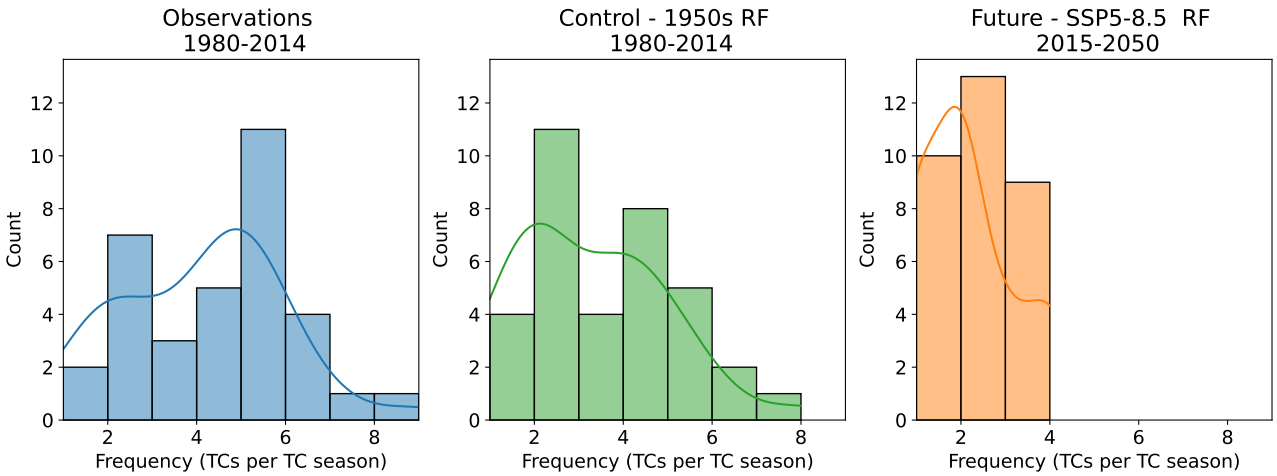

Figure 20: **Distribution of the Frequency of TCs per TC Season Passing Near Land** (Left) Frequency of observed TCs. (Center) Frequency of TCs in the control simulation with 1950s radiative forcing. (Right) Frequency of TCs in the future simulation forced with SSP5-8.5. Kruskal-Wallis p-value of 1.2799e-05.

Figure 21 shows the distribution of intensity (max sustained wind speeds, m/s) for each TC passing near land. Here it can be noted that the observed intensities have a somewhat flat distribution, with a small peak at lower intensities between 20 and 30 m/s. The observed intensities have tails extending well in both directions, representing the full range of very weak TCs to TCs with the highest intensities. In the control and future simulations, a peak between 20 and 30 m/s and a lack of intensity greater than around 55 m/s is shown. The lack of

tails extending to intensities greater than 45 m/s in both the control and future simulations is attributed to the limit given by the model resolution. With a horizontal resolution of 50 km, the GCM used in this study does not have a high enough resolution to detect more intense storms than what is shown. The statistical significance of these intensity distributions confirms with a p-value of 2.6413e-13 that the intensities of storms that pass near land greatly vary between observations and the control and future scenarios.

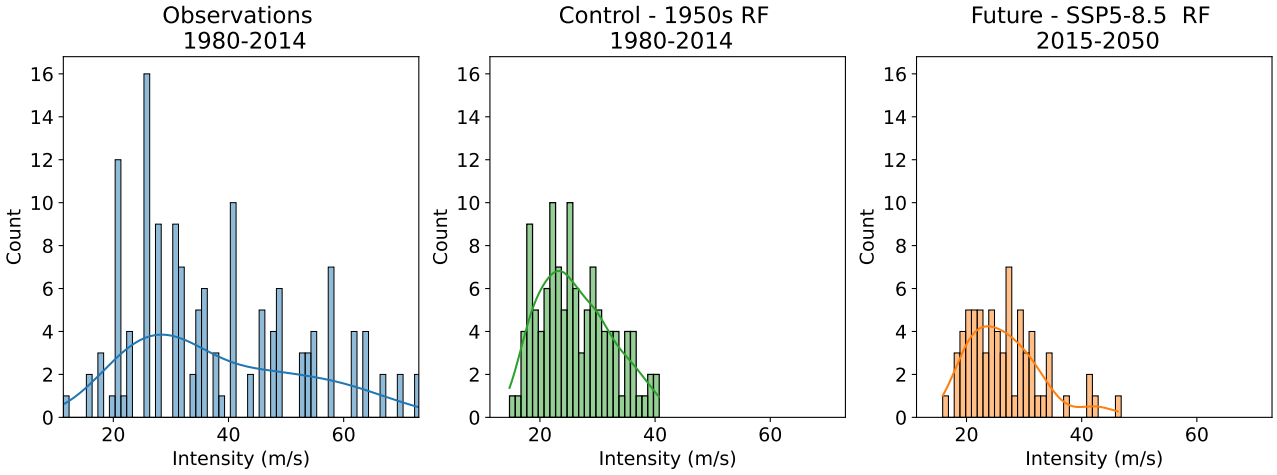

Figure 21: **Distribution of Intensity (max sustained wind) for TCs Passing Near Land** (Left) Intensity (max sustained wind in m/s) of observed TCs. (Center) Intensity of TCs in the control simulation with 1950s radiative forcing. (Right) Intensity of TCs in the future simulation forced with SSP5-8.5. Kruskal-Wallis p-value of 2.6413e-13.

Figure 22 shows the distribution of the duration (in days) of each TC observed passing near land. The observed duration of TCs show a distinct peak of TCs that last around 10 days, with very few TCs surviving for longer than 20 days. The control and future simulations, however, show a much broader distribution than observations. The control simulation has a slight plateau from 15-25 days, with a much longer tail extending past 50 days. The the future simulation is flatter than the control simulation, with no discernible peak but with a similar extended tail. The control and future simulation distributions indicate that there is perhaps not a great enough weight on factors that would cause a TC passing near land in observation to dissipate, such as traveling too close or too far from the equator and transitioning into an extratropical or subtropical storm. This distinction between TC dissipation and extratropical and subtropical transition was not made by the identification method as outlined in Section 3.2.1, and therefore could account for the extended duration shown in the simulations. The statistical significance confirms with a p-value of 6.1057e-30 that these distributions are indeed significantly different.

The question of if the more intense TCs passing near land have a greater duration can also be asked, and Figure 23 shows the distribution of duration of TCs greater than 35 m/s that pass near land. The observations show a high peak of TCs surviving less than 15 days and not exceeding 30 days, while both the control and future simulations show a almost no curve. The control and future simulations indicate that there are very few TCs that pass within 100km of land and also have wind speeds (at some point) of $>$ 35 m/s at all, and therefore no relationship can be discerned. A p-value of 8.3908e-08 confirms that these distributions are significantly different from one another.

Figure 24 shows a linear regression fit of the observed frequency of TCs per TC season that pass near land. The observational data shows a weak negative relationship between time and the number of TCs that come near land, with low statistical significance suggesting that a warming

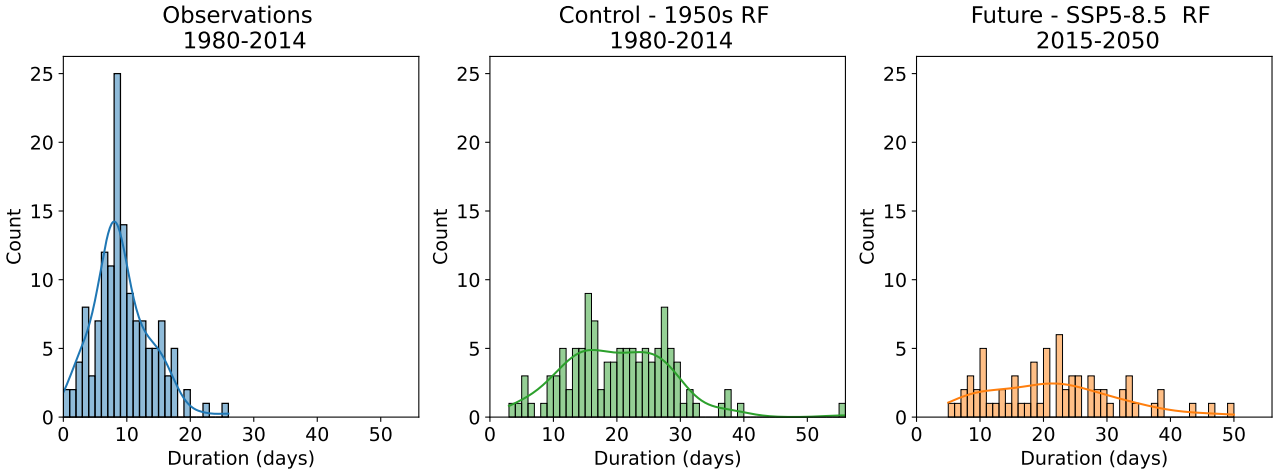

Figure 22: **Distribution of the Duration of TCs Passing Near Land** (Left) Duration of observed TCs. (Center) Duration of TCs in the control simulation with 1950s radiative forcing. (Right) Duration of TCs in the future simulation forced with SSP5-8.5. Kruskal-Wallis p-value of 6.1057e-30.

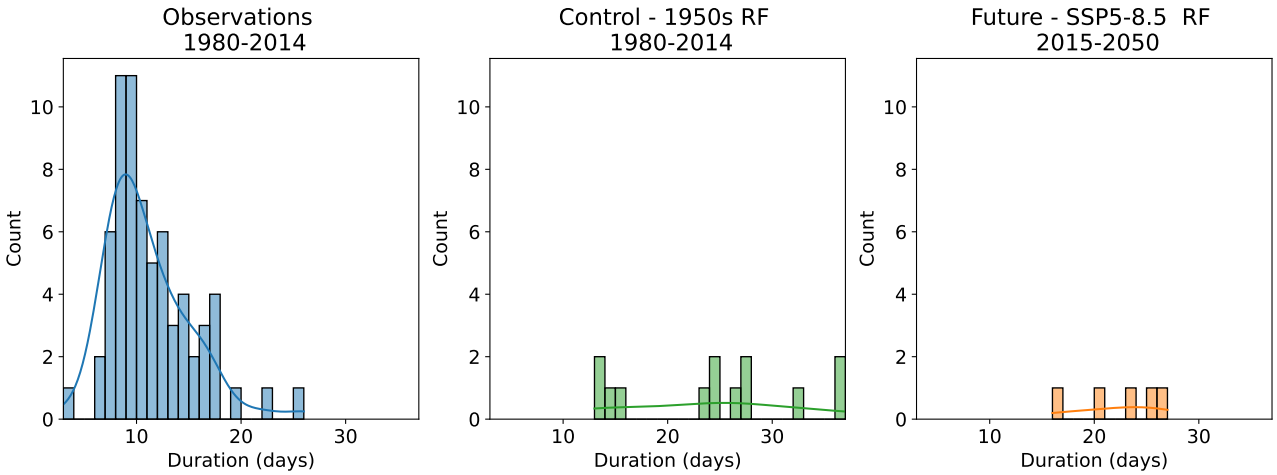

Figure 23: **Distribution of the Duration of TCs with Sustained Wind Speeds $>$ 35 m/s** (Left) Duration of observed TCs. (Center) Duration of TCs in the control simulation with 1950s radiative forcing. (Right) Duration of TCs in the future simulation forced with SSP5-8.5. Kruskal-Wallis p-value of 8.3908e-08.

climate does not have a significant impact on how frequently TCs occur. The control simulation regression fit is similar to the observations, with a very weak negative (if not negligible) relationship and low statistical significance suggesting time and a warming climate does not have any significant impact on the number of TCs that occur and pass near land. Under a warmer climate in the future simulation, the regression fit shows a stronger negative linear relationship between time and the number of TCs, with a high statistical significance represented by a p-value of 0.0136. Figure 24 can be interpreted to represent very low if not negligible changes in the number of TCs occurring and passing near land in the SWIO in observation, even a slight decrease in the the observed numbers, with some indication that under a warmer climate (such as that of SSP5-8.5), there will be fewer TCs passing near land.

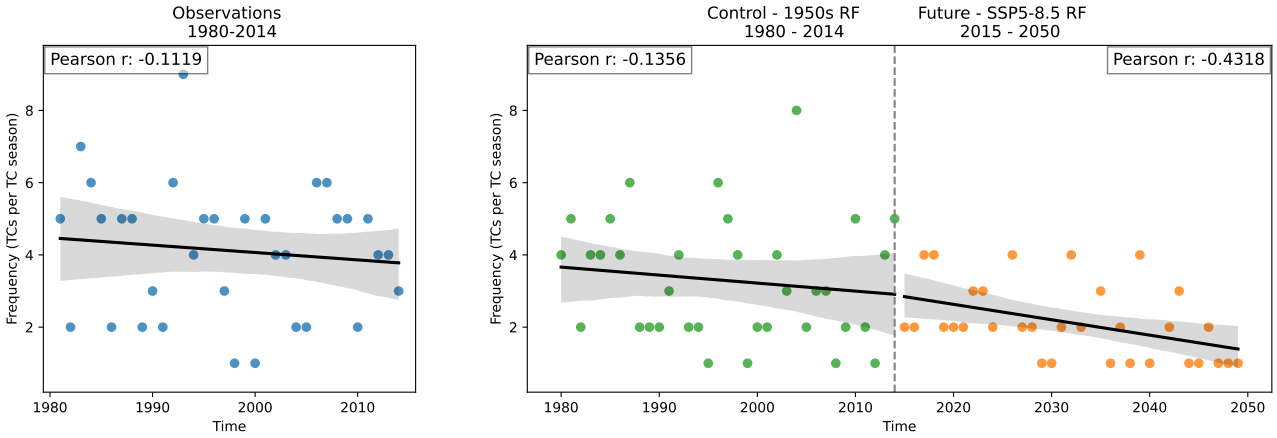

Figure 24: **Regression of the Frequency of TCs per TC Season Passing Near Land** (Left) Linear regression of observed frequency of TCs in each TC season that pass near land. Each point represents an individual TC season. (Right) Linear regression of the frequency of TCs in each TC season that pass near land in the control simulation with 1950s radiative forcing and the future simulation forced with SSP5-8.5.

Figure 25 shows a linear regression fit of duration of each TC per season. The observational data shows a weak positive linear relationship with high confidence between time and the duration of individual TCs, indicating that as time passes (and therefore the climate warms) the duration of TCs passing near land have been gradually increasing. The p-value of 0.0018 indicates that this correlation coefficient is statistically significant, and supports the presence of some correlation between a warmer climate and an increased duration of the TCs passing near land. The control and future simulations, however, show weaker positive relationships and with a low statistical significance. This indicates that although there is some observational evidence to suggest an increase in duration with a warmer climate, this is not reflected in the model simulations.
It can therefore be asked if the broader duration categories (short-lasting storms and long-lasting storms) show any differences compared to the regression in Figure 25. Figure 26 shows 5-year running mean of the 25th, 50th (median) and 75th percentiles of the duration values of each TC. The observational percentiles closely follow the shape of the regression in Figure 16, with the 25th percentile consistently low while the 50th and 75th percentiles fluctuate slightly more, indicating that the longer lasting storms passing near land could be lasting slightly longer as the climate warms. The control and future simulation percentiles show greater variation from one another, but do not show consistent deviation to indicate a difference between the upper (75th) and lower (25th) percentiles to indicate that there is a difference between longer lasting and shorter lasting TCs that pass near land as the climate warms.
Figure 27 shows a linear regression fit of intensity of each TC per TC season that passes near land. The observed TCs shows a weak positive linear relationship between the season and the

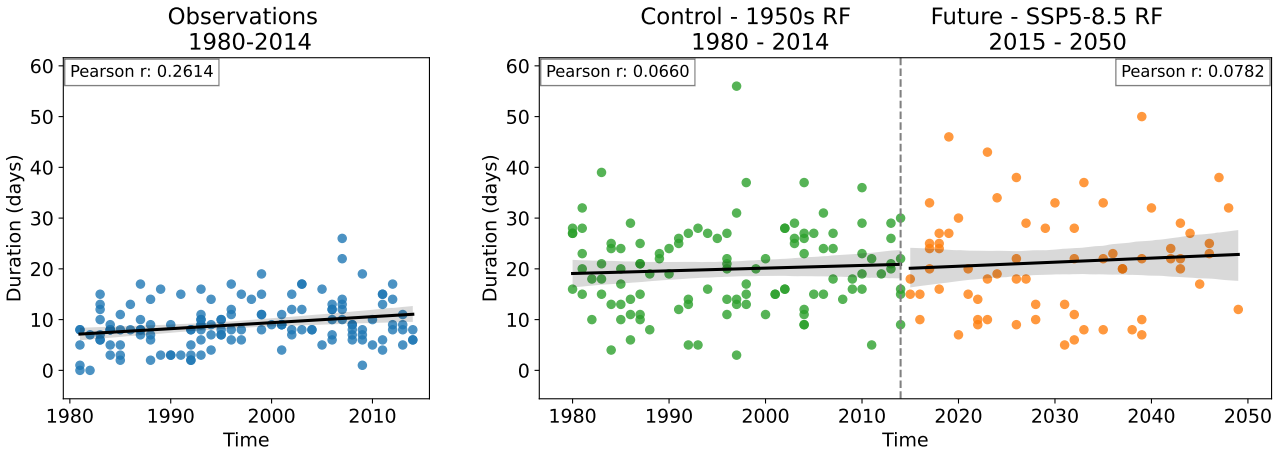

Figure 25: **Regression of the Duration of TCs Passing Near Land** (Left) Linear regression of observed duration of TCs passing near land in each TC season. Each point represents an individual TC. (Right) Linear regression of TC duration in each TC season in the control simulation with 1950s radiative forcing and the future simulation forced with SSP5-8.5.

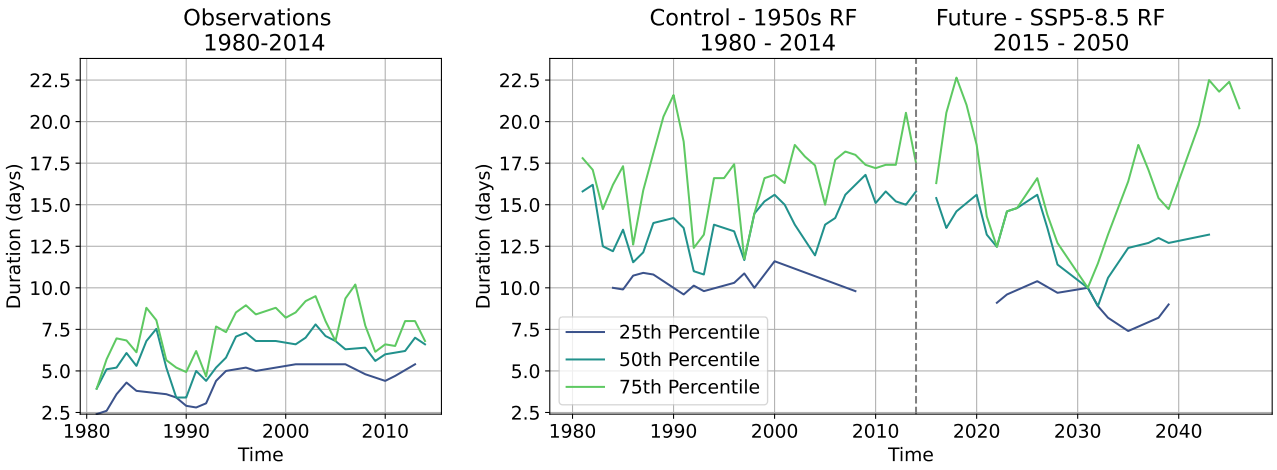

Figure 26: **Percentile 5-Year Running Mean of TC Duration - Near Land** (Left) 5-year running mean of the 25th, 50th, and 75th percentile of the duration of observed TCs passing near land. (Right) 5-year runing mean of the 25th, 50th, and 75th percentile of the control simulation with 1950s radiative forcing and the future simulation forced by SSP5-8.5. Control and future simulations are delimited with a vertical dashed line.

intensity of individual TCs, indicating that as time passes (and therefore the climate warms) the intensity of TCs have been slightly increasing. The p-value of 0.0085 indicates that this correlation coefficient is statistically significant, and supports the presence of some correlation between a warmer climate and an increased intensity of TCs. The control simulation shows a negligible trend, with a low statistical significance, indicating almost no relationship between the season and the intensity of the TCs. The future simulation shows a negligible relationship between time and the intensity of TCs passing near land, with low statistical significance. The discrepancy between the observations and the control and future simulations could be in part due to the model's limited horizontal resolution, which prohibits the model from identifying the most intense TCs. With the inclusion of higher intensity TCs in the control and future simulations, this might result in trends more similar to the observed TC intensities.

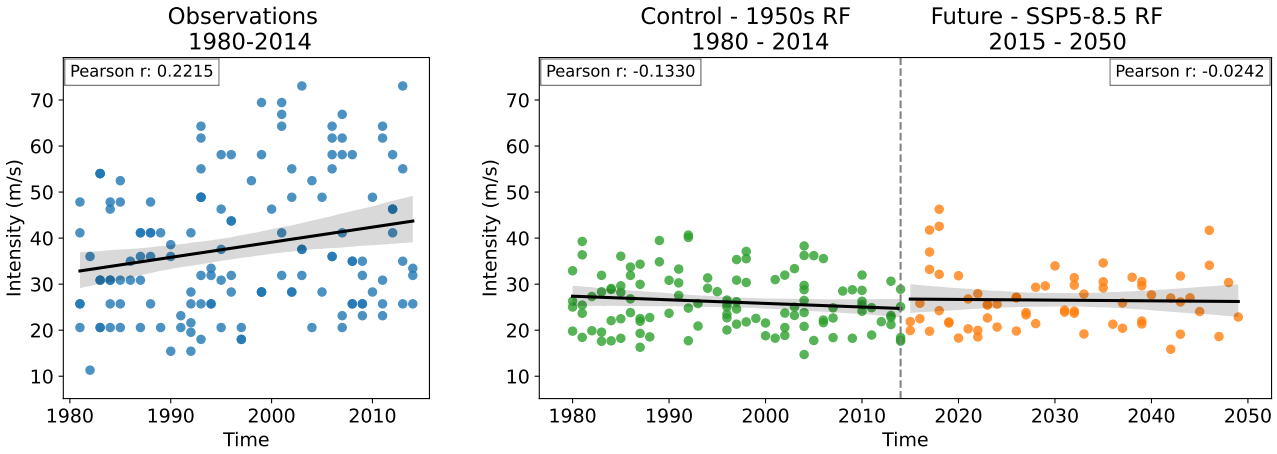

Figure 27: **Regression of the Intensity of TCs Passing Near Land** (Left) Linear regression of observed maximum intensity (measured in max sustained wind speeds in m/s) of TCs in each TC season that pass near land. Each point represents an individual TC. (Right) Linear regression of TC maximum intensity in each TC season for storms passing near land in the control simulation with 1950s radiative forcing and the future simulation forced with SSP5-8.5.

Similarly to the duration results, it can also therefore be asked if the broader intensity categories (low intensity and high intensity TCs) show any differences than the regression in Figure 27. Figure 28 shows 5-year running mean of the 25th, 50th (median) and 75th percentiles of the intensity values of each TC. The observational percentiles vary greatly with the shape of the data shown Figure 16, particularly with the 75th percentile (more intense TCs) while the 50th and 75th percentiles fluctuate slightly less, indicating that the more intense TCs passing near land could be becoming more intense as the climate warms. The control and future simulation percentiles show less variation from one another and do not show great deviation to indicate a difference between the upper (75th) and lower (25th) percentiles to indicate that there is a difference between more and less intense TCs that pass near land as the climate warms.

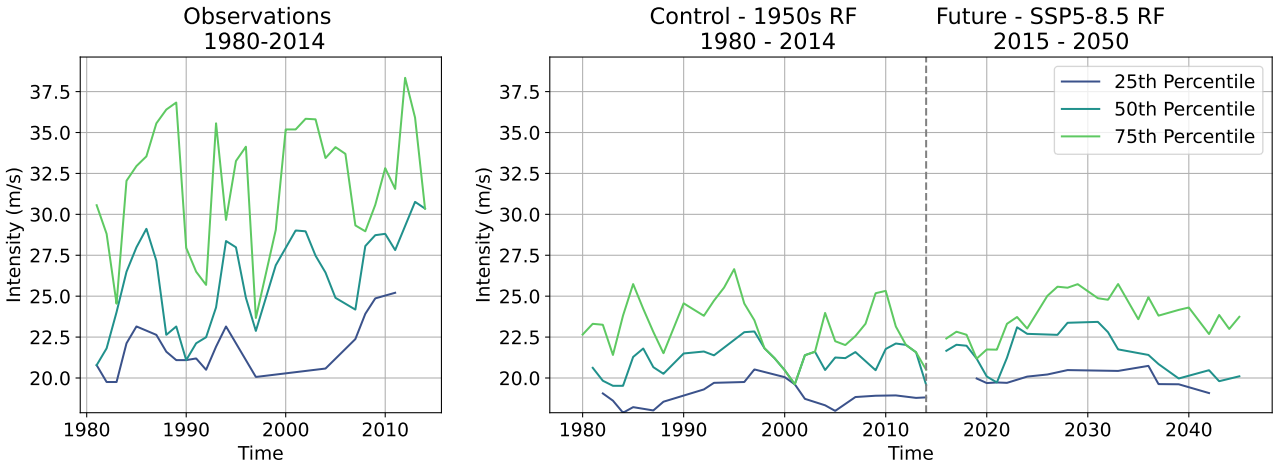

Figure 28: **Percentile 5-Year Running Mean of TC Intensity Near Land** (Left) 5-year running means of the 25th, 50th and 75th percentile of the max intensity of observed TCs passing near land. (Right) 5-year running means of the 25th, 50th, and 75th percentiles of the control simulation with 1950s radiative forcing and the future simulation forced by SSP5-8.5. Control and future simulations are delimited with a vertical dashed line.

4.2.3 Landfall

The analysis in this subsection includes all TCs that have the maximum sustained wind speeds present within the previously defined boundaries of the SWIO basin, irregardless of where the TC track begins or ends, as well as an additional criteria that the TC track must make landfall, as defined in Section 3.2.4. From the values as presented in Table 4.1 alone, it seems that the control simulation identifies significantly more TCs than observations would indicate as making landfall, with a greater proportion of them passing making landfall than both the observed TCs and the future simulation TCs. The future simulation has a comparable number of identified TCs to the observed TCs, but still notably higher.

Figure 29 shows the distribution of the frequency of TCs in each TC season that make landfall. The observational TCs show first a slight plateau at fewer than 2 TCs per season making landfall, with peak around 4 TCs per TC season making landfall. It is also notable that observations show no greater than 6 TCs making landfall in a TC season. The control simulation shows a flattened and curve with a high plateau between 3 and 6 TCs making landfall in each season. The future simulation shows a peak between 3 and 4 TCs making landfall per season. These distributions can be indicative of either more TCs being identified as making landfall in the model simulations (particularly in the control simulation) compared to observations. Additionally, similarly to Section 4.2.1 what has been identified as a TC following the methods in Section 3.2.1 might not have been a TC if the same conditions were to have occurred in observation, and therefore too many TCs might be considered in the model simulations. Both interpretations are likely in this instance. The statistical significance of these three distributions as described in Section 3.2.3 confirms with a p-value of 0.0005 that the distributions represented by the three histograms are significantly different across the TCs that make landfall in the SWIO basin. Although it is worth noting, that these distributions are the most statistically significant of all distributions presented in this section.

Figure 30 shows the distribution of intensity (maximum sustained wind speeds in m/s) for each TC that makes landfall. Here it can be noted that the observed intensities have a somewhat flat distribution, with no discernible peak. The observed intensities have tails extending well in both directions, representing the full range of very weak TCs to TCs with the highest

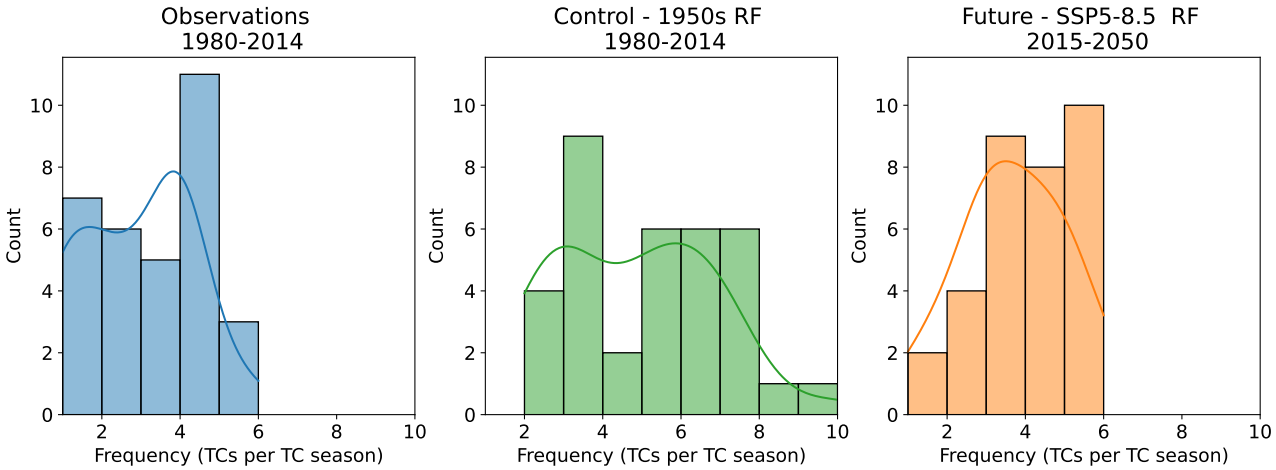

Figure 29: **Distribution of the Frequency of Landfall TCs per TC Season in the SWIO** (Left) Frequency of observed landfall TCs. (Center) Frequency of TCs in the control simulation with 1950s radiative forcing. (Right) Frequency of TCs in the future simulation forced with SSP5-8.5. Kruskal-Wallis p-value of 0.0005.

intensities. In the control and future simulations, a high peak between 20 and 30 m/s and a lack of intensity greater than around 55 m/s is shown. The lack of tails extending to intensities greater than 55 m/s in both the control and future simulations is attributed to the limit given by the model resolution. With a horizontal resolution of 50 km, the GCM used in this study does not have a high enough resolution to detect more intense TCs than what is shown. The statistical significance of these intensity distributions confirms with a p-value of 1.2178e-12 that the intensities of TCs that make landfall greatly vary between observations and the control and future scenarios.

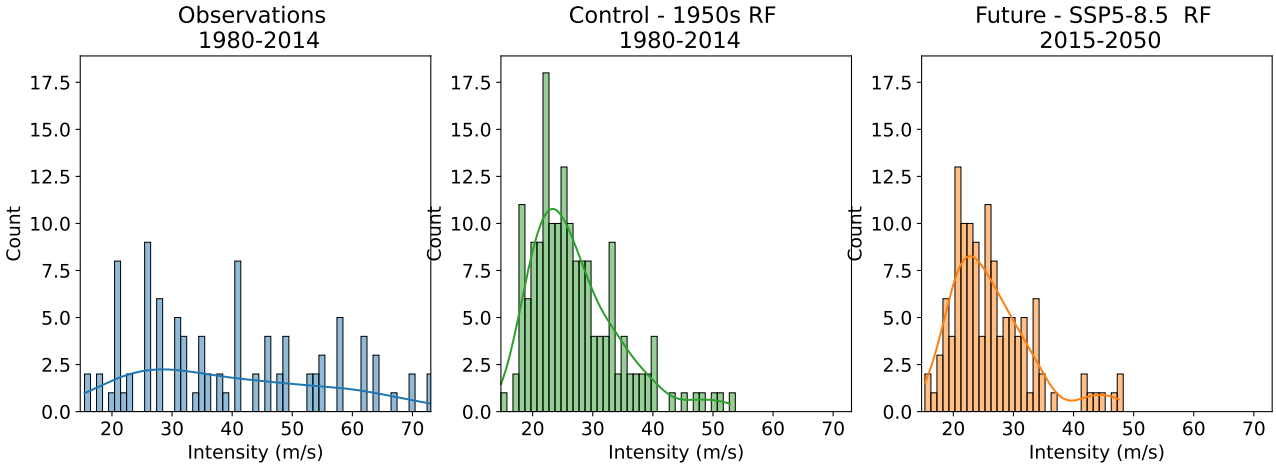

Figure 30: **Distribution of Intensity for TCs Making Landfall** (Left) Intensity (max sustained wind in m/s) of observed TCs. (Center) Intensity of TCs in the control simulation with 1950s radiative forcing. (Right) Intensity of TCs in the future simulation forced with SSP5-8.5. Kruskal-Wallis p-value of 1.2178e-12.

Figure 31 shows the distribution of the duration (in days) of each TC making landfall. The observed duration of TCs show a distinct peak of TCs lasting between around 10 days, with very few TCs surviving for longer than 20 days. The control and future simulations, however, show a much broader distribution than observations. The control simulation has a peak from 15-25 days, with a much longer tail extending past 50 days. The peak in the future simulation

is flatter than the control simulation, extending from 15-30 days with a similar extended but slightly shorter (not exceeding 50 days) tail. The control and future simulation distributions indicate that there is perhaps not a great enough weight on factors that would cause a TC passing near land in observation to dissipate, such as traveling too close or too far from the equator and transitioning into an extratropical or subtropical storm. This distinction between TC dissipation and extratropical and subtropical transition was not made by the identification method as outlined in Section 3.2.1, and therefore could account for the extended duration shown in the simulations. The statistical significance confirms with a p-value of 2.6023e-30 that these distributions are indeed significantly different.

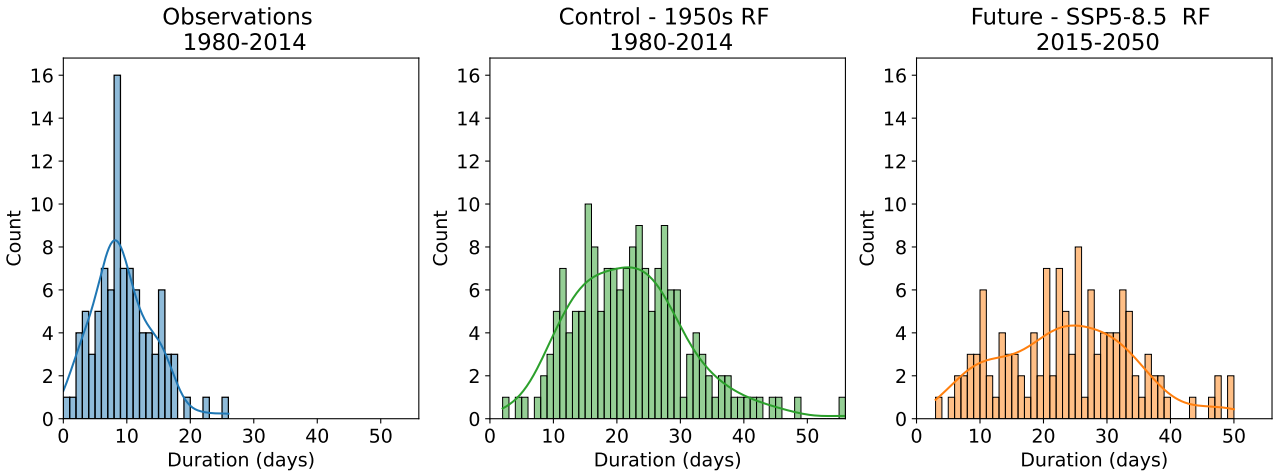

Figure 31: **Distribution of the Duration of TCs Making Landfall** (Left) Duration of observed TCs making landfall. (Center) Duration of TCs in the control simulation with 1950s radiative forcing. (Right) Duration of TCs in the future simulation forced with SSP5-8.5. Kruskal-Wallis p-value of 2.6023e-30.

The question of if the more intense TCs passing near land have a greater duration can also be asked, and Figure 32 shows the distribution of duration of TCs greater than 35 m/s that make landfall. The observations show a high peak of TCs surviving less than 12 days and not exceeding 30 days, while both the control and future simulations show a flattened curve with no discernible peak. The control and future simulations indicate that (similarly to Figure 31) the model scenarios the accounting for transition to an extratropical or subtropical and subsequent difference in definition of a TC and a beginning of either of these types of storms is necessary to more accurately reflect observations. A p-value of 1.4461e-10 confirms the that these distributions are significantly different from one another.

Figure 33 shows a linear regression fit of the frequency of TCs per TC season that make landfall. The observational data shows a weak negative relationship between time and the number of TCs that make landfall, with low statistical significance suggesting that the season does not have a significant impact on how frequently landfall TCs occur. The control simulation regression fit is slightly different to the observations, with a very weak (if not negligible) positive relationship, although with low statistical significance suggesting that time does not have any significant impact on the number of TCs that occur and make landfall. Under a warmer climate in the future simulation, the regression fit shows a weak negative linear relationship between the season and the number of TCs, but also with a low significance. Figure 33 can be interpreted to represent very low if not negligible changes in the number of TCs occurring and make landfall in the SWIO, even a slight decrease in the the observed numbers, although the relationships for observed TCs and both simulations is not significant.

Figure 34 shows a linear regression fit of duration of each TC per season making landfall. The observational data shows a weak positive linear relationship with statistical significance

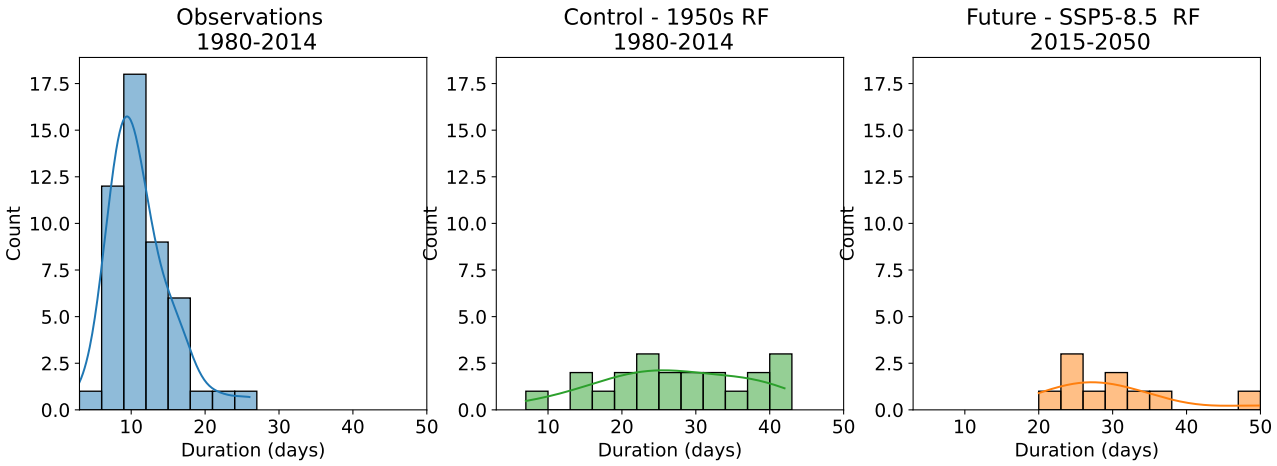

Figure 32: **Distribution of the Duration of TCs Making Landfall with Sustained Wind Speeds $>$ 35 m/s** (Left) Duration of observed TCs making landfall, which at some point in the lifetime had a max sustained wind speed $>$ 35 m/s. (Center) Duration of TCs in the control simulation with 1950s radiative forcing. (Right) Duration of TCs in the future simulation forced with SSP5-8.5. Kruskal-Wallis p-value is 1.4461e-10.

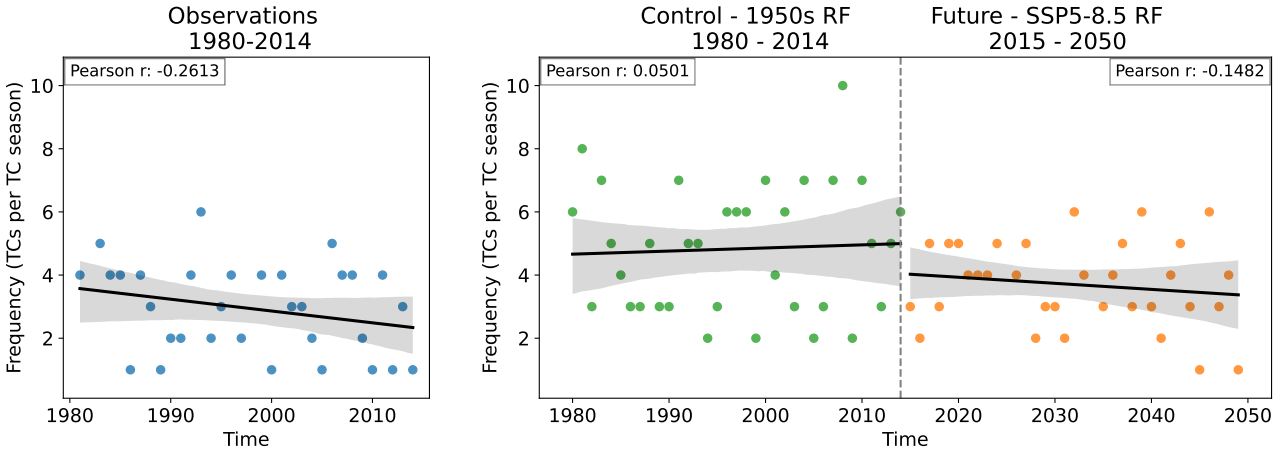

Figure 33: **Regression of the Frequency of TCs per TC Season Making Landfall** (Left) Linear regression of observed frequency of TCs in each TC season that make landfall. Each point represents an individual TC season. (Right) Linear regression of TCs in each TC season that make landfall in the control simulation with 1950s radiative forcing and the future simulation forced with SSP5-8.5.

between time and the duration of individual TCs with a p-value of 0.0105, indicating that as time passes (and therefore the climate warms) the duration of TCs making landfall have been slightly increasing. The control and future simulations, however, show a weaker positive relationships without statistical significance. This indicates that the model simulations do not reflect the same weak positive relationship in duration increasing over time that the observations show.

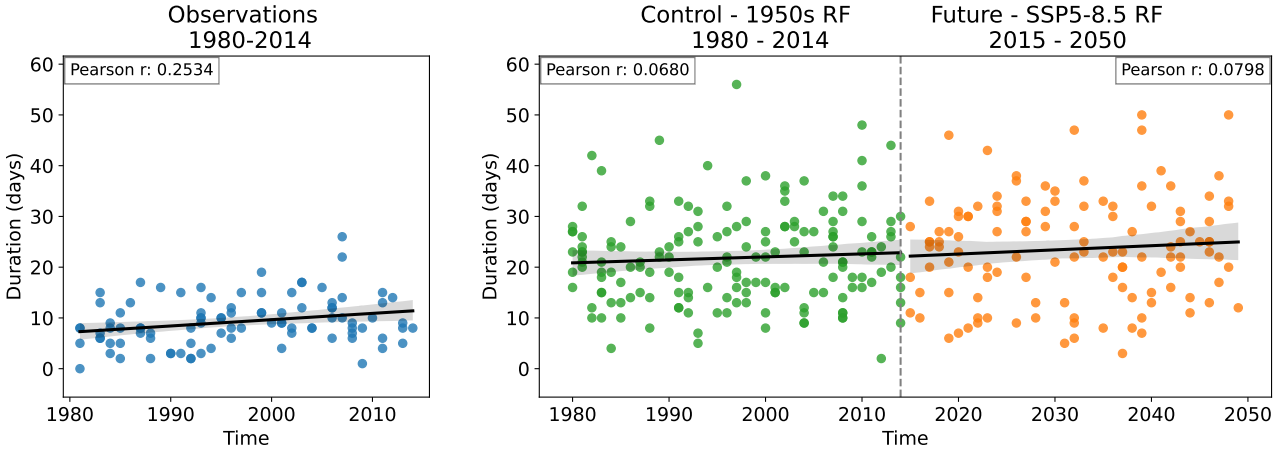

Figure 34: **Regression of the Duration of TCs Making Landfall** (Left) Linear regression of observed duration (days) of TCs that make landfall. Each point represents an individual TC. (Right) Linear regression of TCs that make landfall in the control simulation with 1950s radiative forcing and the future simulation forced with SSP5-8.5.

It can therefore be asked if the broader duration categories (short-lasting storms and long-lasting storms) show any differences than the regressions in Figure 34. Figure 35 shows 5-year running mean of the 25th, 50th (median) and 75th percentiles of the duration values of each landfall TC. The observational percentiles closely follow the shape of the regression in Figure 34, with the 25th percentile consistently low while the 50th and 75th percentiles fluctuate slightly more, indicating that the longer lasting storms making landfall could be lasting slightly longer as the climate warms. The control and future simulation percentiles show greater variation from one another, but do not show consistent deviation to indicate a difference between the upper (75th) and lower (25th) percentiles to indicate that there is a difference between longer lasting and shorter lasting TCs that make landfall as the climate warms.

Figure 36 shows a linear regression fit of intensity of each TC per season that makes landfall. The observed TCs shows a weak positive linear relationship between the season and the intensity of individual TCs, indicating that as time passes (and therefore the climate warms) the intensity of TCs have been slightly increasing. The p-value of 0.0105 indicates that this correlation coefficient is statistically significant, and supports the presence of some correlation between a warmer climate and an increased intensity of TCs. The control simulation also shows a weak positive relationship, with low statistical significance, indicating almost no relationship between the season and the intensity of the TCs. The future simulation also shows a weak positive trend, although also with low statistical significance. The discrepancy between the observations and the control and future simulations could be in part due to the model's limited horizontal resolution, which prohibits the model from identifying the most intense TCs. With the inclusion of higher intensity TCs in the control and future simulations, this might result in trends more similar to the observed TC intensities.

Similarly to the duration results, it can also therefore be asked if the broader intensity categories (low intensity and high intensity TCs) show any differences than the regression in Figure 36.

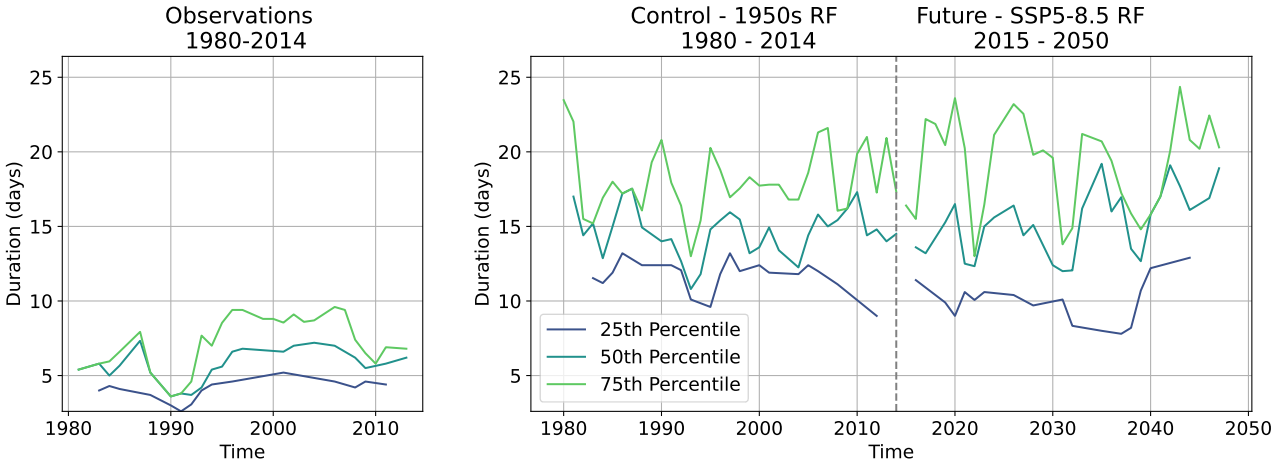

Figure 35: **Percentile 5-Year Running Mean of Landfall TC Duration** (Left) 5-year running mean of the 25th, 50th and 75th percentile of the duration of observed TCs making landfall. (Right) 5-year running mean of the 25th, 50th, and 75th percentile of the control simulation with 1950s radiative forcing and the future simulation forced by SSP5-8.5. Control and future simulations are deliminated with a vertical dashed line.

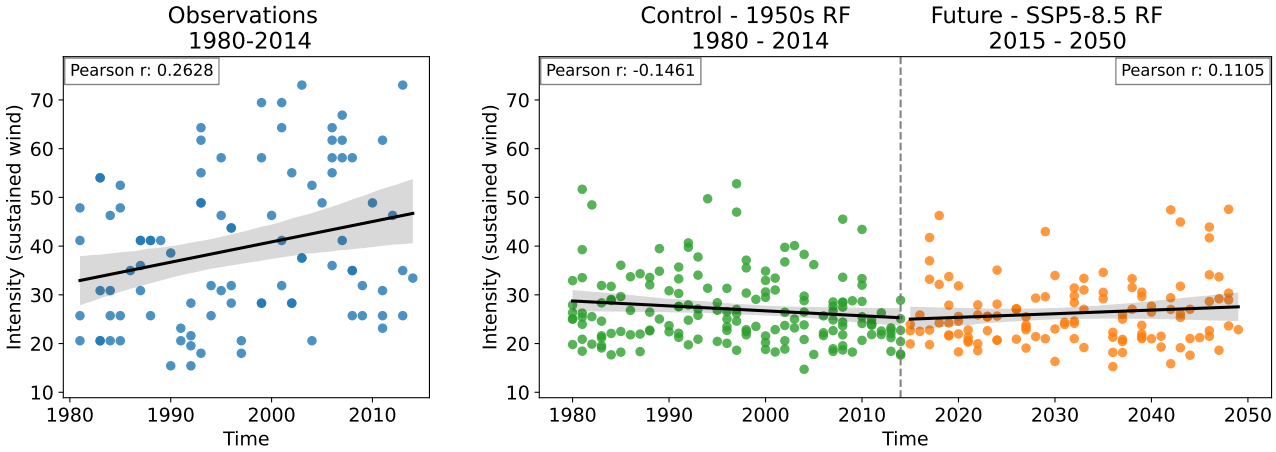

Figure 36: **Regression of the Intensity of TCs Making Landfall** (Left) Linear regression of observed max intensity of TCs that make landfall. Each point represents an individual TC. (Right) Linear regression of the max intensity of TCs that make landfall in the control simulation with 1950s radiative forcing and the future simulation forced with SSP5-8.5.

Figure 37 shows 5-year running mean of the 25th, 50th (median) and 75th percentiles of the duration values of each TC making landfall. The observational percentiles vary greatly with the shape of the data shown Figure 36, particularly with the 75th percentile (more intense TCs) while the 50th percentile fluctuates slightly less, and the 25th even less, indicating that the longer lasting storms passing near land could be lasting slightly longer as the climate warms. The control and future simulation percentiles show less variation from one another and do not show great deviation to indicate a difference between the upper (75th) and lower (25th) percentiles to indicate that there is a difference between longer lasting and shorter lasting TCs that pass near land as the climate warms.

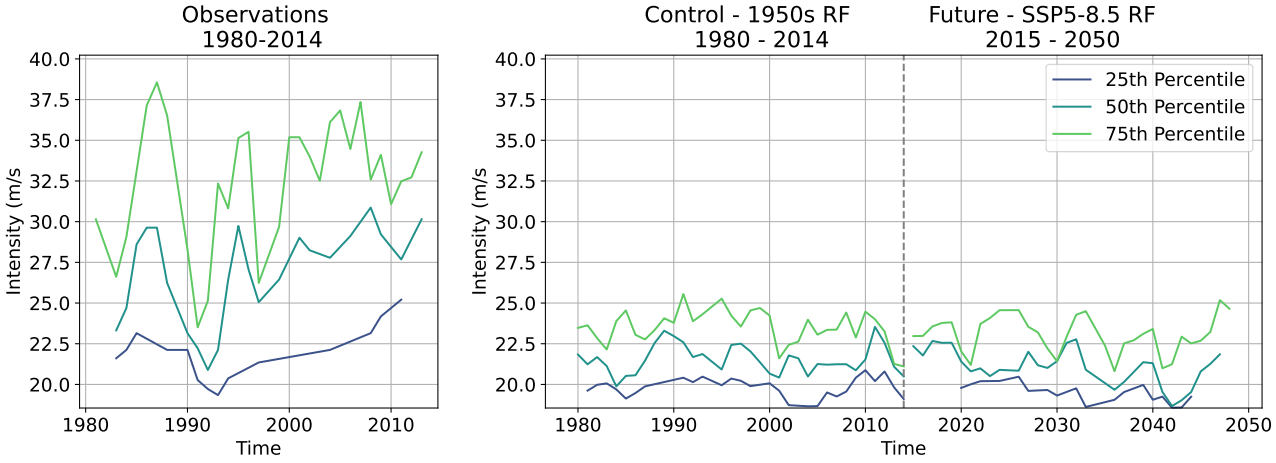

Figure 37: **Percentile 5-Year Running Mean of Landfall TC Intensity** (Left) 5-year running means of the 25th, 50th, and 75th percentile of the max intensity of observed TCs passing near land. (Right) 5-year running means of the 25th, 50th, and 75th percentiles of the control simulation with 1950s radiative forcing and the future simulation forced by SSP5-8.5. Control and future simulations are delimited with a vertical dashed line.

4.3 Damage Estimation

The following section presents the results of the damage estimation via mean sea level pressure (MSLP) as an indicator as outlined by the methods in Section 3.2.5.
Figure 38 shows the distribution of the MSLP (in hPa) of each TC for the entire SWIO basin. The observed MSLP shows a slight peak of TCs with MSLP between 980 and 990 hPa, indicating that the majority of observed TCs in the SWIO basin reach a Category 1 classification on the adjusted Saffir-Simpson scale as shown in Table 3.3. The control and future simulations, however, show a much more distinct peak at higher MSLPs, with few TCs reaching Category 1 status. The control simulation has a high peak around 1000 hPa, with a shorter tail going no lower than 955 hPa (Category 3). The peak in the future simulation is slightly lower than the control simulation, but peaking also around 1000 hPa with a short tail not extending past 960 hPa. The control and future simulation distributions indicate that the model is limited by its horizontal resolution in identifying TCs that would cause greater amounts of damage. The statistical significance confirms with a p-value of 5.8427e-103 that these distributions are indeed significantly different.

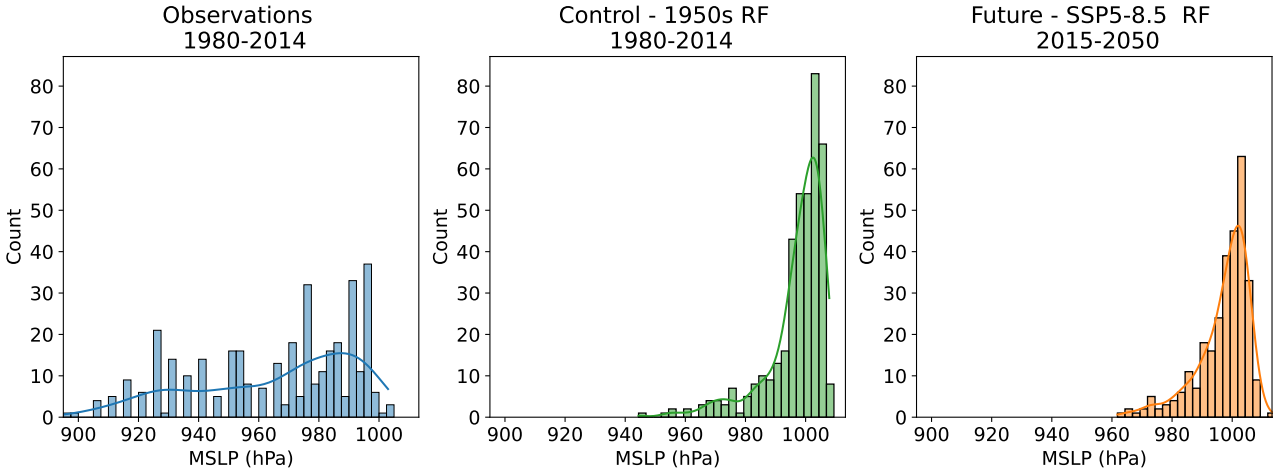

Figure 38: **Distribution of MSLP** (Left) MSLP of all observed TCs in the SWIO basin. (Center) MSLP of of TCs in the control simulation with 1950s radiative forcing. (Right) MSLP of TCs in the future simulation forced with SSP5-8.5. Kruskal-Wallis p-value of 5.8427e-103.

Figure 39 shows a linear regression fit of MSLP of each TC per season in the SWIO basin. The observed MSLP shows a weak (if not negligible) negative linear relationship between time and the MSLP of individual TCs with low significance, indicating almost no relationship between the MSLP of TCs and a warming climate. Likewise, both the control and future simulations show negligible relationships between time and MSLP, with low statistical significance. The regression analysis shows almost no discernible relationship between MSLP and a warming climate.
To further analyze the relationship that MSLP has with a warming climate, figure 40 shows shows 5-year running mean of the 25th, 50th (median) and 75th percentiles of the duration values of each TC. The observations show a slight variation of the 25th percentile lower than the 50th and 75th, while the control and future simulations show very little distinction between the 25th, 50th and 75th percentiles. This indicates that in observations, MSLP (and therefore damage done by the TCs) is increasing as the more intense storms increase with time under a warming climate.

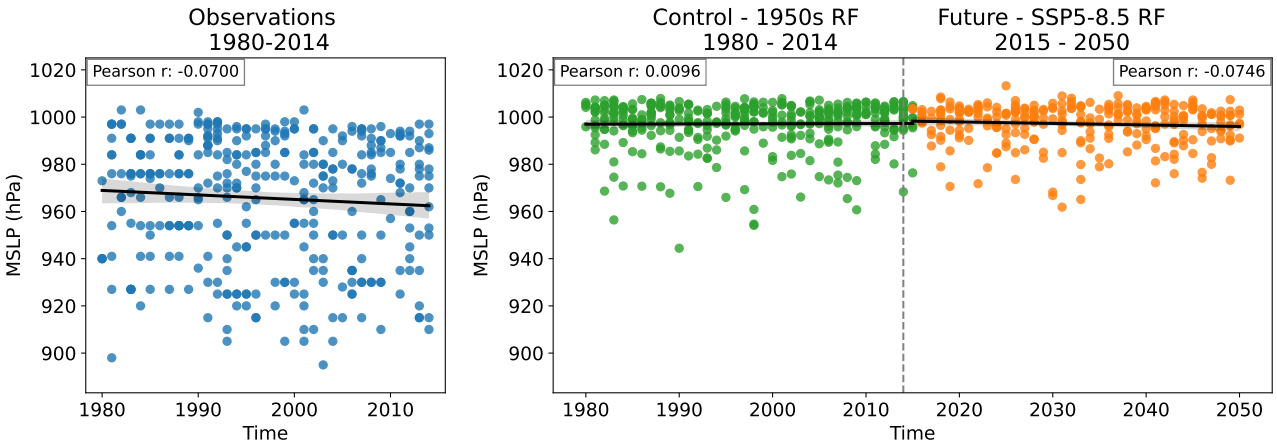

Figure 39: **Linear Regression of MSLP of all TCs in the SWIO** Linear regression of MSLP of observed TCs. Each point represents an individual TC. (Right) Linear regression of the MSLP of TCs in the control simulation with 1950s radiative forcing and the future simulation forced with SSP5-8.5.

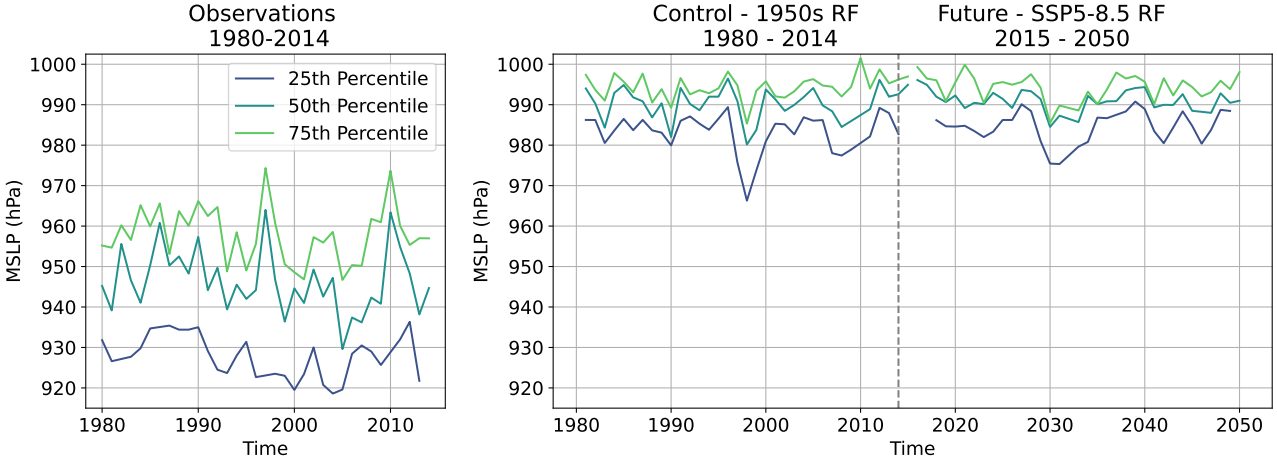

Figure 40: **Percentiles of MSLP versus Season** (Left) 5-year running means of the 25th, 50th and 75th percentiles of the MSLP of observed TCs in the SWIO basin. (Right) 5-year running means of the 25th, 50th, and 75th percentiles of the control simulation with 1950s radiative forcing and the future simulation forced by SSP5-8.5. Control and future simulations are delimited with a vertical dashed line.

4.4 Results Summary

Tables 4.2 and 4.3 provide an overview of the results of the statistical tests done for the analysis in Section 4.2. All distribution analysis showed statistical evidence that the distributions of observations, control and future simulations were very different from one another across the variables tested. Results of the linear regression analysis showed most notably, statistically significant relationships between increases in intensity and duration of TCs in observations. These relationships were not well reflected in the model simulations. Another notable result was the statistical significance of a decrease in the frequency of TCs passing near land in the future simulation, although this was not reflected in observations or in the control simulation.

		Kruskal-Wallis p-value
All TCs in the SWIO	Frequency	2.6606e-05
	Intensity	2.6579e-22
	Duration	8.9581e-84
	Duration of TCs with wind speeds >35 m/s	7.5912e-31
	MSLP	5.8427e-103
Near Land TCs	Frequency	1.2799e-05
	Intensity	2.6413e-13
	Duration	6.1057e-30
	Duration of TCs with wind speeds >35 m/s	8.3908e-08
Landfall TCs	Frequency	0.0005
	Intensity	1.2178e-12
	Duration	2.6023e-30
	Duration of TCs with wind speeds >35 m/s	1.4461e-10

Table 4.2: Overview of all the Kruskal-Wallis p-values calculated for the distributions presented in this section.

		Observations		Control-1950 Simulation		Highres-Future Simulation	
		Pearson r	p-value	Pearson r	p-value	Pearson r	p-value
All TCs in the SWIO	Frequency	0.0342	0.8453	-0.0133	0.9394	-0.0262	0.8812
	Intensity	0.1935	0.0002	0.0063	0.9901	0.0809	0.1675
	Duration	0.1905	0.0002	0.0629	0.2110	0.0725	0.2169
	MSLP	-0.0700	0.1862	0.0096	0.8491	-0.0746	0.2035
Near Land TCs	Frequency	-0.1119	0.5286	-0.1356	0.4318	-0.4318	0.0136
	Intensity	0.2215	0.0085	-0.1330	0.1564	-0.0242	0.8445
	Duration	0.2614	0.0018	0.0660	0.4831	0.0782	0.5263
Landfall TCs	Frequency	-0.2613	0.1485	0.0501	0.7752	-0.1482	0.4104
	Intensity	0.2628	0.0105	-0.1461	0.0580	0.1105	0.2257
	Duration	0.2534	0.0137	0.0680	0.3798	0.0798	0.3825

Table 4.3: Overview of all Pearson r (correlation coefficients) and p-values calculated for the linear regressions presented in this section.

5 Discussion

In this chapter the results of the analysis will be discussed. First, the tracking algorithm method is assessed for how well it represented observed TCs in the SWIO in Section 5.1. Then, the future TC season characteristics in the SWIO under a warming climate are discussed in Section 5.2. Finally, impacts to the region in the form of TC impact on vanilla agriculture in Madagascar will be discussed in Section 5.3.

5.1 Discussion of Methods: How well does the tracking algorithm method represent observed tropical cyclones?

The methodology as presented in Section 3.2 and subsequently examined presents several advantages within the context of this study. The basis of core elements of the methodology on previous studies using a well defined TC tracking algorithm provides an established framework for the detection of TCs in the SWIO. Likewise, specific criteria and filters for identifying TCs and distinguishing them from other synoptic systems aid in the clarity of 'what a TC is' as defined in this study, and therefore which systems were relevant to include in the analysis. The use of checks against model output for confirmation also aids in the validation process outlined in Section 3.2 Section, as well as the use of relevant statistical analysis to investigate the relevant variables presented throughout the study in a comprehensive way.
Alternatively, there are areas of limitation and potential sources of error present in the methodology of this study. Due to limitations in time and computing resources, certain criteria and filters (such as an assessment of the coherent vertical structure condition of TCs and the transitions to extratropical and subtropical storms) for more in-depth TC identification were not included. These omissions may impact the resulting data upon which the analysis was conducted, and therefore the conclusions drawn and presented. Likewise, the assumptions that visual correlation between surface wind speeds and vorticity in model output to the calculated TC tracks as a confirmation method may introduce subjectivity and potential bias. An additional or alternative method for verifying model output could strengthen the overall analysis. Additionally, the use of EC-Earth3p-HR exclusively in this study may introduce biases based on the specific characteristics of this model. Given further time, the model simulations from all models described in Table 3.1 remain relevant to this study and if included, would provide a more comprehensive view on TCs in the SWIO.
Given these methodological considerations, some general characteristics of the EC-Earth3p-HR model play a role in the findings of this study. The future projections of both the frequency and characteristics of TCs have rooted dependence in the forcing environment and how those elements will change under a warmer climate (Murakami et al., 2012; Zhao & Held, 2012). Higher model resolutions with small ensembles ((M. J. Roberts et al., 2015; Zhao et al., 2009)) and large ensembles with a singular resolution (Mei et al., 2019; Yoshida et al., 2017) are necessary to adequately represent the inter-annual variability of TCs that is seen in observations. EC-Earth3P-HR and the other models listed in Table **??** have the ability to form a comprehensive small ensemble with high resolutions, which (given the inclusion of additional models), gives credibility to the model results of this study. More specifically, M. J. Roberts et al. (2020) finds that there is a distinct increase in the TC frequency with resolution (compared to observations) in several models including EC-Earth3p-HR, while many models have a shifted ratio of NH to SH TCs than is seen in observations, skewed towards an overproduction in the SH. Features of the model such as the hemispheric asymmetry can indicate that the model simulations result in too many SH TCs, while additional limitations in observational best track data specifically

in the SH (due to a lack of tropical depressions and subtropical cyclones represented in best track data) further enhance this asymmetry and influence the analysis (Strachan et al., 2013). The behavior of TCs in the SWIO is influenced by a variety of factors described in Section 2. Key tropic features for cyclogenesis occurrence (overview in Table **??**) may play a role in understanding the TC conditions found in this study. Key atmospheric and oceanic conditions such as SSTs, wind shear and moisture availability play crucial roles in TC development. The impact of these atmospheric and oceanic conditions on TCs is not explicitly addressed in this study, but can be important factors to consider in future analysis of TCs in the SWIO.

It is noTable that in addition to climate drivers and atmospheric conditions, other influences can also affect TC behavior in the SWIO. For instance, regional oceanic and atmospheric circulations, such as the Hadley and Walker Cells, Inter-tropical Convergence Zone (ITCZ), Indian Ocean Dipole (IOD), the El Nino-Southern Oscillation (ENSO) and the Madden-Julian Oscillation (MJO), can modulate the frequency, intensity, and tracks of TCs (Seneviratne et al., 2021). These regional oceanic and atmospheric circulations are discussed further in Section 2. Within the context of EC-Earth3P-HR in particular, the ENSO amplitude in the beginning of austral summer (corresponding with the TC season) is noted to have an systematic underestimation, which could influence ENSO events which bring warm SSTs into the SWIO via the Walker cell (outlined in Section 2). However, Ash and Matyas (2012) finds that ENSO alone is not enough to account for all variability of the TC tracks, duration and intensity and that the IOD SST anomaly also plays a large role. The broad range of natural variability present in the SWIO makes trend detection and attribution to climate change impacts difficult, as the uncertainties in these modes of variability lead to further uncertainties in the projected changes in TC activity.

Additional evaluation elements could be included in this study for more robust findings. In particular, the inclusion of multiple ensemble members for the EC-Earth3p-HR model, as well as inclusions of other models and respective ensemble members would have added to the robustness of the findings. In light of this, the all-basin analysis and damage estimation analysis as outlined in Sections 3.2.3 and 3.2.5 were conducted for a second EC-Earth3P-HR model ensemble member (member *r2i1p2f1*), an overview of which can be found in Appendix A. This further analysis into the addition of an ensemble member did not show a great difference in any distributions of any of the variables (frequency, intensity, duration, MSLP), but rather reflected the results of the single member analysis quite closely. Regression analysis also showed similar (or negligibly different) relationship between frequency, intensity, duration and MSLP, likewise for the percentile analysis. While the addition of the second model ensemble member did not influence the results found in Section 4.2 A comprehensive evaluation of the abilities of EC-Earth3p-HR and the *TRACK* algorithm (in particular) to accurately capture the essential characteristics of TCs in the SWIO would provide a more solid foundation on which to base the results of this analysis. The model needs to capture the conditions that facilitate the genesis of TCs in the SWIO region based on the conditions described in Section 2, as well as the intensification process and track movement and dissipation. The ability of EC-Earth3p-HR and the TRACK algorithm to evaluate the dissipation characteristics would be of particular interest as an additional element of consideration in this study. Comparing *TRACK*'s predicted dissipation rates and the timing of TC decay with the observed best-track would provide insights into its skill in simulating the dissipation process in the SWIO, and would make a useful consideration in evaluating in particular the duration element of TCs in the SWIO. By further comparing the *TRACK*'s outputs with observed best-track data, assessments of the strengths and limitations of *TRACK* and EC-Earth3p-HR and further areas of improvement can be made.

5.2 Discussion of Results: What do future tropical cyclone seasons look like in the SWIO?

The resulting identification and visual confirmation of TCs as presented in Sections 4.1.1 and 4.1.2 provide a base assumption that the analysis methodology outlined in Section 3.2 is reasonably robust to provide insights into TC trends in the SWIO. Figure 5 showing the spatial distribution of TC tracks calls to attention the control and future simulations tendency to have TC tracks which pass both within 5°of the equator, and also south of 30°S. These two extremes are areas where the Coriolis force is no longer adequate for cyclone genesis ((McBride & Zehr, 1981). What is most likely being displayed in Figure 5 is a representation of the model and tracking algorithm's lack of ability to discern where a TC transitions to an extratropical storm or a subtropical storm. Likewise, an under representation of tropical depressions and subtropical storms in observational data most likely enhances this disparity between the three maps in Figure 5.

By examining the resulting number of TCs analyzed as shown in Table 4.1, the control simulation in particular shows a higher number of TCs than is observed and in the future simulation, which is attributed to the characteristics described in Section 5.1, particularly due to the characteristics of TCs worldwide (as discussed in Section 2) showing that as the climate warms, TC frequency has been slightly decreasing. As the control simulation shows 1950s radiative forcing conditions, it is likely then that this slightly negative trend with warmer conditions would not be present, and the control simulation would show more TCs. It is also noTable that the observations show more TCs coming near land than in the model simulations, which can be attributed to a lack of resolution in the land coordinates used to calculate the distances between TC tracks and land. As the SWIO is characterized by having many small islands throughout the basin, an increased land mask resolution could play a role in this disparity. It is also noTable that the control and future simulations have a higher proportion of TCs calculated to make landfall than as seen in observations, and additionally a higher proportion of landfall TCs to near land TCs than is seen in observations. TC track paths and likewise if a TC does or does not make landfall is influenced by a variety of factors such as the conditions surrounding the prevailing modes of variability (as discussed in Section 2 and in Section 5.1). The presence of high pressure systems can influence the path of TCs, as these systems create areas of sinking air, resulting in sTable atmospheric conditions and a anti-clockwise flow of air in the SH. TCs tend to move around the periphery of high-pressure systems, following the path of least resistance. Likewise, the same conditions relevant to TC genesis (as outlined in Table **??** also contribute to the direction that a TC takes through the basin, where the TC will follow a path of least resistance into areas (for example) with warmer SSTs and away from areas with colder SSTs that cause dissipation, where warmer SSTs are available for the TC to travel through.

When it comes to landfall, several additional factors can influence whether a tropical cyclone makes landfall or remains over the ocean. The topography around the area where the TC is in influences the TC, and Barbary et al. (2019) finds that within 100 km of land, the land influences the TC and likewise effects from the TC influence land in terms of experienced weather conditions related to TCs. Mountains, coastlines, and other geographical features can disrupt the storm's circulation and cause it to weaken or change course. However, the size and intensity of the TC plays a large role, as larger and more intense TCs tend to be able to overcome the disruption caused by land features in its path, and therefore make landfall (Wahiduzzaman & Yeasmin, 2019). As the natural variability in the factors that can 'steer' a TC is high, there is low confidence in the attribution of TC tracks to climate change influences and therefore the disparity between the number of near land and landfall TCs shown in Table 4.1 is a reflection of this natural variability in the control and future simulations.

The results of this study most clearly indicate weak positive relationships between time and the

intensity and duration of observed TCs in the SWIO, as well as for the TCs which pass near land and make landfall. This relationship is not well reflected the control and future simulations, which show only one statistically significant relationship between a decrease in the frequency of near land TCs over time in the future simulation. In particular, the model simulations showed TCs that had much longer duration, but reached much lower intensities than was observed. The model simulations showed little agreement throughout all sub-categories of TCs (all basin, near land and landfall), and in fact highlighted the limitations of EC-Earth3p-HR as described in Section 5.1. Uncertainties come primarily from the model simulation results due to the methodological limitations, however there is additional limited confidence due to data limitations in so called 'best-track' data (as used in this study and outlined in Section 3.1), particularly due to limited inclusion of sub-tropical storms (Schreck et al., 2014). Model resolution is a great challenge in this study, which is particularly reflected in the distribution analysis of all basin, near land and landfall TCs. When examining the percentiles of duration and intensity, if the percentile analysis indicated that (for example) intense storms were getting more intense, then there would be greater spreads (as time increased) in the percentile lines. This was however not seen clearly with the exception of the intensities of observed TCs across the SWIO basin, as well as TCs that pass near land and make landfall. If the model resolution greater and more able to fully resolve TC conditions, then it could be expected that the control and future simulations would show shifted distributions more closely aligning with what was seen in observations.

Comparing the SWIO basin results to global projections on TC trends described in chapter 2, there are agreements with the results found in this study. (Seneviratne et al., 2021) notes similar low confidence in long term trends of TC frequency or intensity based metrics, as is found in this study. Some evidence of positive trends in TC intensity found in studies (see Section 2) similarly conducted over the satellite era also demonstrate positive trends in TC intensity. While this study did not expand on other elements such as rapid intensification events, poleward migration of peak intensity, and a slowdown in translation speeds, these elements would be relevant to consider when comparing the TC conditions at present and in the future in the SWIO to global trends.

5.3 Discussion of Impacts: How will future tropical cyclones impact vanilla agriculture in the SWIO, particularly in Madagascar?

Understanding the behavior of cyclones in the SWIO is of great importance in global context. First and foremost, the SWIO is a region that is prone to the occurrence of TCs, and their impacts can be significant. The ability to accurately predict TC behavior in this region is crucial to inform future adaptation strategies as the potential impacts of TCs on coastal communities such as Madagascar and others throughout the SWIO region are varied. TC impacts include strong winds, storm surges, heavy precipitation and flooding, all of which can lead to property damage, loss of lives, and disruption of essential services. Coastal communities, particularly though with limited resources and inadequate infrastructure, are more vulnerable to these impacts (Mavume et al., 2009; Seneviratne et al., 2021).

While all of the impacts that TCs cause can significantly affect coastal communities and economies, when discussing in particular the impact that TCs in the SWIO have on vanilla agriculture in Madagascar, this study finds several attributes to be particularly significant. Weather conditions from TC activity can be particularly damaging to vanilla crops as discussed in Sections 1 and 2. Excess wind and water, as well as flooding are particularly damaging to the vanilla plant, causing a lack of crop yield as well as water logging, vine damage, and soil erosion.

The results of this study find that with the increase in intensity and duration of TCs, Madagascar and the vanilla agricultural region will likely not experience an increase in the frequency of TCs, but the TCs that do occur will have higher wind speeds and lower MSLP, an indication that damage to the region will gradually increase with TC occurrence as time passes. All of which poses a higher risk of infrastructure damage, crop destruction, and other socio-economic impacts to the vanilla agricultural production system in the region. While precipitation was not directly analyzed in this study, the extended duration of TCs also extend exposure to high winds and precipitation, as well as flooding which can be detrimental to the vanilla crop and hinder post-cyclone recovery efforts. These trends highlight the growing vulnerability of vanilla agriculture in the SWIO region, and adaptation strategies for vulnerable coastal communities can be based around the anticipation of TCs to be longer lasting and with greater duration, while not necessarily increasing in frequency.

6 Conclusion and Outlook

This study has evaluated the future trends of TCs under a changing climate in the SWIO, and assessed how these future trends will impact the region and in particular its vanilla agriculture. This was done utilizing storm tracks derived from EC-Earth3P-HR model simulations conducted under CMIP6 HighResMIP protocol by the PRIMAVERA project group, as well as observational best track data data from the SWIO basin. Storms from the period beginning on the 1st of October 1980 through the 30th of May 2015 were considered to remove pre-satellite era uncertainties, and cross checks between model output and the calculated storm tracks are made to verify the *TRACK* algorithm output. To this end, a variety of analysis was conducted to derive future trends from modeled simulations incorporating a high emissions climate change scenario, and then compared to a control simulation as well as observational trends for the SWIO basin. Future damages were estimated using MSLP as predictor. As a result, the questions of *how well does the tracking algorithm method applied to model data represent observed tropical cyclones from best track data*, and *what do future tropical cyclone seasons look like in the SWIO basin under a high emissions changing climate scenario* as well as *how will future tropical cyclones impact vanilla agriculture in the SWIO, specifically on the island of Madagascar* can be addressed.

Regarding the tracking algorithm method, there are several advantages to the methodology used in this study. The building upon previous TC identification methods via the use of a well-defined tracking algorithm provides a solid framework for detection of TCs in the SWIO region. Additionally, filtering for TC conditions helps to ensure the clarity and relevence of the analysis. The inclusion of model output checks and statistical analysis further enhances the validation process. However, there are limitations and potential sources of error in the methodology. Due to time and computing constraints, certain criteria and filters for more in-depth TC identification were not included. This omission may affect the resulting data and conclusions. The subjective nature of visual correlation between surface wind speeds and vorticity in model output as a confirmation method introduces potential bias. Using additional and alternative methods for algorithm verification could strengthen the analysis. Additionally, the exclusive use of EC-Earth3p-HR model simulations may introduce biases based on its specific characteristics, and including simulations from other models would provide a more comprehensive view of TCs in the SWIO.

Regarding future TCs and TC seasons under a changing climate, the results of this study indicate agreement with well documented global trends of gradual increases in TC intensity and duration, with a noted lack in increased frequency. However, these trends were primarily seen in observations, with discrepancies or no discernible trends in the model simulation output. Uncertainties arise from methodological and data limitations, as well as model resolution challenges. Overall, there is low confidence in long-term trends of TC frequency or intensity in the SWIO, consistent with global projections, in part due to the relevance of climate drivers and atmospheric conditions in shaping TC characteristics. Factors such as sea surface temperatures, wind shear, and moisture availability play crucial roles in TC development. Other regional oceanic and atmospheric circulations, such as the Hadley and Walker Cells, ITCZ, IOD, ENSO, and MJO, also influence TC behavior in the SWIO.

The results of this study find that with the gradual increases in intensity and duration of TCs in the SWIO basin, the impacts on coastal communities and agriculture (such as the vanilla production in Madagascar) will likely be experienced as increased damage due to higher wind speeds and lower pressure TCs, coupled with increased exposure to both precipitation, wind speeds, and MSLP as TCs have a longer duration in a warming climate. These conditions pose a higher risk of infrastructure damage, crop destruction and other socio-economic impacts to the

vanilla agricultural production in Madagascar and in the rest of the SWIO basin, highlighting growing vulnerabilities under a changing climate.
In light of this, this analysis would benefit primarily from the inclusion of all models and ensemble members available as described in table 3.1 to help eliminate internal variability within the models, and provide a more robust foundation for comparison to observations. As models with higher resolutions are developed, their inclusions will also be critical in future TC analysis globally, as even the high resolution models present in HighResMIP lack the horizontal resolution required to produce conditions where TCs can be calculated as intensifying past a Category 3 classification. The horizontal resolution of the models is a critical limitation to the accuracy of the analysis of TCs. Additionally, a thorough evaluation of the natural modes of variability (such as ENSO, IOD, MJO, and ITCZ) present and influencing TCs in the SWIO basin would provide additional clarity into the inter-seasonal and inter-annual variability of TC genesis conditions. Further analysis on TC characteristics such as translation speed and poleward peak intensity migration would also be highly relevant for this study, particularly relating to the impacts on vanilla agriculture in Madagascar and for coastal communities throughout the SWIO basin under a changing climate.

Bibliography

Ash, K. D., & Matyas, C. J. (2012). The influences of ENSO and the subtropical Indian Ocean Dipole on tropical cyclone trajectories in the southwestern Indian Ocean. *International Journal of Climatology*, *32*(1), 41–56. https://doi.org/10.1002/joc.2249

Bakkensen, L. A., & Mendelsohn, R. O. (2016). Risk and Adaptation: Evidence from Global Hurricane Damages and Fatalities [Publisher: The University of Chicago Press]. *Journal of the Association of Environmental and Resource Economists*, *3*(3), 555–587. https://doi.org/10.1086/685908

Balaguru, K., Foltz, G. R., & Leung, L. R. (2018). Increasing Magnitude of Hurricane Rapid Intensification in the Central and Eastern Tropical Atlantic. *Geophysical Research Letters*, *45*(9), 4238–4247. https://doi.org/10.1029/2018GL077597

Barbary, D., Leroux, M.-D., & Bousquet, O. (2019). The orographic effect of Reunion Island on tropical cyclone track and intensity. *Atmospheric Science Letters*, *20*(2), e882. https://doi.org/10.1002/asl.882

Bengtsson, L., Hodges, K. I., & Esch, M. (2007). Tropical cyclones in a T159 resolution global climate model: Comparison with observations and re-analyses [Publisher: Taylor & Francis]. *Tellus A: Dynamic Meteorology and Oceanography*, *59*(4), 396–416. https://doi.org/10.1111/j.1600-0870.2007.00236.x

Bowyer, P. (2000). Phenomenal waves with a transitioning tropical cyclone (luis, the queen, and the buoys). *Preprints, 24th Conf. on Hurricanes and Tropical Meteorology, Fort Lauderdale, FL, Amer. Meteor. Soc*, *294*, 295.

Brown, M. L. (2009). Madagascar's cyclone vulnerability 11 and the global vanilla economy. *Political Economy of Hazards and Disasters*, 241–64.

Brownell, R., Hogan, C., May, S., Nielsen, C., Pennestri, C., Roques, D., Rosskam, S., & Todd, H. (2009). The state of vanilla: Challenges and opportunities. *Perfum. Flavor*, *34*, 20–22.

Cappucci, M. (2023). Cyclone Freddy is officially Earth's most energetic storm on record - The Washington Post. Retrieved May 4, 2023, from https://web.archive.org/web/20230313053428/https://www.washingtonpost.com/weather/2023/03/12/cyclone-freddy-records-ace-longevity/

C.D. (2018). Why there is a worldwide shortage of vanilla. *The Economist*. Retrieved May 4, 2023, from https://www.economist.com/the-economist-explains/2018/03/28/why-there-is-a-worldwide-shortage-of-vanilla

Chen, S., Elsberry, R. L., & Harr, P. A. (2017). Modeling Interaction of a Tropical Cyclone with Its Cold Wake [Publisher: American Meteorological Society Section: Journal of the Atmospheric Sciences]. *Journal of the Atmospheric Sciences*, *74*(12), 3981–4001. https://doi.org/10.1175/JAS-D-16-0246.1

Cherchi, A., Fogli, P. G., Lovato, T., Peano, D., Iovino, D., Gualdi, S., Masina, S., Scoccimarro, E., Materia, S., Bellucci, A., & Navarra, A. (2019). Global Mean Climate and Main Patterns of Variability in the CMCC-CM2 Coupled Model. *Journal of Advances in Modeling Earth Systems*, *11*(1), 185–209. https://doi.org/10.1029/2018MS001369

Consortium (EC-Earth), E.-E. (2018). EC-Earth-Consortium EC-Earth3P-HR model output prepared for CMIP6 HighResMIP control-1950. https://doi.org/10.22033/ESGF/CMIP6.4548

Correll, D. S. (1953). Vanilla-its botany, history, cultivation and economic import. *Economic Botany*, *7*(4), 291–358. https://doi.org/10.1007/BF02930810

Fitchett, J. M. (2018). Recent emergence of CAT5 tropical cyclones in the South Indian Ocean [Publisher: Academy of Science of South Africa]. *South African Journal of Science*, *114*(11-12), 1–6. https://doi.org/10.17159/sajs.2018/4426

Fitchett, J. M., & Grab, S. W. (2014). A 66-year tropical cyclone record for south-east Africa: Temporal trends in a global context. *International Journal of Climatology*, *34*(13), 3604–3615. https://doi.org/10.1002/joc.3932

Foley, G. R., & Hanstrum, B. N. (1994). The Capture of Tropical Cyclones by Cold Fronts off the West Coast of Australia [Publisher: American Meteorological Society Section: Weather and Forecasting]. *Weather and Forecasting*, *9*(4), 577–592. https://doi.org/10.1175/1520-0434(1994)009<0577:TCOTCB>2.0.CO;2

Gray, W. M. (1998). The formation of tropical cyclones. *Meteorology and Atmospheric Physics*, *67*(1), 37–69. https://doi.org/10.1007/BF01277501

Grinsted, A., Ditlevsen, P., & Christensen, J. H. (2019). Normalized US hurricane damage estimates using area of total destruction, 19002018. *Proceedings of the National Academy of Sciences*, *116*(48), 23942–23946. https://doi.org/10.1073/pnas.1912277116

Grotch, S. L., & MacCracken, M. C. (1991). The Use of General Circulation Models to Predict Regional Climatic Change [Publisher: American Meteorological Society Section: Journal of Climate]. *Journal of Climate*, *4*(3), 286–303. https://doi.org/10.1175/1520-0442(1991)004<0286:TUOGCM>2.0.CO;2

Gutjahr, O., Putrasahan, D., Lohmann, K., Jungclaus, J. H., von Storch, J.-S., Brüggemann, N., Haak, H., & Stössel, A. (2019). Max Planck Institute Earth System Model (MPI-ESM1.2) for the High-Resolution Model Intercomparison Project (HighResMIP) [Publisher: Copernicus GmbH]. *Geoscientific Model Development*, *12*(7), 3241–3281. https://doi.org/10.5194/gmd-12-3241-2019

Haarsma, R., Acosta, M., Bakhshi, R., Bretonnière, P.-A. B., Caron, L.-P., Castrillo, M., Corti, S., Davini, P., Exarchou, E., Fabiano, F., Fladrich, U., Fuentes Franco, R., García-Serrano, J., Von Hardenberg, J., Koenigk, T., Levine, X., Meccia, V., Van Noije, T., Van Den Oord, G., … Wyser, K. (2020). *HighResMIP versions of EC-Earth: EC-Earth3P and EC-Earth3P-HR. Description, model performance, data handling and validation* (preprint). Climate and Earth System Modeling. https://doi.org/10.5194/gmd-2019-350

Haarsma, R. J., Roberts, M. J., Vidale, P. L., Senior, C. A., Bellucci, A., Bao, Q., Chang, P., Corti, S., Fučkar, N. S., Guemas, V., von Hardenberg, J., Hazeleger, W., Kodama, C., Koenigk, T., Leung, L. R., Lu, J., Luo, J.-J., Mao, J., Mizielinski, M. S., … von Storch, J.-S. (2016). High Resolution Model Intercomparison Project (HighResMIP v1.0) for CMIP6 [Publisher: Copernicus GmbH]. *Geoscientific Model Development*, *9*(11), 4185–4208. https://doi.org/10.5194/gmd-9-4185-2016
Data section - description of highres mip

Hodges, K. I. (1995). Feature Tracking on the Unit Sphere [Publisher: American Meteorological Society Section: Monthly Weather Review]. *Monthly Weather Review*, *123*(12), 3458–3465. https://doi.org/10.1175/1520-0493(1995)123<3458:FTOTUS>2.0.CO;2

Hodges, K. I. (1999). Adaptive Constraints for Feature Tracking [Publisher: American Meteorological Society Section: Monthly Weather Review]. *Monthly Weather Review*, *127*(6), 1362–1373. https://doi.org/10.1175/1520-0493(1999)127<1362:ACFFT>2.0.CO;2

IPCC. (2021). Summary for policymakers (V. Masson-Delmotte, P. Zhai, A. Pirani, S. Connors, C. Péan, S. Berger, N. Caud, Y. Chen, L. Goldfarb, M. Gomis, M. Huang, K. Leitzell, E. Lonnoy, J. Matthews, T. Maycock, T. Waterfield, O. Yelekçi, R. Yu, & B. Zhou, Eds.) [In Press].

Jones, E. C., & Murphy, A. D. (2009). *The Political Economy of Hazards and Disasters* [Google-Books-ID: uY1YaNM402MC]. Rowman Altamira.

Jones, S. C., Harr, P. A., Abraham, J., Bosart, L. F., Bowyer, P. J., Evans, J. L., Hanley, D. E., Hanstrum, B. N., Hart, R. E., Lalaurette, F., Sinclair, M. R., Smith, R. K., & Thorncroft, C. (2003). The Extratropical Transition of Tropical Cyclones: Forecast Challenges,

Current Understanding, and Future Directions [Publisher: American Meteorological Society Section: Weather and Forecasting]. *Weather and Forecasting*, *18*(6), 1052–1092. https://doi.org/10.1175/1520-0434(2003)018<1052:TETOTC>2.0.CO;2

Jury, M. R. (1993). A preliminary study of climatological associations and characteristics of tropical cyclones in the SW Indian Ocean. *Meteorology and Atmospheric Physics*, *51*(1), 101–115. https://doi.org/10.1007/BF01080882

Jury, M. (2022). Chapter 3: Climate, The Climate of Madagascar. In S. M. Goodman & A. Andrianarimisa (Eds.), *The new natural history of Madagascar*. Princeton University Press. https://books.google.dk/books?hl=da&lr=&id=IJhwEAAAQBAJ&oi=fnd&pg=PA91&dq=tropical+cyclones+madagascar&ots=dSV-ZQCO6z&sig=edZMwxBhHnrK-bTe5bq_8XSkAI0&redir_esc=y#v=onepage&q=tropical%20cyclones%20madagascar&f=false

Kang, N.-Y., & Elsner, J. B. (2012). Consensus on Climate Trends in Western North Pacific Tropical Cyclones [Publisher: American Meteorological Society Section: Journal of Climate]. *Journal of Climate*, *25*(21), 7564–7573. https://doi.org/10.1175/JCLI-D-11-00735.1

Kaplan, J., & DeMaria, M. (1995). A Simple Empirical Model for Predicting the Decay of Tropical Cyclone Winds after Landfall [Publisher: American Meteorological Society Section: Journal of Applied Meteorology and Climatology]. *Journal of Applied Meteorology and Climatology*, *34*(11), 2499–2512. https://doi.org/10.1175/1520-0450(1995)034<2499:ASEMFP>2.0.CO;2

Karnauskas, K. B., Zhang, L., & Emanuel, K. A. (2021). The Feedback of Cold Wakes on Tropical Cyclones. *Geophysical Research Letters*, *48*(7), e2020GL091676. https://doi.org/10.1029/2020GL091676
e2020GL091676 2020GL091676

Kishtawal, C. M., Jaiswal, N., Singh, R., & Niyogi, D. (2012). Tropical cyclone intensification trends during satellite era (1986–2010). *Geophysical Research Letters*, *39*(10). https://doi.org/10.1029/2012GL051700

Klotzbach, P. J., Bell, M. M., Bowen, S. G., Gibney, E. J., Knapp, K. R., & Schreck, C. J. (2020). Surface Pressure a More Skillful Predictor of Normalized Hurricane Damage than Maximum Sustained Wind [Publisher: American Meteorological Society Section: Bulletin of the American Meteorological Society]. *Bulletin of the American Meteorological Society*, *101*(6), E830–E846. https://doi.org/10.1175/BAMS-D-19-0062.1

Knapp, K. R., Kruk, M. C., Levinson, D. H., Diamond, H. J., & Neumann, C. J. (2010). The International Best Track Archive for Climate Stewardship (IBTrACS): Unifying Tropical Cyclone Data [Publisher: American Meteorological Society Section: Bulletin of the American Meteorological Society]. *Bulletin of the American Meteorological Society*, *91*(3), 363–376. https://doi.org/10.1175/2009BAMS2755.1
IBTrACS dataset

Knutson, T., Camargo, S. J., Chan, J. C. L., Emanuel, K., Ho, C.-H., Kossin, J., Mohapatra, M., Satoh, M., Sugi, M., Walsh, K., & Wu, L. (2020). Tropical Cyclones and Climate Change Assessment: Part II: Projected Response to Anthropogenic Warming [Publisher: American Meteorological Society Section: Bulletin of the American Meteorological Society]. *Bulletin of the American Meteorological Society*, *101*(3), E303–E322. https://doi.org/10.1175/BAMS-D-18-0194.1

Kossin, J. P. (2018). A global slowdown of tropical-cyclone translation speed [Number: 7708 Publisher: Nature Publishing Group]. *Nature*, *558*(7708), 104–107. https://doi.org/10.1038/s41586-018-0158-3

Kossin, J. P., Emanuel, K. A., & Vecchi, G. A. (2014). The poleward migration of the location of tropical cyclone maximum intensity [Number: 7500 Publisher: Nature Publishing Group]. *Nature*, *509*(7500), 349–352. https://doi.org/10.1038/nature13278

Kossin, J. P., Olander, T. L., & Knapp, K. R. (2013). Trend Analysis with a New Global Record of Tropical Cyclone Intensity [Publisher: American Meteorological Society Section: Journal of Climate]. *Journal of Climate*, *26*(24), 9960–9976. https://doi.org/10.1175/JCLI-D-13-00262.1

Kruskal, W. H., & Wallis, W. A. (2012). Use of Ranks in One-Criterion Variance Analysis [Publisher: Taylor & Francis Group]. *Journal of the American Statistical Association*. Retrieved May 9, 2023, from https://www.tandfonline.com/doi/abs/10.1080/01621459.1952.10483441

Kuhlbrodt, T., Jones, C. G., Sellar, A., Storkey, D., Blockley, E., Stringer, M., Hill, R., Graham, T., Ridley, J., Blaker, A., Calvert, D., Copsey, D., Ellis, R., Hewitt, H., Hyder, P., Ineson, S., Mulcahy, J., Siahaan, A., & Walton, J. (2018). The Low-Resolution Version of HadGEM3 GC3.1: Development and Evaluation for Global Climate. *Journal of Advances in Modeling Earth Systems*, *10*(11), 2865–2888. https://doi.org/10.1029/2018MS001370

Laing, A., & Evans, J.-L. (2011). Chapter 8: Tropical Cyclones. In *Introduction to Tropical Meteorology* (2nd). The University Corporation for Atmospheric Research. Retrieved May 5, 2023, from https://ftp.comet.ucar.edu/memory-stick/tropical/textbook_2nd_edition/navmenu.php_tab_9_page_2.2.0.htm

Laney, R. M. (2004). A process-led approach to modeling land change in agricultural landscapes: A case study from Madagascar. *Agriculture, Ecosystems & Environment*, *101*(2-3), 135–153. https://doi.org/10.1016/j.agee.2003.09.004

Levinson, D. H., Knapp, K. R., Kruk, M. C., J., H., & Kossin, J. P. (2010). The International Best Track Archive for Climate Stewardship (IBTrACS) Project: Overview of Methods and Indian Ocean Statistics. In Y. Charabi (Ed.), *Indian Ocean Tropical Cyclones and Climate Change* (pp. 215–221). Springer Netherlands. https://doi.org/10.1007/978-90-481-3109-9_26

Lu, J., Vecchi, G. A., & Reichler, T. (2007). Expansion of the Hadley cell under global warming. *Geophysical Research Letters*, *34*(6). https://doi.org/10.1029/2006GL028443

Malherbe, J., Engelbrecht, F. A., & Landman, W. A. (2013). Projected changes in tropical cyclone climatology and landfall in the Southwest Indian Ocean region under enhanced anthropogenic forcing. *Climate Dynamics*, *40*(11), 2867–2886. https://doi.org/10.1007/s00382-012-1635-2

Maloney, E. D., & Hartmann, D. L. (2000). Modulation of Eastern North Pacific Hurricanes by the Madden–Julian Oscillation [Publisher: American Meteorological Society Section: Journal of Climate]. *Journal of Climate*, *13*(9), 1451–1460. https://doi.org/10.1175/1520-0442(2000)013<1451:MOENPH>2.0.CO;2

Manganello, J. V., Hodges, K. I., Kinter, J. L., Cash, B. A., Marx, L., Jung, T., Achuthavarier, D., Adams, J. M., Altshuler, E. L., Huang, B., Jin, E. K., Stan, C., Towers, P., & Wedi, N. (2012). Tropical Cyclone Climatology in a 10-km Global Atmospheric GCM: Toward Weather-Resolving Climate Modeling [Publisher: American Meteorological Society Section: Journal of Climate]. *Journal of Climate*, *25*(11), 3867–3893. https://doi.org/10.1175/JCLI-D-11-00346.1

Martin, D. A., Andriafanomezantsoa, R., Dröge, S., Osen, K., Rakotomalala, E., Wurz, A., Andrianarimisa, A., & Kreft, H. (2021). Bird diversity and endemism along a land-use gradient in Madagascar: The conservation value of vanilla agroforests. *Biotropica*, *53*(1), 179–190. https://doi.org/10.1111/btp.12859

Mavume, A. F., Rydberg, L., Rouault, M., & Lutjeharms, J. R. E. (2009). Climatology and Landfall of Tropical Cyclones in the South- West Indian Ocean [Number: 1]. *Western*

Indian Ocean Journal of Marine Science, *8*(1). https://doi.org/10.4314/wiojms.v8i1.56672

McBride, J. L., & Zehr, R. (1981). Observational analysis of tropical cyclone formation. Part ii: Comparison of non-developing versus developing systems. *Journal of the Atmospheric Sciences*, *38*(6), 1132–1151. https://doi.org/10.1175/1520-0469(1981)038<1132:OAOTCF>2.0.CO;2

Mei, W., Kamae, Y., Xie, S.-P., & Yoshida, K. (2019). Variability and predictability of north atlantic hurricane frequency in a large ensemble of high-resolution atmospheric simulations. *Journal of Climate*, *32*(11), 3153–3167.

Mei, W., & Xie, S.-P. (2016). Intensification of landfalling typhoons over the northwest Pacific since the late 1970s [Number: 10 Publisher: Nature Publishing Group]. *Nature Geoscience*, *9*(10), 753–757. https://doi.org/10.1038/ngeo2792

Menary, M. B., Kuhlbrodt, T., Ridley, J., Andrews, M. B., Dimdore-Miles, O. B., Deshayes, J., Eade, R., Gray, L., Ineson, S., Mignot, J., Roberts, C. D., Robson, J., Wood, R. A., & Xavier, P. (2018). Preindustrial Control Simulations With HadGEM3-GC3.1 for CMIP6. *Journal of Advances in Modeling Earth Systems*, *10*(12), 3049–3075. https://doi.org/10.1029/2018MS001495

Merrill, R. (1993). Tropical cyclone structure. *Global guide to tropical cyclone forecasting*, 2–1.

Murakami, H., Mizuta, R., & Shindo, E. (2012). Future changes in tropical cyclone activity projected by multi-physics and multi-SST ensemble experiments using the 60-km-mesh MRI-AGCM. *Climate Dynamics*, *39*(9), 2569–2584. https://doi.org/10.1007/s00382-011-1223-x

NOAA. (n.d.). Saffir-simpson hurricane wind scale. Retrieved May 5, 2023, from https://www.nhc.noaa.gov/aboutsshws.php

NumPy. (n.d.). Numpy.percentile — NumPy v1.24 Manual. Retrieved May 9, 2023, from https://numpy.org/doc/stable/reference/generated/numpy.percentile.html

Prasetya, D. A., Nguyen, P. T., Faizullin, R., Iswanto, I., & Armay, E. F. (2020). Resolving the shortest path problem using the haversine algorithm. *Journal of critical reviews*, *7*(1), 62–64.

PRIMAVERA. (n.d.). Our simulations | PRIMAVERA. Retrieved May 2, 2023, from https://www.primavera-h2020.eu/modelling/our-simulations/

Probst, P., Proietti, C., Annunziato, A., Paris, S., & Wania, A. (2017). Tropical cyclone enawo post-event report. *Joint Research Centre (JRC), The European Commission's Science and Knowledge Service: Brussels, Belgium.*

Redmond, G., Hodges, K. I., Mcsweeney, C., Jones, R., & Hein, D. (2015). Projected changes in tropical cyclones over Vietnam and the South China Sea using a 25 km regional climate model perturbed physics ensemble. *Climate Dynamics*, *45*(7), 1983–2000. https://doi.org/10.1007/s00382-014-2450-8
Reference for langauge when talking about cyclones for a specific region

Reuters. (2023). Cyclone Freddy death toll jumps to over 1,000, Malawi president says. *Reuters*. Retrieved May 4, 2023, from https://www.reuters.com/world/africa/cyclone-freddy-death-toll-jumps-over-1000-malawi-president-says-2023-04-12/

Roberts, C. D., Senan, R., Molteni, F., Boussetta, S., Mayer, M., & Keeley, S. P. E. (2018). Climate model configurations of the ECMWF Integrated Forecasting System (ECMWF-IFS cycle 43r1) for HighResMIP [Publisher: Copernicus GmbH]. *Geoscientific Model Development*, *11*(9), 3681–3712. https://doi.org/10.5194/gmd-11-3681-2018

Roberts, M. (2019). CMIP6 HighResMIP: Tropical storm tracks as calculated by the TRACK algorithm. https://catalogue.ceda.ac.uk/uuid/0b42715a7a804290afa9b7e31f5d7753
TRACK algorithm files

Roberts, M. J., Baker, A., Blockley, E. W., Calvert, D., Coward, A., Hewitt, H. T., Jackson, L. C., Kuhlbrodt, T., Mathiot, P., Roberts, C. D., Schiemann, R., Seddon, J., Vannière, B., & Vidale, P. L. (2019). Description of the resolution hierarchy of the global coupled HadGEM3-GC3.1 model as used in CMIP6 HighResMIP experiments [Publisher: Copernicus GmbH]. *Geoscientific Model Development*, *12*(12), 4999–5028. https://doi.org/10.5194/gmd-12-4999-2019

Roberts, M. J., Vidale, P. L., Mizielinski, M. S., Demory, M.-E., Schiemann, R., Strachan, J., Hodges, K., Bell, R., & Camp, J. (2015). Tropical Cyclones in the UPSCALE Ensemble of High-Resolution Global Climate Models [Publisher: American Meteorological Society Section: Journal of Climate]. *Journal of Climate*, *28*(2), 574–596. https://doi.org/10.1175/JCLI-D-14-00131.1

Roberts, M. J., Camp, J., Seddon, J., Vidale, P. L., Hodges, K., Vanniere, B., Mecking, J., Haarsma, R., Bellucci, A., Scoccimarro, E., Caron, L.-P., Chauvin, F., Terray, L., Valcke, S., Moine, M.-P., Putrasahan, D., Roberts, C., Senan, R., Zarzycki, C., & Ullrich, P. (2020). Impact of Model Resolution on Tropical Cyclone Simulation Using the HighResMIP–PRIMAVERA Multimodel Ensemble [Publisher: American Meteorological Society Section: Journal of Climate]. *Journal of Climate*, *33*(7), 2557–2583. https://doi.org/10.1175/JCLI-D-19-0639.1

Rummukainen, M. (2010). State-of-the-art with regional climate models. *Wiley Interdisciplinary Reviews: Climate Change*, *1*(1), 82–96.

Saji, N., & Yamagata, T. (2003). Possible impacts of Indian Ocean Dipole mode events on global climate. *Climate Research*, *25*, 151–169. https://doi.org/10.3354/cr025151

Schneider, T., Bischoff, T., & Haug, G. H. (2014). Migrations and dynamics of the intertropical convergence zone [Number: 7516 Publisher: Nature Publishing Group]. *Nature*, *513*(7516), 45–53. https://doi.org/10.1038/nature13636

Schreck, C. J., Knapp, K. R., & Kossin, J. P. (2014). The Impact of Best Track Discrepancies on Global Tropical Cyclone Climatologies using IBTrACS [Publisher: American Meteorological Society Section: Monthly Weather Review]. *Monthly Weather Review*, *142*(10), 3881–3899. https://doi.org/10.1175/MWR-D-14-00021.1

Scipy. (n.d.). Scipy.stats.pearsonr — SciPy v1.10.1 Manual. Retrieved May 9, 2023, from https://docs.scipy.org/doc/scipy/reference/generated/scipy.stats.pearsonr.html

Seabold, S., & Perktold, J. (2010). Statsmodels: Econometric and statistical modeling with python. *9th Python in Science Conference*.

Seneviratne, S., Zhang, X., Adnan, M., Badi, W., Dereczynski, C., Di Luca, A., Ghosh, S., Iskandar, I., Kossin, J., Lewis, S., Otto, F., Pinto, I., Satoh, M., Vicente-Serrano, S., Wehner, M., & Zhou, B. (2021). Weather and climate extreme events in a changing climate. In V. Masson-Delmotte, P. Zhai, A. Pirani, S. Connors, C. Péan, S. Berger, N. Caud, Y. Chen, L. Goldfarb, M. Gomis, M. Huang, K. Leitzell, E. Lonnoy, J. Matthews, T. Maycock, T. Waterfield, O. Yelekçi, R. Yu, & B. Zhou (Eds.), *Climate change 2021: The physical science basis. contribution of working group i to the sixth assessment report of the intergovernmental panel on climate change* (pp. 1513–1766). Cambridge University Press. https://doi.org/10.1017/9781009157896.013

Singh, V., & Koll, R. (2022). A review of ocean-atmosphere interactions during tropical cyclones in the north indian ocean. *Earth-Science Reviews*, *226*, 103967. https://doi.org/10.1016/j.earscirev.2022.103967

Skirving, W., Marsh, B., De La Cour, J., Liu, G., Harris, A., Maturi, E., Geiger, E., & Eakin, C. M. (2020). CoralTemp and the Coral Reef Watch Coral Bleaching Heat Stress Product Suite Version 3.1 [Number: 23 Publisher: Multidisciplinary Digital Publishing Institute]. *Remote Sensing*, *12*(23), 3856. https://doi.org/10.3390/rs12233856

Strachan, J., Vidale, P. L., Hodges, K., Roberts, M., & Demory, M.-E. (2013). Investigating Global Tropical Cyclone Activity with a Hierarchy of AGCMs: The Role of Model Resolution [Publisher: American Meteorological Society Section: Journal of Climate]. *Journal of Climate*, *26*(1), 133–152. https://doi.org/10.1175/JCLI-D-12-00012.1

Taylor, K. E. (2001). Summarizing multiple aspects of model performance in a single diagram. *Journal of Geophysical Research: Atmospheres*, *106*(D7), 7183–7192. https://doi.org/10.1029/2000JD900719

Taylor, K. E., Juckes, M., Balaji, V., Cinquini, L., Denvil, S., Durack, P. J., Elkington, M., Guilyardi, E., Kharin, S., Lautenschlager, M., Lawrence, B., Nadeau, D., & Stockhouse, M. (2018). CMIP6 Global Attributes DRS, Filenames, Directory Structure and CV's. Retrieved May 3, 2023, from https://docs.google.com/document/d/1h0r8RZr_f3-8egBMMh7aqLwy3snpD6_MrDz1q8n5XUk/edit

Theodorsson-Norheim, E. (1986). Kruskal-Wallis test: BASIC computer program to perform nonparametric one-way analysis of variance and multiple comparisons on ranks of several independent samples. *Computer Methods and Programs in Biomedicine*, *23*(1), 57–62. https://doi.org/10.1016/0169-2607(86)90081-7

Ullrich, P. A., & Zarzycki, C. M. (2017). TempestExtremes: A framework for scale-insensitive pointwise feature tracking on unstructured grids [Publisher: Copernicus GmbH]. *Geoscientific Model Development*, *10*(3), 1069–1090. https://doi.org/10.5194/gmd-10-1069-2017

Uyanık, G. K., & Güler, N. (2013). A Study on Multiple Linear Regression Analysis. *Procedia - Social and Behavioral Sciences*, *106*, 234–240. https://doi.org/10.1016/j.sbspro.2013.12.027

Voldoire, A., Saint-Martin, D., Sénési, S., Decharme, B., Alias, A., Chevallier, M., Colin, J., Guérémy, J.-F., Michou, M., Moine, M.-P., Nabat, P., Roehrig, R., Salas y Mélia, D., Séférian, R., Valcke, S., Beau, I., Belamari, S., Berthet, S., Cassou, C., ... Waldman, R. (2019). Evaluation of CMIP6 DECK Experiments With CNRM-CM6-1. *Journal of Advances in Modeling Earth Systems*, *11*(7), 2177–2213. https://doi.org/10.1029/2019MS001683

Wahiduzzaman, M., & Yeasmin, A. (2019). Statistical forecasting of tropical cyclone landfall activities over the North Indian Ocean rim countries. *Atmospheric Research*, *227*, 89–100. https://doi.org/10.1016/j.atmosres.2019.04.034

Weaver, B., & Wuensch, K. L. (2013). SPSS and SAS programs for comparing Pearson correlations and OLS regression coefficients. *Behavior Research Methods*, *45*(3), 880–895. https://doi.org/10.3758/s13428-012-0289-7

Weinkle, J., Landsea, C., Collins, D., Musulin, R., Crompton, R. P., Klotzbach, P. J., & Pielke, R. (2018). Normalized hurricane damage in the continental United States 1900–2017 [Number: 12 Publisher: Nature Publishing Group]. *Nature Sustainability*, *1*(12), 808–813. https://doi.org/10.1038/s41893-018-0165-2

Williams, K. D., Copsey, D., Blockley, E. W., Bodas-Salcedo, A., Calvert, D., Comer, R., Davis, P., Graham, T., Hewitt, H. T., Hill, R., Hyder, P., Ineson, S., Johns, T. C., Keen, A. B., Lee, R. W., Megann, A., Milton, S. F., Rae, J. G. L., Roberts, M. J., ... Xavier, P. K. (2018). The Met Office Global Coupled Model 3.0 and 3.1 (GC3.0 and GC3.1) Configurations. *Journal of Advances in Modeling Earth Systems*, *10*(2), 357–380. https://doi.org/10.1002/2017MS001115

WMO. (2016). Tropical cyclone naming. Retrieved May 5, 2023, from https://public.wmo.int/en/our-mandate/focus-areas/natural-hazards-and-disaster-risk-reduction/tropical-cyclones/Naming

WMO. (2023). Tropical Cyclone Freddy may set new record | World Meteorological Organization. Retrieved May 4, 2023, from https://web.archive.org/web/20230313145433/https://public.wmo.int/en/media/news/tropical-cyclone-freddy-may-set-new-record

Yoshida, K., Sugi, M., Mizuta, R., Murakami, H., & Ishii, M. (2017). Future changes in tropical cyclone activity in high-resolution large-ensemble simulations. *Geophysical Research Letters*, *44*(19), 9910–9917.

Zarzycki, C. M., & Ullrich, P. A. (2017). Assessing sensitivities in algorithmic detection of tropical cyclones in climate data. *Geophysical Research Letters*, *44*(2), 1141–1149. https://doi.org/10.1002/2016GL071606

Zhang, C. (2013). Madden–Julian Oscillation: Bridging Weather and Climate [Publisher: American Meteorological Society Section: Bulletin of the American Meteorological Society]. *Bulletin of the American Meteorological Society*, *94*(12), 1849–1870. https://doi.org/10.1175/BAMS-D-12-00026.1

Zhao, M., & Held, I. M. (2012). TC-Permitting GCM Simulations of Hurricane Frequency Response to Sea Surface Temperature Anomalies Projected for the Late-Twenty-First Century [Place: Boston MA, USA Publisher: American Meteorological Society]. *Journal of Climate*, *25*(8), 2995–3009. https://doi.org/https://doi.org/10.1175/JCLI-D-11-00313.1

Zhao, M., Held, I. M., Lin, S.-J., & Vecchi, G. A. (2009). Simulations of Global Hurricane Climatology, Interannual Variability, and Response to Global Warming Using a 50-km Resolution GCM [Publisher: American Meteorological Society Section: Journal of Climate]. *Journal of Climate*, *22*(24), 6653–6678. https://doi.org/10.1175/2009JCLI3049.1

A Appendix

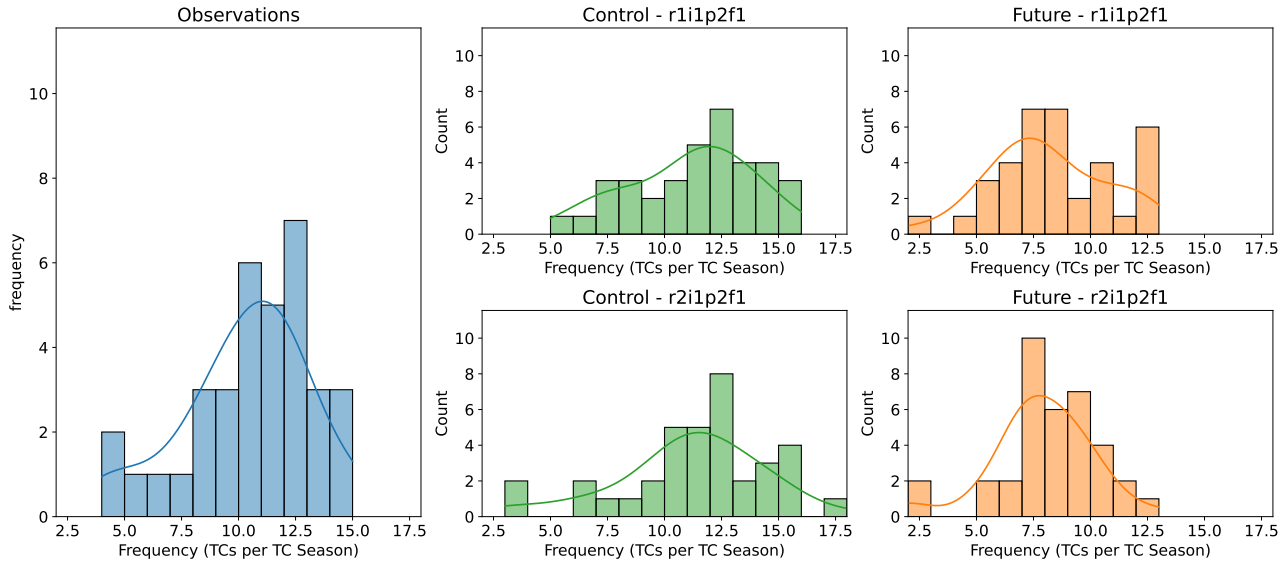

Figure 41: **Distribution of the Frequency of TCs per TC Season in Two EC-Earth3P-HR Ensemble Members** (Left) Distribution of the frequency of observed TCs per TC season across the entire SWIO basin. (Upper center) Distribution of the frequency of TCs in EC-Earth3P-HR model ensemble r1i1p2f1 for the control simulation with 1950s radiative forcing. (Lower center) Distribution of the frequency of of TCs in EC-Earth3P-HR model ensemble r1i1p2f1 for the control simulation with 1950s radiative forcing. (Upper right) Distribution of the frequency of TCs in EC-Earth3P-HR model ensemble r1i1p2f1 for the future simulation forced with SSP5-8.5. (Lower right) Distribution of the frequency of TCs in EC-Earth3P-HR model ensemble r2i1p2f1 for the future simulation forced with SSP5-8.5. Kruskal-Wallis p-value of 2.0072e-08.

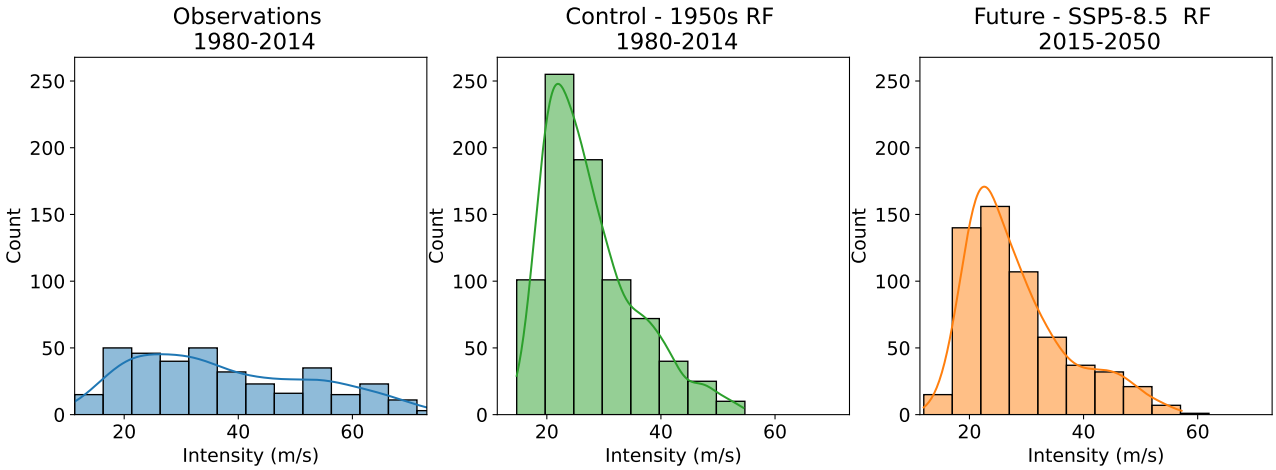

Figure 42: **Distribution of Intensity of TCs in Two EC-Earth3P-HR Ensemble Members** (Left) Distribution of observed TC intensities in the SWIO. (Center) Distribution of the intensities of TCs in both ensemble member r1i1p2f1 and r2i1p2f1 for the control simulation with 1950s radiative forcing. (Right) Distribution of the intensities of TCs in both ensemble member r1i1p2f1 and r2i1p2f1 for the future simulation forced with SSP5-8.5. Kruskal-Wallis p-value of 1.3215e-26.

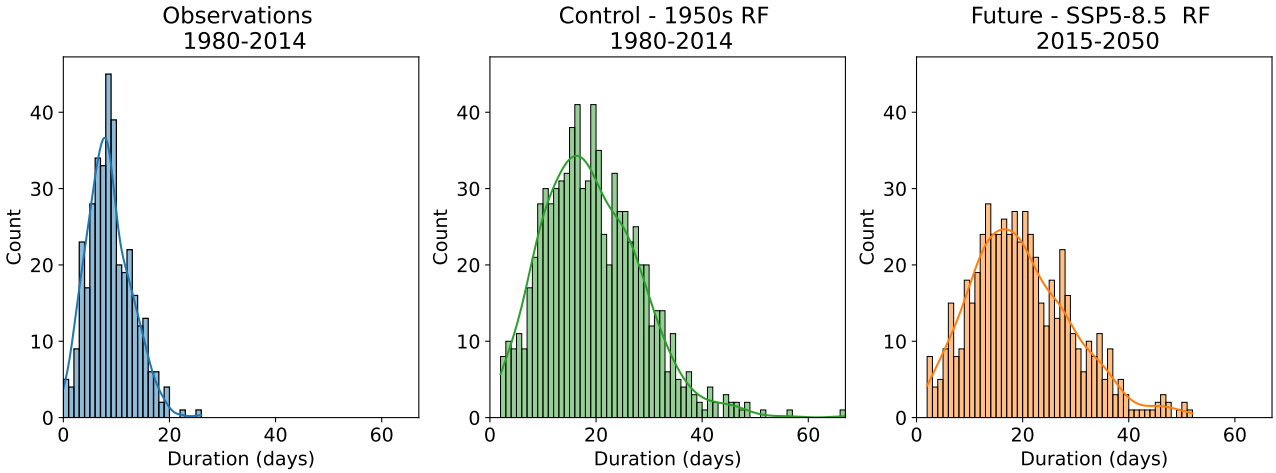

Figure 43: **Distribution of Duration of TCs in Two EC-Earth3P-HR Ensemble Members** (Left) Distribution of the duration of observed TCs in the SWIO. (Center) Distribution of the duration of TCs in both ensemble member r1i1p2f1 and r2i1p2f1 for the control simulation with 1950s radiative forcing. (Right) Distribution of the duration of TCs in both ensemble member r1i1p2f1 and r2i1p2f1 for the future simulation forced with SSP5-8.5. Kruskal-Wallis p-value of 6.065e-99.

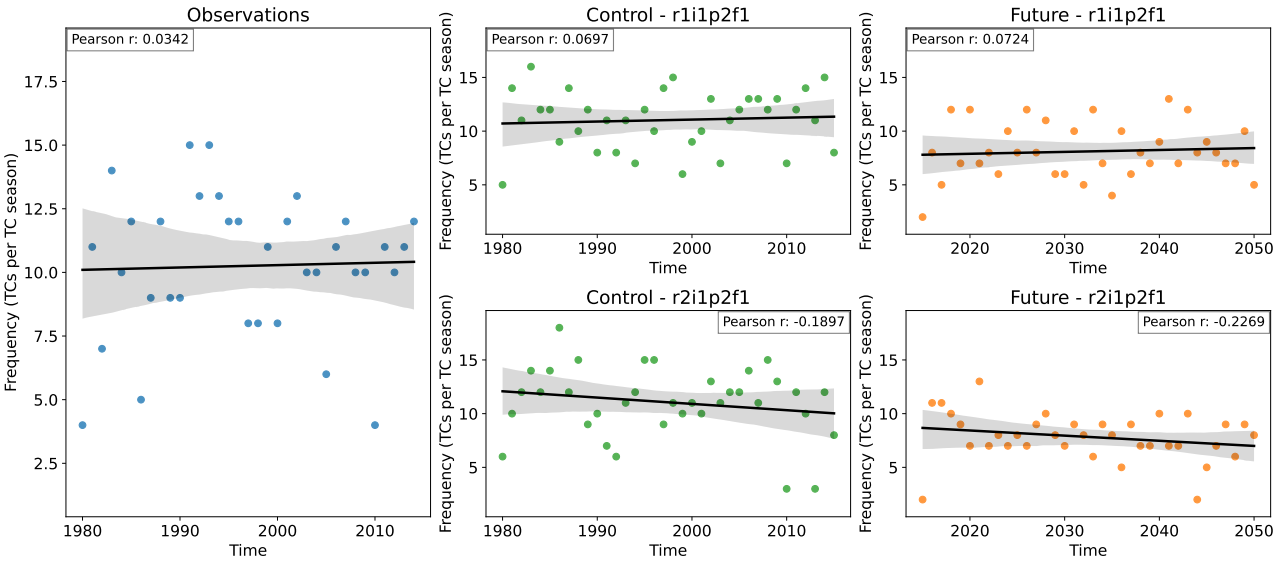

Figure 44: **Linear Regression of the Frequency of TCs per TC Season in Two EC-Earth3P-HR Ensemble Members** (Left) Linear regression of the frequency of observed TCs per TC season. (Upper center) Linear regression of the frequency of TCs in ensemble member r1i1p2f1 for the control simulation with 1950s radiative forcing. (Lower center) Linear regression of the frequency of TCs in ensemble member r2i1p2f1 for the control simulation with 1950s radiative forcing. (Upper right) Linear regression of the frequency of TCs in ensemble member r1i1p2f1 for the future simulation forced by SSP5-8.5. (Lower right) Linear regression of the frequency of TCs in ensemble member r2i1p2f1 for the future simulation forced by SSP5-8.5.

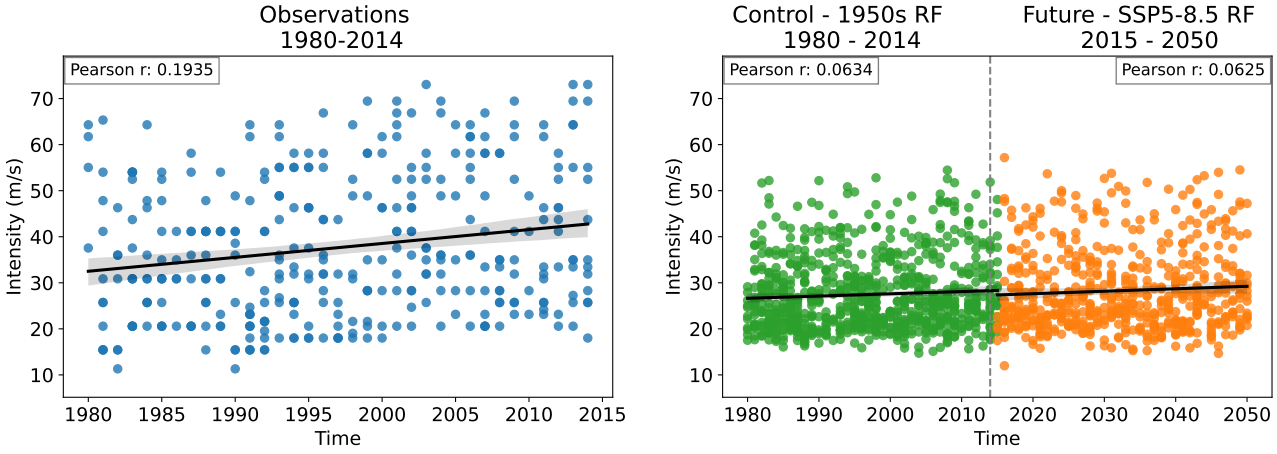

Figure 45: **Linear Regression of the Intensity of TCs in Two EC-Earth3P-HR Ensemble Members** (Left) Linear regression of the intensity of observed TCs in the SWIO basin. (Right) Linear regressions of intensity of both ensemble members r1i1p2f1 and r2i1p2f1 combined for the control and future simulations, respectively. Control and future simulations delimited with a vertical dashed line.

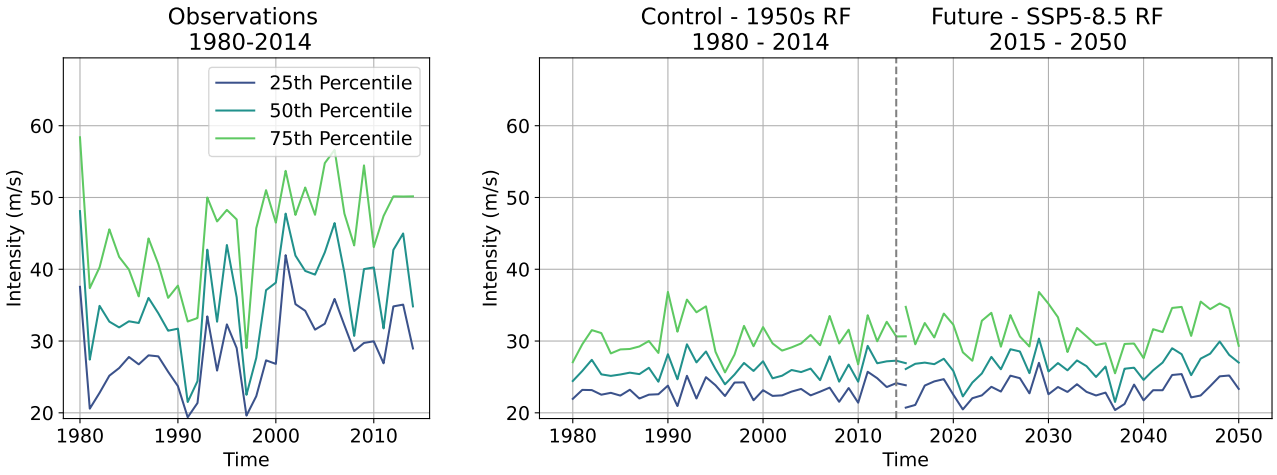

Figure 46: **Percentile 5-Year Running Mean of SWIO TC Intensity for Two EC-Earth3P-HR Ensemble Members** (Left) 5-year running mean of the 25th, 50th and 75th percentile of the intensity of observed TCs in the SWIO. (Right) 5-year running mean of the 25th, 50th, and 75th percentile of both ensemble members r1i1p2f1 and r2i1p2f1 combined for the control and future simulations, respectively. Control and future simulations delimited with a vertical dashed line.

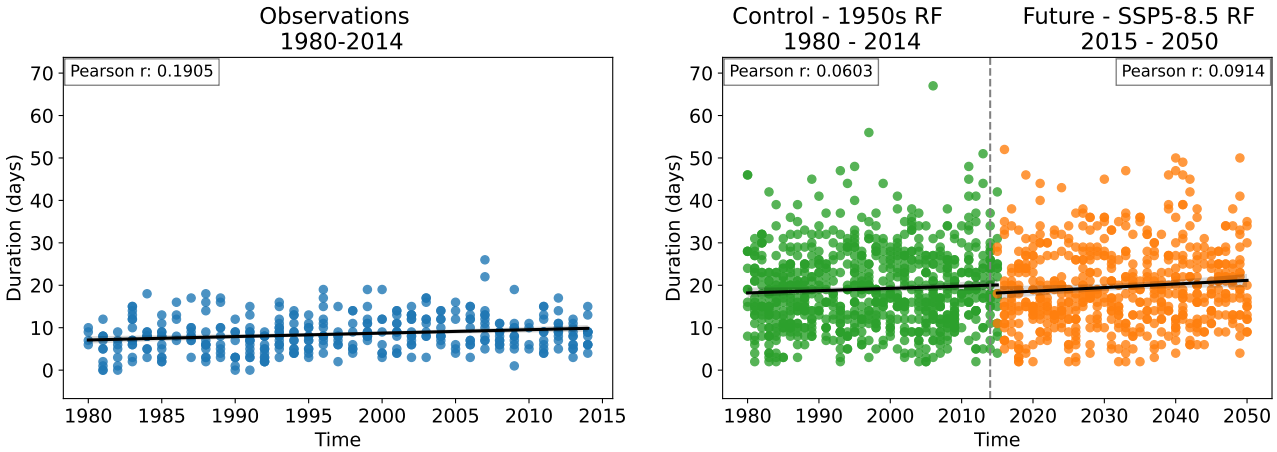

Figure 47: **Linear Regression of the Duration of TCs in Two EC-Earth3P-HR Ensemble Members** (Left) Linear regression of the duration of observed TCs in the SWIO basin. (Right) Linear regressions of intensity of both ensemble members r1i1p2f1 and r2i1p2f1 combined for the control and future simulations, respectively. Control and future simulations delimited with a vertical dashed line.

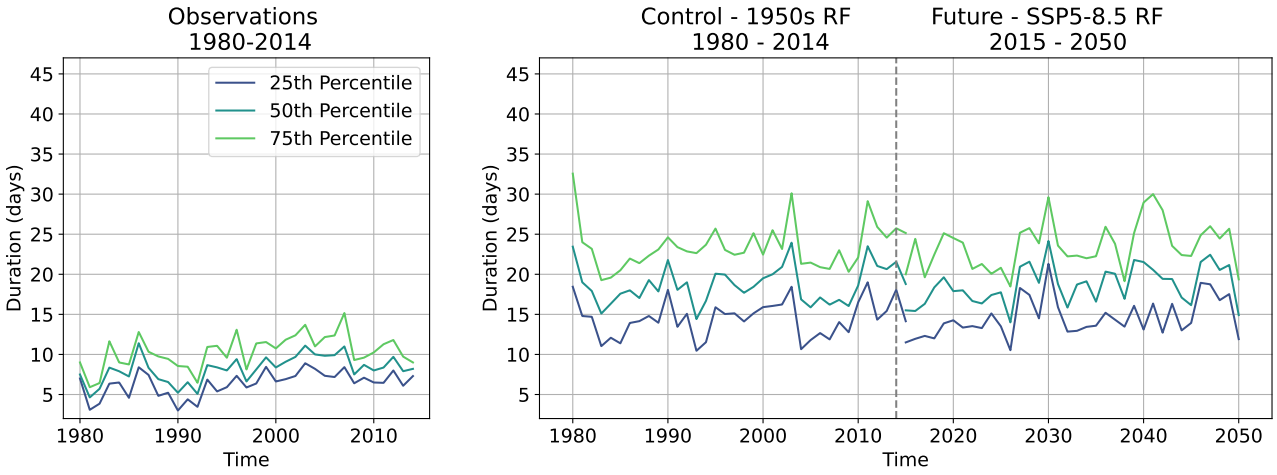

Figure 48: **Percentile 5-Year Running Mean of SWIO TC Duration for Two EC-Earth3P-HR Ensemble Members** (Left) 5-year running mean of the 25th, 50th and 75th percentile of the duration of observed TCs in the SWIO. (Right) 5-year running mean of the 25th, 50th, and 75th percentile of both ensemble members r1i1p2f1 and r2i1p2f1 combined for the control and future simulations, respectively. Control and future simulations delimited with a vertical dashed line.

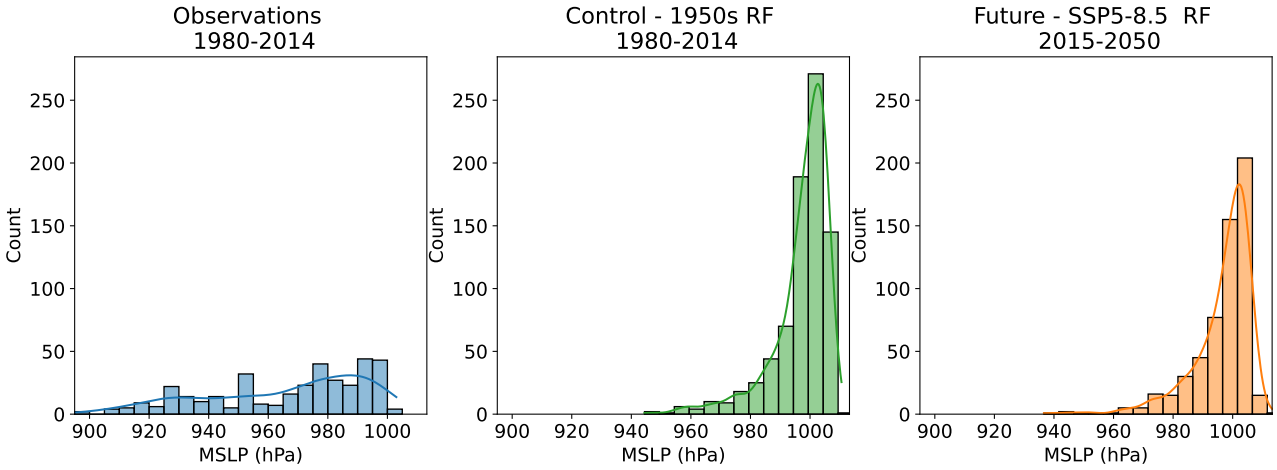

Figure 49: **Distribution of MSLP for TCs in Two EC-Earth3P-HR Ensemble Members** (Left) Distribution of the MSLP for observed TCs in the SWIO. (Center) Distribution of the MSLP of TCs in both ensemble member r1i1p2f1 and r2i1p2f1 for the control simulation with 1950s radiative forcing. (Right) Distribution of the MSLP of TCs in both ensemble member r1i1p2f1 and r2i1p2f1 for the future simulation forced with SSP5-8.5. Kruskal-Wallis p-value of 5.8751e-102.

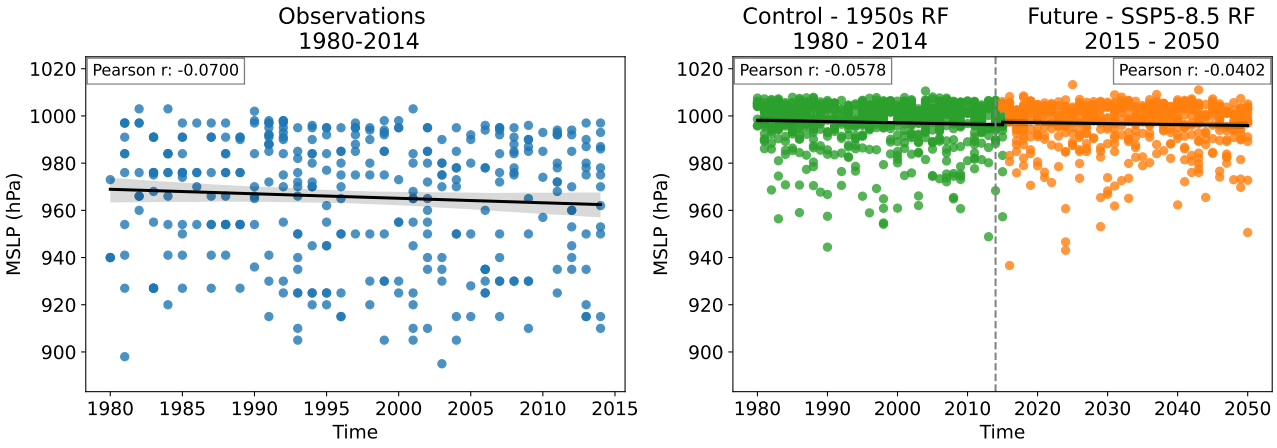

Figure 50: **Linear Regression of the MSLP of TCs in Two EC-Earth3P-HR Ensemble Members** (Left) Linear regression of the MSLP of observed TCs in the SWIO basin. (Right) Linear regressions of MSLP of both ensemble members r1i1p2f1 and r2i1p2f1 combined for the control and future simulations, respectively. Control and future simulations delimited with a vertical dashed line.

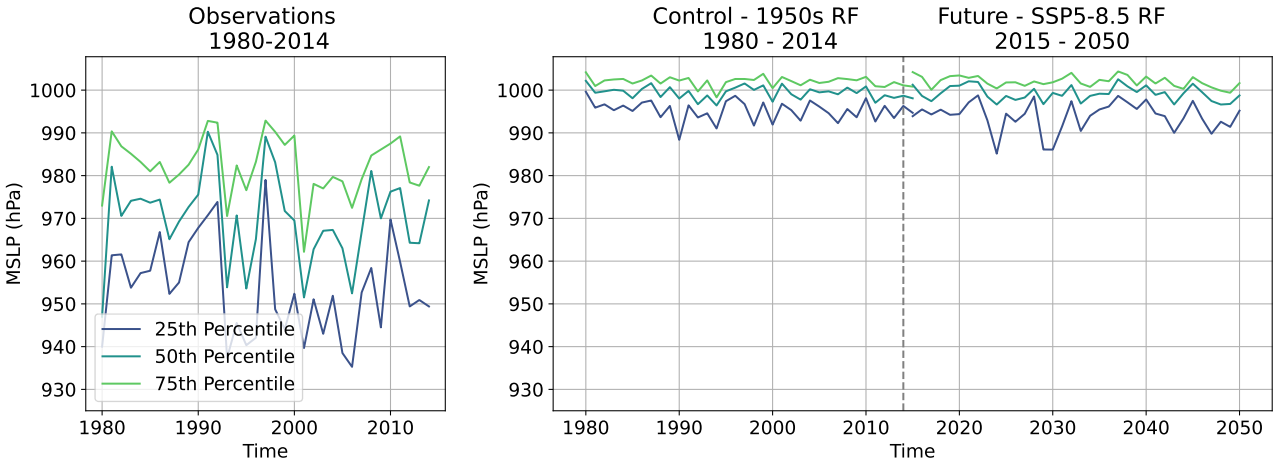

Figure 51: **Percentile 5-Year Running Mean of SWIO TC MSLP for Two EC-Earth3P-HR Ensemble Members** (Left) 5-year running mean of the 25th, 50th and 75th percentile of the MSLP of observed TCs in the SWIO. (Right) 5-year running mean of the 25th, 50th, and 75th percentile of the MSLP of both ensemble members r1i1p2f1 and r2i1p2f1 combined for the control and future simulations, respectively. Control and future simulations delimited with a vertical dashed line.